MICROWAVE SINTERING AND CHARACTERIZATION OF ALUMINA
AND ALUMINA MATRIX CERAMIC NANOCOMPOSITES

A THESIS SUBMITTED TO
THE GRADUATE SCHOOL OF NATURAL AND APPLIED SCIENCES
OF
MIDDLE EAST TECHNICAL UNIVERSITY

BY

BURCU KAYIPLAR

IN PARTIAL FULLFILLMENT OF THE REQUIREMENTS
FOR
THE DEGREE OF MASTER OF SCIENCE
IN
METALLURGICAL AND MATERIALS ENGINEERING

APRIL 2010

Approval of the thesis:

MICROWAVE SINTERING AND CHARACTERIZATION OF ALUMINA AND ALUMINA MATRIX NANOCOMPOSITES

submitted by **BURCU KAYIPLAR** in partial fulfillment of the requirements for the degree of **Master of Science in Metallurgical and Materials Engineering Department, Middle East Technical University** by,

Prof. Dr. Canan ÖZGEN   ＿＿＿＿＿
Dean, Graduate School of **Natural and Applied Sciences**

Prof. Dr. Tayfur ÖZTÜRK   ＿＿＿＿＿
Head of Department, **Metallurgical and Materials Engineering**

Assist. Prof. Dr. Arcan F. DERİCİOĞLU   ＿＿＿＿＿
Supervisor, **Metallurgical and Materials Engineering Dept., METU**

Examining Committee Members:

Prof. Dr. Muharrem TİMUÇİN   ＿＿＿＿＿
Metallurgical and Materials Engineering Dept., METU

Assist. Prof. Dr. Arcan F. DERİCİOĞLU   ＿＿＿＿＿
Metallurgical and Materials Engineering Dept., METU

Prof. Dr. Abdullah ÖZTÜRK   ＿＿＿＿＿
Metallurgical and Materials Engineering Dept., METU

Assoc. Prof. Dr. Caner DURUCAN   ＿＿＿＿＿
Metallurgical and Materials Engineering Dept., METU

Assoc. Prof. Dr. Zafer EVİS   ＿＿＿＿＿
Engineering Sciences Dept., METU

Date: 29.04.2010

I hereby declare that all information in this document has been obtained and presented in accordance with academic rules and ethical conduct. I also declare that, as required by these rules and conduct, I have fully cited and referenced all material and results that are not original to this work.

Name, Last Name: Burcu KAYIPLAR

Signature   :

ABSTRACT

MICROWAVE SINTERING AND CHARACTERIZATION OF ALUMINA AND ALUMINA MATRIX CERAMIC NANOCOMPOSITES

Kayıplar, Burcu

M.S., Department of Metallurgical and Materials Engineering
Supervisor: Assist. Prof. Dr. Arcan F. Dericioğlu

April 2010, 106 pages

Efficiency of microwave heating on the sintering of ceramic materials has been investigated in comparison to conventional processing. Monolithic alumina with or without sintering additives such as MgO, CaO, Y_2O_3 were fabricated by both conventional and microwave sintering at temperatures ranging from 1000˚C to 1600˚C with a constant soaking time of 1 hour. Based on the densification results on monolithic alumina, nanometer-sized SiC or stabilized ZrO_2 particle-dispersed alumina matrix ceramic nanocomposites were sintered by both methods at 1300˚C and 1500˚C for 1 hour. Sintered ceramic materials were characterized in terms of densification, microstructural evolution, chemical composition and mechanical properties such as hardness and indentation fracture toughness.

Microwave sintering was determined to be a remarkably effective method in the production of Al_2O_3 ceramics at considerably low temperatures (≤1400˚C) compared to conventional sintering in achieving enhanced relative densities reaching to ~97% with improved microstructural characteristics and mechanical properties. Usage of sintering additives at temperatures higher than 1400˚C was determined to be effective in densifying Al_2O_3 by both methods. Second phase

particle incorporation yielded poor densification resulting in a decrease of hardness of the fabricated ceramic nanocomposites; however, their fracture toughness improved considerably caused by the crack deflection at the dispersed particles and grain boundaries reaching to ~4 MPa·m$^{1/2}$ in the case of SiC particle-dispersed nanocomposites. Compared to conventional sintering, microwave sintering is more effective in the processing of alumina and alumina matrix nanocomposites leading to similar densification values along with improved microstructural and mechanical characteristics at lower temperatures in shorter soaking periods.

Keywords: Ceramic nanocomposites, ceramic processing, microwave sintering, Al_2O_3, SiC, stabilized ZrO_2, microstructure, mechanical properties.

ÖZ

ALUMİNA VE ALUMİNA MATRİSLİ SERAMİK NANOKOMPOZİT MALZEMELERİN MİKRODALGA İLE SİNTERLENMESİ VE KARAKTERİZASYONU

Kayıplar, Burcu

Y.Lisans, Metalurji ve Malzeme Mühendisliği Bölümü

Tez Yöneticisi: Yrd. Doç. Dr. Arcan F. Dericioğlu

Nisan 2010, 106 sayfa

Mikrodalga ısıtmanın seramik malzemelerin sinterlenmesi üzerindeki etkinliği konvansiyonel yöntemle mukayese edilerek incelenmiştir. MgO, CaO ve Y_2O_3 gibi sinterlemeye yardımcı katkı maddeleri içeren veya içermeyen monolitik alumina (Al_2O_3) 1000˚C ila 1600˚C sıcaklık aralığında 1 saatlik sabit bekleme süresi ile hem konvansiyonel hem de mikrodalga sinterleme yöntemleri ile üretilmiştir. Monolitik aluminanın yüzde yoğunlaşım sonuçlarına dayanarak, nanometre boyutundaki SiC veya kararlılaştırılmış ZrO_2 parçacıkları dağıtılmış alumina matrisli seramik nanokompozitler her iki metodla 1300 ve 1500°C'de 1 saat süre ile sinterlenmiştir. Sinterlenmiş seramik malzemeler yüzde yoğunlaşım değerleri, mikroyapısal değişimleri, kimyasal bileşimleri ve sertlik ve girinti kırılma tokluğu gibi mekanik özellikleri bakımından incelenmiştir.

Mikrodalga sinterlemenin konvansiyonel sinterlemeye kıyasla nispeten düşük sıcaklıklarda (≤1400˚C) gelişmiş mikroyapılı, ~%97'ye varan yüksek yoğunlaşım oranlarına ve daha iyi mekanik özelliklere sahip Al_2O_3 seramiklerinin üretiminde daha etkili bir yöntem olduğu belirlenmiştir. 1400˚C'den daha yüksek sıcaklıklarda sinterlemeye yardımcı katkı maddelerinin kullanımının her iki yöntemle de aluminanın yoğunlaştırılmasında etkin olduğu belirlenmiştir.

İkincil faz parçacıklarının ilavesi ile düşük yoğunluğa ve bu sebeple düşük sertlik değerlerine sahip seramik nanokompozitler elde edilmiştir, ancak SiC parçacıkları dağıtılmış nanokompozitlerin kırılma tokluğu parçacık ve tane sınırlarında görülen kırık sapması davranışı ile $\sim$4 MPa·m$^{1/2}$ seviyelerine yükselmiştir. Konvasiyonel sinterlemeye kıyasla, mikrodalga sinterleme daha düşük sinterleme sıcaklık ve sürelerinde sağladığı daha yüksek yoğunlaşım oranları ve gelişmiş mikroyapısal ve mekanik özellikler ile alumina matrisli nanokompozitlerin üretiminde çok daha etkin bir yöntem olduğunu ortaya koymuştur.

Anahtar kelimeler: Seramik nanocompozitler, seramik prosesleri, mikrodalga sinterleme, Al$_2$O$_3$, SiC, stabilize ZrO$_2$, mikroyapı, mekanik özellikler.

To My Family

ACKNOWLEDGMENTS

First of all, I would like express my deepest gratitude to my advisor Assist. Prof. Dr. Arcan F. Dericioğlu for his supervision, knowledge, advice, encouragement and patience throughout the entire stage of this dissertation. I am so grateful to my advisor for letting me benefit from his profound knowledge and experience. During my study, his supports and understanding helped me to overcome difficult times.

I would also like to express my sincere thanks to Cengiz Tan for his kind interest during SEM studies, Necmi Avcı for performing XRD measurements and Yusuf Yıldırım for his kind helps during my metallographic studies.

I would also like to thank to all of my friends at the Department of Metallurgical and Materials Engineering, METU, especially, Selen Gürbüz, Elvan Tan, Göksu Gürer, Onur Rauf Bingöl and Volkan Kalem, for their moral support and unforgettable favors.

On the other hand, I am also grateful to my friends Derya Erdem and Derya Kapusuz for always being beside me to support at every time of my life throughout the last two years.

Finally, I would like to express my very special thanks to my parents for their support, encouragement and trust in me throughout my life.

TABLE OF CONTENTS

LIST OF TABLES

LIST OF FIGURES

CHAPTER 1

INTRODUCTION

Alumina (Al_2O_3) is a widely used, relatively feasible structural ceramic for many engineering applications because of its specific features such as high stiffness to weight ratio, high temperature stability, resistance to corrosion and abrasion etc. Nevertheless, their low fracture resistance limits the widespread usage of monolithic Al_2O_3 ceramics in various engineering applications [1]. To overcome this deficiency, studies have focused on forming nanocomposites by dispersing ceramic nano-particles in alumina matrix. Conventional processing of such ceramic materials is usually inefficient in terms of tooling/maintenance cost and time because of the high temperatures and/or simultaneous pressure application required. The deficiencies associated with conventional processes can be overcome by an alternative method, namely microwave sintering, which has been demonstrated to reveal improved densification, microstructural morphology and mechanical properties at lower temperatures and times in the processing of ceramics and ceramic nanocomposites.

In the current study, preliminary aim was to make a comparative analysis between the sintering efficiencies of conventional and microwave heating methods based on monolithic Al_2O_3 as a representative material. For this purpose introductory experiments were conducted on the microwave sintering of monolithic Al_2O_3 at varying temperatures between 1000 and 1600˚C. Results showed that microwave sintering is more effective than its conventional counterpart at temperatures below 1400˚C, which is remarkably low for the processing of alumina ceramics, where ~15% higher relative densification has been achieved at these mild temperatures. In correlation with the achieved densification levels, hardness of microwave sintered monolithic Al_2O_3 followed an increasing trend with the process

1

temperature up to 1500°C, after which hardness values of both conventional and microwave sintered Al$_2$O$_3$ started to decrease due to abnormal grain growth.

In addition to the microwave sintering studies on plain Al$_2$O$_3$, three different types of sintering aids were added to further improve its densification by inhibiting abnormal grain growth especially observed at elevated temperatures. Nevertheless, it was determined that usage of sintering aids did not provide additional improvement in densification at temperatures lower than 1400°C for both microwave and conventional sintering, where the relative density of microwave sintered plain monolithic Al$_2$O$_3$ has already reached to ~97%. Microstructural observation of sintered Al$_2$O$_3$ ceramics revealed that addition of sintering aids suppressed grain boundary mobility excessively at the low sintering temperature regime. At higher sintering temperatures hardness values of sintering aid containing Al$_2$O$_3$ ceramics processed by both methods increased reaching to values as high as ~19 GPa due to enhanced densification, where that of plain Al$_2$O$_3$ showed a decreasing tendency caused by the abnormal grain growth. Similarly, decreasing indentation fracture toughness of conventional sintered monolithic Al$_2$O$_3$ was attributed to abnormal grain growth. On the other hand, indentation fracture toughness values of microwave sintered Al$_2$O$_3$ ceramics did not show remarkable change with temperature and sintering additive type showing the effective suppression of grain growth related complications by the use of microwave heating.

During its principal stage, current study has focused on the processing of nanometer-sized SiC (Al$_2$O$_3$/SiC$_p$) and yttrium stabilized ZrO$_2$ (Al$_2$O$_3$/YSZ$_p$) particle-dispersed Al$_2$O$_3$ matrix ceramic nanocomposites by both conventional and microwave sintering at two different temperatures of 1300°C and 1500°C. Addition of SiC or YSZ particles led to reduction in densification compared to monolithic Al$_2$O$_3$ for both of the methods. The negative effect of particle dispersion on densification was less pronounced in the case of zirconia addition compared to that observed in SiC addition to Al$_2$O$_3$. Hardness values of the Al$_2$O$_3$/SiC$_p$ nanocomposites were considerably lower than those of the monolithic

2

Al$_2$O$_3$ due to the inefficient densification which did not show a strong second phase content dependence. Contrary to the observed change in hardness, indentation fracture toughness of Al$_2$O$_3$/SiC$_p$ nanocomposites processed by both methods showed an improvement reaching up to ~4 MPa.m$^{1/2}$ compared to that of monolithic Al$_2$O$_3$ which is on the order of ~2.5 MPa.m$^{1/2}$. Achieved fracture toughness improvement was attributed to the change of fracture mode of Al$_2$O$_3$ from inter to transgranular by the addition of SiC particles which is more dominant in the case of microwave sintering. Different than those of the Al$_2$O$_3$/SiC$_p$ nanocomposites, hardness of Al$_2$O$_3$/YSZ$_p$ nanocomposites did not reveal remarkable difference with respect to the hardness values of monolithic Al$_2$O$_3$, even though the densification achieved in Al$_2$O$_3$/YSZ$_p$ nanocomposites was relatively lower. On the other hand, as opposed to the fracture toughness improvement achieved in Al$_2$O$_3$/SiC$_p$ nanocomposites, indentation fracture toughness of Al$_2$O$_3$/YSZ$_p$ nanocomposites showed a decreasing trend with increasing ZrO$_2$ content mainly because of the reduction in densification.

In conclusion, according to the results of this study, microwave sintering was determined to be an efficient alternative method specifically for the fabrication of alumina and alumina matrix nanocomposites because of the relative densification, microstructure evolution and resulting mechanical properties achieved at lower temperatures in shorter soaking periods compared to conventional sintering. Despite the presence of difficulties associated with microwave sintering such as accurate temperature measurement and stabilization together with the material and geometry dependence of volumetric heating, this alternative processing method should further be studied in detail for various material systems due to the prospective practical advantages such as time and energy savings it provides in addition to the above-mentioned improvements from the materials science point of view.

CHAPTER 2

LITERATURE REVIEW

2.1 Solid State Sintering Theory

Production techniques like casting, machining, forging, stamping, welding are not readily applicable to ceramic materials because of their refractory and brittle nature. Thus, they are generally produced by powder metallurgical methods which mainly involve blending and mixing of ceramic powders, pressing them to desired shapes and subsequent heat treatment of the compacts –sintering- (Fig. 2.1). In some cases, heat and pressure can be applied at the same time to increase densification of final product by the methods like hot pressing or hot isostatic pressing.

Raw Powders   Formed Product after Pressing   Sintered Product
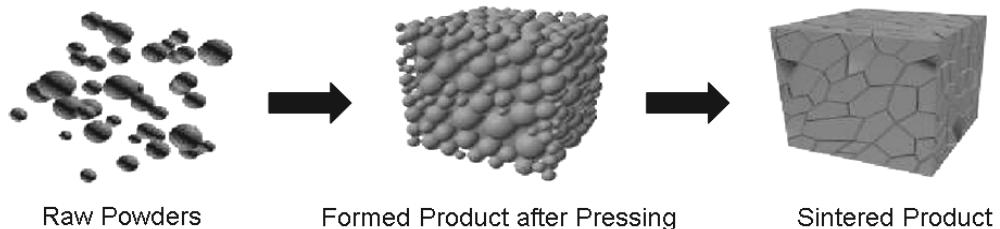
Figure 2.1 Main processes of powder metallurgy.

Sintering is the process of heating a compressed material (green compact) or a powder mass to a temperature below its melting point to allow bonding of the particles and reduce porosity (densification) which strengthens the compact [2, 3]. The main driving force during solid state sintering is the tendency to decrease free energy of the system associated with surfaces/interfaces. System decreases its

4

total free energy by with the reduction of total free surfaces, elimination of solid/vapor interfaces, creation of grain boundaries and ultimately by grain growth. Therefore, increasing surface area of the initial powders, i.e. starting with finer particles, increases total surface energy, and thus enhances sintering rate.

Mass transport is the main mechanism of solid state sintering which occurs by atomic diffusion. Transport of the materials is affected by externally applied pressure, curvature of the particle surfaces and chemical reactions due to change in the surface energy. Increasing temperature increases the mobility of the atomic features which gives rise to neck formation between touching particles by mass transport. Figure 2.2 shows the mass transport mechanisms occuring during solid state sintering process. Surface diffusion (1), lattice diffusion from the surface (2) and vapor transport (evaporation-condensatiton) mechanisms (3) are non-densifying mechanisms, atoms move from the particle surfaces to the neck causing neck growth and coarsening of the particles without densification. Most important densification mechanisms are grain boundary diffusion (4) and lattice diffusion (5) from grain boundaries and from the bulk to the pores which result in densification and shrinkage beside the neck formation [3].
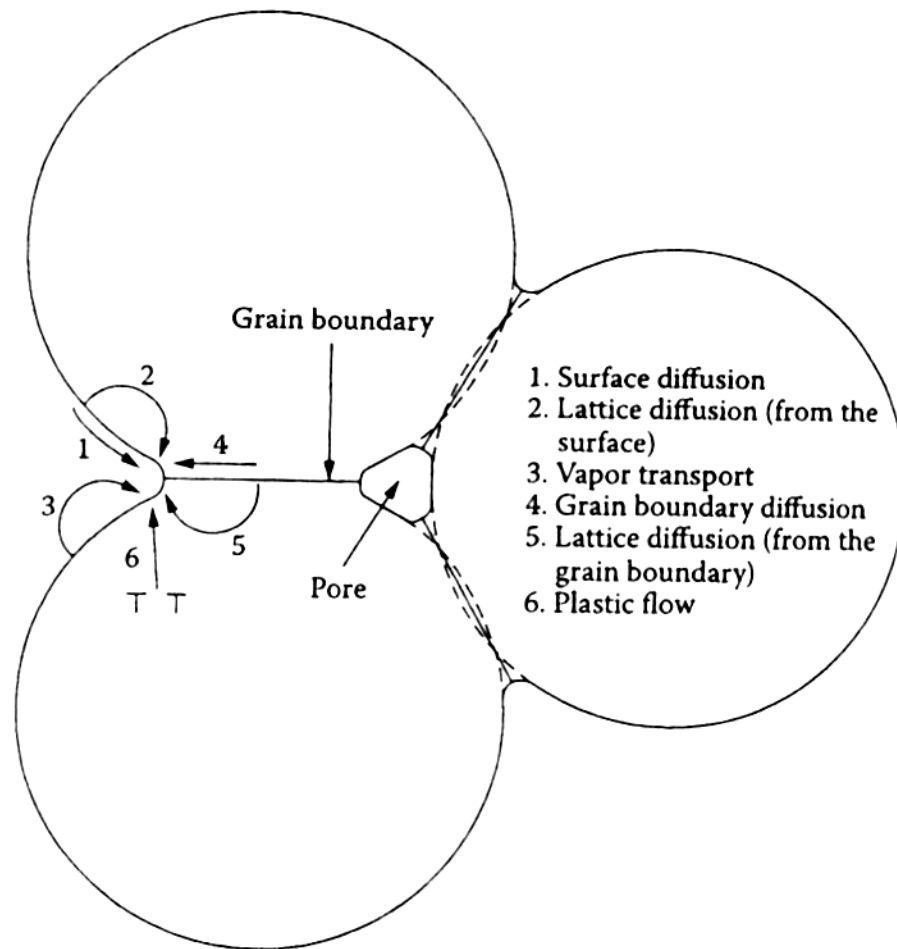
Figure 2.2 Schematic representation of the sintering mechanisms [3].

Sintering proceeds in consequtive three stages which are first, intermediate and final stages. At the first stage, small contacts between the particles of green compact start to grow and necks form between particles as in Figure 2.3 (a) and (b). Shrinkage (densification) is rather poor during this stage (~5%). Second stage is the most important one in terms of densification. After the neck formation, individual particles start to loose their identity. A continuous, channel-like structure of pores occur, grain growth starts and grain boundaries extend from pore to pore. This stage continues until pores become isolated and closed Figure 2.3 (c). Most of the achieved densification (nearly 90%) occurs during this stage. At the final stage, all of the pores become isolated and smoother Figure 2.3 (d). Mobility of pores and grain boundaries start to decrease at this stage which results

6

in lower densification rate. As a result, achievement of fully densified, non-porous structure is very difficult because of residual voids containing enclosed gases which cannot diffuse out as a consequence of local equilibrium established between gas pressure and interface surface tension. Application of pressure and temperature simultaneously or sintering in vacuum or liquid phase sintering can help overcome this limitation.
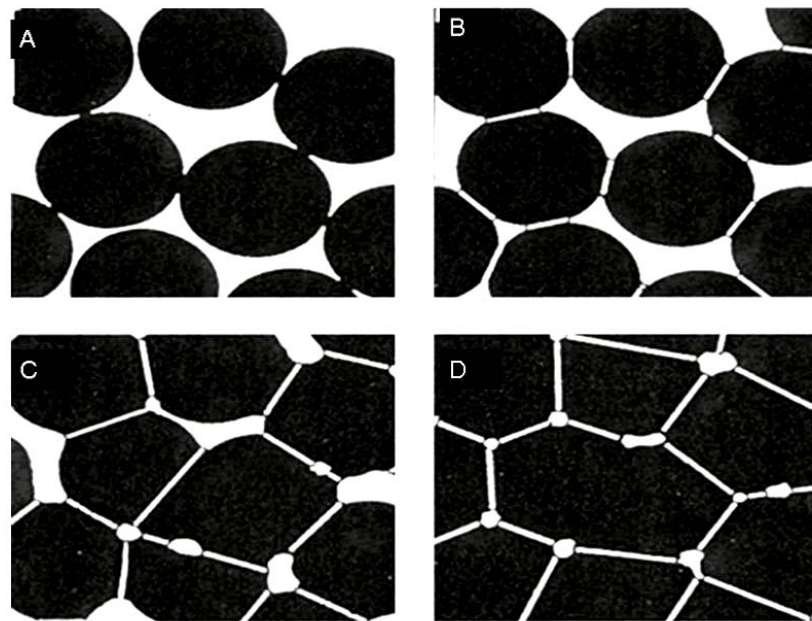
Figure 2.3 Three stages of sintering following (a) bond growth, (b) Initial stage (the pore volume shrinks), (c) Intermediate stage (grain boundaries form at the contacts), (d) Final stage (pores become smoother) [4].

During the final stage, grain growth occurs in addition to pore elimination. Average grain size increases with time yet grain size distribution remarks homogeneous. Total dwell time at high temperatures is an important factor that affects grain growth and grain size distribution. It can cause discontinuous exaggerated grain growth called "abnormal grain growth (AGG)." During abnormal grain growth some grains grow at a higher rate with respect to their

7

neighbors which results in larger grains within a much smaller grain sized matrix. It effects densification due to pores trapped within the larger grains and render full densification almost impossible. Furthermore, abnormally large grains can be detrimental for mechanical properties. Reasons of abnormal grain growth can be listed as higher grain boundary mobility and lower energy of some grains than the surrounding matrix, non-uniform powder packing and inhomogeneous segregation of dopants or impurities on the grain boundaries [2, 3, 5-7].

In order to inhibit abnormal grain growth and enhance densification very small amounts of additives which form transient liquid phase around the matrix particles during sintering is used. Insoluble, homogeneously distributed secons phase additives prevent grain boundary motion by pinning. For example, addition of MgO to Al_2O_3 suppresses grain growth and enhances pore mobility and shrinkage [6, 8]. Another way to overcome AGG is the addition of fine and inert second phase inclusions which can also provide strengthening effect. Second phase particles increase diffusion distances and change interfacial reactions which retard the grain growth of the primary phase. For example, addition of sub-micron SiC particles to Si_3N_4 or Al_2O_3 matrices or ZrO_2 additions to α-Al_2O_3 reduce grain sizes and improve strengths of the materials [7, 8]. In addition to these methods, rapid heating rate could also be a good alternative to obtain fine grain size and higher densification. Samples can pass low temperature regions, where surface diffusion mechanism is more active, by high heating rates, so fine grained microstructure could be brought up to high temperatures where lattice and grain boundary diffusions are predominant [9]. Fast firing, microwave sintering and plasma sintering are some examples to rapid heating methods.

Microwave Sintering Theory

2.2.1 Electromagnetic Radiation and Microwaves

Electromagnetic (EM) radiation is a form of energy generated by accelerating electric charges which are in the wave form at a travelling speed of light. The radiated waves are composed of electric and magnetic fields which oscillate at the right angles to each other and also at the right angles to the propagation direction of the waves. Electromagnetic waves cover a wide range of frequencies in the range of 10^4 to 10^{20} Hz which are classified as radio waves, microwaves, infrared radiation, visible light, ultraviolet radiation, X-rays and gamma rays. Figure 2.4 shows the spectrum of electromagnetic wave. [10, 11]. Microwaves (MWs) are a form of electromagnetic waves with frequencies ranging from 0.3 to 300 GHz and wavelengths ranging from 0.001 to 1 m (Fig. 2.4) [3].
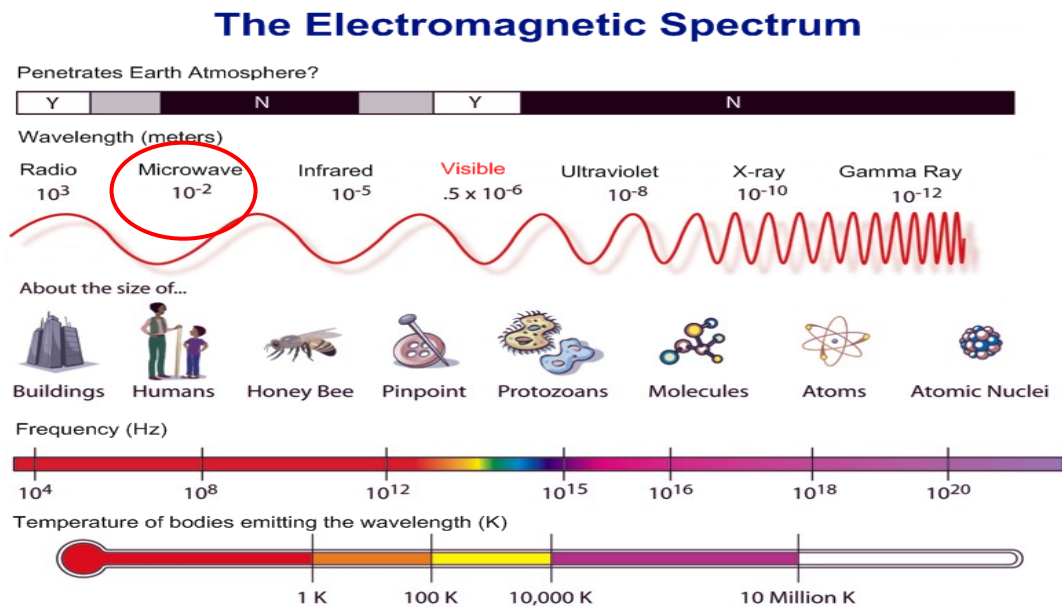
Figure 2.4 Electromagnetic wave spectrum [10].

After the discovery of electromagnetic induction by Faraday in 1831, Maxwell began to work on Faraday's concept and suggested the theory of electromagnetics. Following the study of Maxwell, electromagnetic waves first detected by Hertz using electrical sources [3, 11]. The properties of microwaves like electrical and magnetic field components, amplitude and phase angle as well as the ability to propagate enable the interaction of microwaves with materials and production of heat in some materials [3]. Firstly, discovery of microwaves led to the development of radar concepts during World War II to detect the enemy aircrafts and submarines. After that discovery, application areas of the microwaves started to expand in addition to radar applications. Some of the microwave applications include communication, navigation, radar detection, microwave heating of materials (i.e. drying of food items, sintering of ceramics and metals etc.), power transmission, electronic warfare, medical applications (i.e. MRI) and weather control [10].

2.2.2 Interaction of Materials with Microwaves

Microwave heating is a function of the material being processed. Materials absorb electromagnetic energy and convert it into heat, largely within the sample itself; unlike the conventional heating where there are significant thermal energy losses because of the indirect heating of the materials. Generated heat depends on the interaction of material with the electric and magnetic field components of the microwave. Microwave frequencies couple with internal polarized species and create oscillations of free electrons, ions, molecules, space charges and lattice. Polarization of a material is a consequence of its dielectric constant of material in an electric field, and loss tangent is a measure of absorption of microwaves by the material. The dielectric constant is defined by complex permittivity (ε^*) for dielectric materials, where complex permeability (μ^*) is used for magnetic materials. Following formula defined the complex permittivity:

$$\varepsilon^* = \varepsilon' - i\varepsilon'' = \varepsilon^o (\varepsilon_{r'} - i\varepsilon_{eff''}) \qquad \text{Eq. 2.1}$$

where ε^I is dielectric constant, ε^{II} is dielectric loss factor, ε^o is permittivity of free space, ε_{r^I} is relative dielectric constant, $\varepsilon_{eff^{II}}$ is effective relative dielectric loss factor, and i= $\sqrt{-1}$. Loss tangent is defined by the formula of

$$\tan\delta = \frac{\varepsilon_{eff^{II}}}{\varepsilon_{r^I}} = \frac{\sigma}{2\pi f \varepsilon^o \varepsilon^I} \qquad \text{Eq. 2.2}$$

where it represents the losses arising from all possible mechanisms for a certain frequency, f, of incident wave in GHz, and conductivity, σ, of the material. The average absorbed energy can be calculated by using

$$P = \pi E_0^2 f \varepsilon^0 \varepsilon^{"} = \pi E_0^2 f \varepsilon^0 \varepsilon^I \tan\delta \qquad \text{Eq. 2.3}$$

where P is the average power dissipated per unit volume and E_0 is the amplitude of the electric field [3, 12].

The dielectric constant and loss tangents of the materials are functions of temperature which means that the degree of interaction between microwaves and especially ceramics changes with temperature. Most of structural ceramics reveal dielectric loss mechanism in microwave field, such as Al_2O_3, ZrO_2 and Si_3N_4. They have low absorption ability at lower temperature and an increased absorption at higher temperatures. Figures 2.5 and 2.6 shows the changes of loss tangents and dielectric loss factors of several ceramics with temperature [3]. Change in tangent loss of SiC and ZrO_2 with temperature has been implemented to Fig. 2.5 schematically combining various data given in literature [13] due to lack of accurate quantitative data comparing the tangent loss of SiC with those of the others.
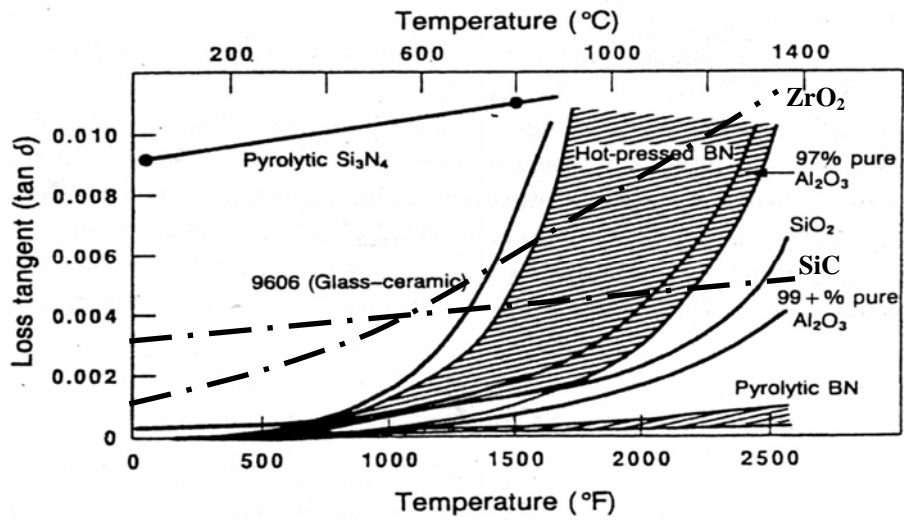
Figure 2.5 Dielectric loss tangent change with temperature (for the frequencies between 8-10 GHz) for some ceramic materials [3, 13].
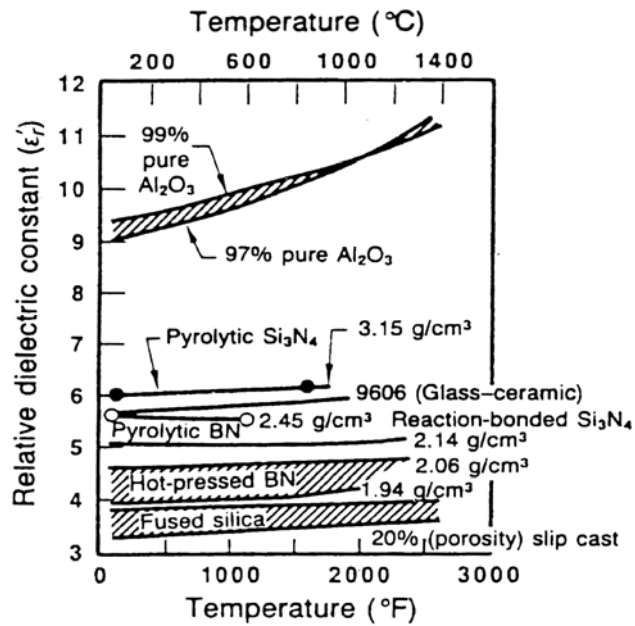
Figure 2. 6 Change of dielectric constant as a function of temperature (for the frequencies between of 8-10 GHz) for some ceramic materials [3].

Depending on the electrical and magnetic properties, materials can be divided into three categories in terms of their interaction with microwaves. Materials with low loss tangents are transparent to microwaves and absorbance of microwaves is very low. At room temperature Al_2O_3, MgO and SiO_2 are transparent to microwaves; however, after a certain critical temperature they start to couple with microwaves [3]. Extremely high loss materials, which are considered to be opaque to microwaves, such as metals, have a thin skin depth and they reflect microwaves. Materials which have intermediate loss tangent values at room temperatures absorb microwaves more efficiently and coupling starts at room temperature. In addition to those materials incorporation of second phase microwave absorbing particles to low loss ceramics can alter the absorption of microwaves (Fig. 2.7) [3, 12].
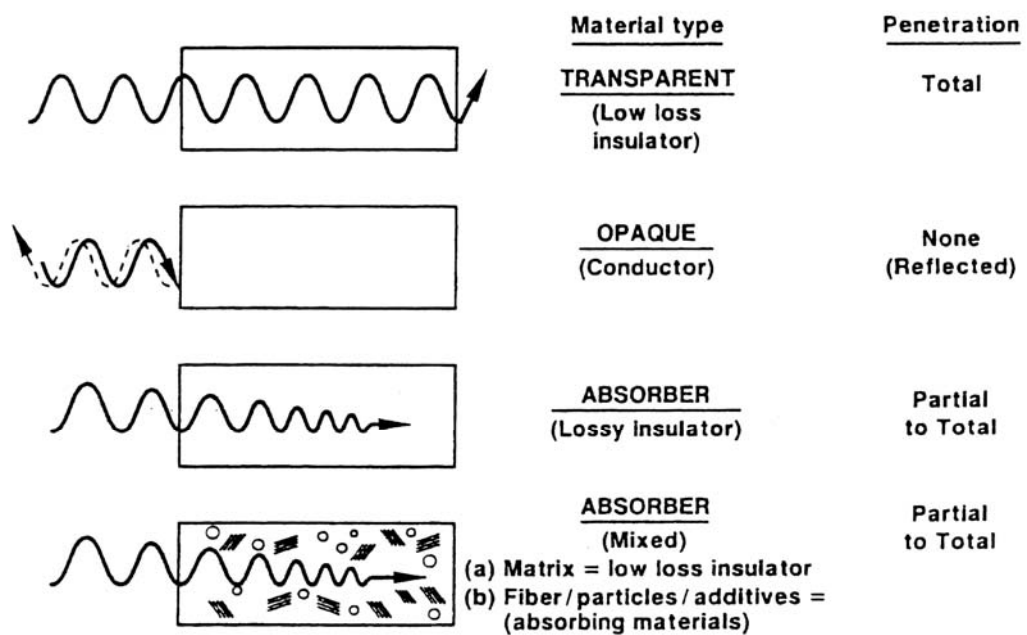
Figure 2.7 Schematic diagram illustrating the interaction of MWs with materials [3].

13

Skin depth, SD, is an important parameter which is the propagation depth of microwaves through the material and defined by

$$SD = \frac{1}{\sqrt{\pi f \mu \sigma}} = \frac{c}{\sqrt{2}\pi f \sqrt{\varepsilon'} \tan \delta} .$$ Eq. 2.4

where, f is frequency, μ is magnetic permittivity, and σ is conductivity. According to this formula, frequency of the microwave and the tangent loss of the material is inversely proportional to its skin depth [3, 12]

2.1.3 Comparison of Conventional and Microwave Sintering

Fundamentally, microwave heating of the materials differs from conventional heating methods. In conventional furnace heating, heat is generated by an external source (i.e. resistive heating element) and transferred to the material by thermal electromagnetic radiation. Maximum intensity, I, of this radiation, which is in the infrared range, is very small ($I<<10^{-4}$) for the majority of solid materials. Consequently, energy is localized within a thin layer near the surface of the material leading to thermal energy transfer from hotter near surface to the colder inner region. Therefore core temperature is lower than the outside of the material [Yu V bykov, high temp microw processing of mtls]. Figure 2.8 shows the heat distribution during conventional heating process.
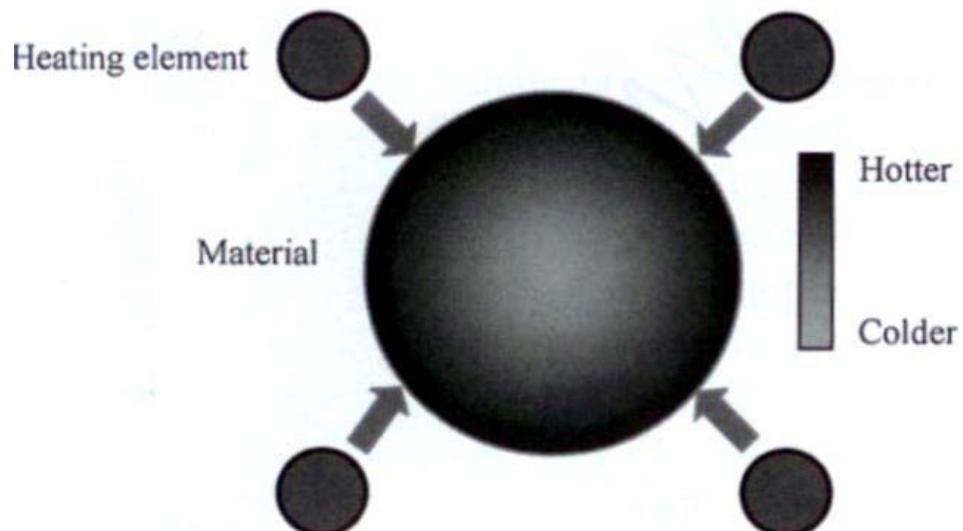
Figure 2.8 Heat distribution within a material during conventional heating process [10].

Contrary to the conventional sintering heating is generated within the material during microwave processing due to the penetration of microwaves into the material. However, in microwave sintering heat is generated at the core and radiates towards the colder outer zone of the material, and thus, heat losses occur from the surface of the material. Therefore, core of the material is generally hotter than the surface of the material (Fig. 2.9).
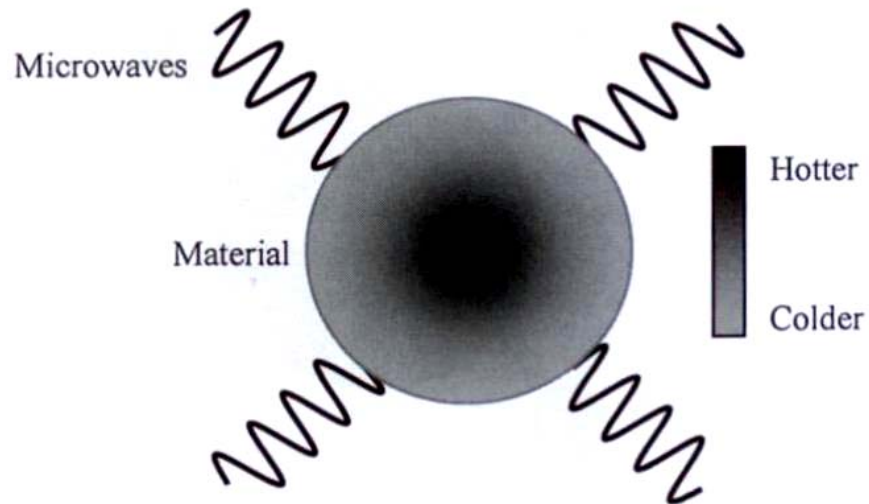
Figure 2.9 Heat distribution within a material during microwave heating process [10].

Hybrid heating method is an optimum solution for heating low loss materials and inhibits temperature gradients within the material during microwave sintering process. By placing susceptors (high loss materials at room temperature) around the sintered component uniform heating is achieved during microwave sintering. By this method, heat evolves from both inside to outside and outside to inside of the material being sintered. Hybrid heating is also provides advantageous for heating of low loss materials by microwaves. Using susceptors makes it possible to microwave sinter materials like Al_2O_3 and MgO which are transparent to microwaves at room temperature. Susceptors are used to heat them to temperatures where these materials start to couple with microwaves. Figure 2.10 illustrates the hybrid heating mechanism schematically [10].
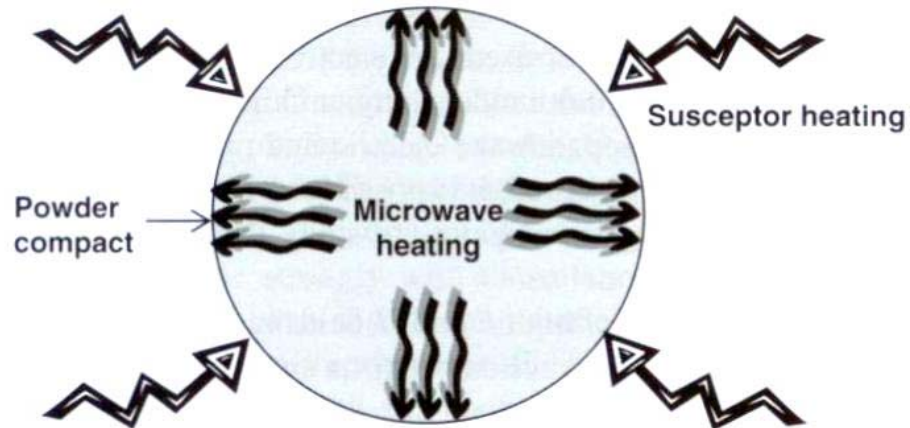
Figure 2.10 Schematic of heating directions during hybrid heating using microwa
ves [10].

In general, advantageous of the microwave sintering over conventional methods can be listed as;

❑ Time and energy saving.

❑ Rapid heating rates (>400ºC/min).

❑ Considerably reduced processing time and temperature.

❑ Fine microstructures, and hence, improved mechanical properties and product performance.

❑ Unlike conventional heating, a volumetrically distributed heat source due to the penetration of microwaves into materials.

However, there are some difficulties related to microwave sintering such as;

❑ Accurate control of the sintering process and
❑ Uniform heating of complex shapes [14, 15].

2.3 Microwave Sintering of Ceramic Materials

The ability of many ceramics to absorb MW radiation above a critical temperature has led to the use of microwaves for processing of ceramics including drying, clinkering, sintering, melting and joining [16]. At present, microwaves at 915 MHz and 2.45 GHz frequencies are almost universally used for industrial and

scientific applications where interaction of the material and the EM wave results in generation of heat [12]. Reasons for the growing interest in the use of microwave energy in ceramic industry include rapid heating, enhanced densification rate and improvement in final microstructures [15]. Microwave heating of ceramics has also the potential to provide cost savings relative to the conventional heating systems, which is directly related to lower activation energy observed during microwave sintering [17, 18]. Although many potential advantages of utilizing microwaves to process ceramics have long been recognized, there are very limited studies about this particular subject [12]. Alumina [17], zirconia [19], tungsten carbide, PZT ceramics [20], hydroxyapatite [21], ferrites, glass ceramics, uranium oxide [12] are some of the ceramic materials on which microwave sintering studies have been conducted.

2.3.1 Microwave Sintering of Monolithic Alumina

Among the polymorphs of Al_2O_3, which are alpha, eta, gamma, delta, theta and kappa, alpha (α) Al_2O_3 is the most stable phase of alumina at all temperatures and ambient pressure. Theoretically, phase transformation of α-Al_2O_3 (corundum) can be obtained after 78 GPa, however experimental studies showed that no phase transformation occurs up to 175 GPa pressure [22]. Stability of α-Al_2O_3 makes it the most preferred polymorph of Al_2O_3 for many engineering applications. Usefulness of Al_2O_3 comes from its superior set of properties which are high strength, high melting temperature, abrasion resistance, electrical and chemical resistivity as well as optical transparency [2, 22]. These properties put alumina forward among the other common oxide ceramics. Some examples to the conventional usage of monolithic alumina can be summarized as pottery sculpture, sanitary ware, tiles and furnace components. Besides its traditional usage, recent studies have been shown that monolithic alumina can be a good advanced ceramic candidate as catalyst substrates, arc lamps tubes, laser hosts, capacitors, transistors and biomaterials. [22]

To manufacture dense alumina, application of melting techniques is not preferable. This is mainly because of the difficult process control and poor feasibility resulting from high melting point of Al_2O_3 (2054˚C). This method is generally used when manufacturing materials like gem stones and laser hosts where cost is of secondary importance. Other alumina materials are produced by powder processing completed by sintering. In this case typically ceramic powder is first consolidated to the desired shape (green compact), and then firing is performed to densify the material. For Al_2O_3, sintering temperatures are generally higher than 1400˚C. Pressureless sintering, hot-pressing, hot isostatic pressing and plasma spraying are some examples of conventional processing techniques used for the production of alumina ceramics. However, they are usually inefficient in terms of tooling/maintenance cost and time. To overcome this problem usage of *microwave sintering* technique has been suggested as a new method which provides higher densification at relatively lower sintering temperatures and times compared to conventional sintering [17, 18, 23]. Results showed that to achieve comparable densification values conventional sintering has to be conducted at temperatures 200-250˚C higher than those used for microwave sintering which is thought to be the consequence of lowered activation energy of microwave sintering compared to conventional sintering which are 85-160 kJ/mole and 520-575 kJ/mole, respectively [17, 18]. This leads to the accelerated diffusion of O^{2-} in the structure during sintering, and hence enhanced densification [17, 18]. Microwave sintering can also provide finer microstructures as a consequence of rapid heating and sintering. Microwave sintering activates grain boundary as well as lattice diffusion at the early stages of sintering where surface diffusion mechanism is predominant in conventional sintering which causes rapid grain growth. Contrarily, during microwave sintering, material can pass through the early stages more rapidly, and thus small grain sizes can be sustained at higher temperature regimes. With the help of the MgO addition and fast firing ultrafine microstructured Al_2O_3 were obtained by microwave sintering [24]. On the other hand, recent studies have showen that grain growth is not necessarily dependent on heating rate. Grain growth paths seemed to be similar for conventional and microwave methods for identical densification values [17, 18].

Studies have demonstrated that microwave heating is an effective method to produce fully densified monolithic Al_2O_3 at relatively lower temperatures compared to conventional sintering, which provides energy and cost savings. Following this observation, some studies have particularly focused on the commercialization potential of microwave sintering method. Cheng et al. built a continuous microwave sintering set-up for the production of large batch (up to 10 kg) alumina abrasive grits. Results showed that to obtain fully densified products by a continuous process sintering time and temperature should be controlled quite sensitively. Besides the densification data, results showed that hardness and abrasion index of the grits were superior than those of conventional sintered products.

As mentioned earlier, Al_2O_3 can be optically transparent material when in single crystalline form (sapphire) or in highly pure and fine grained polycrystalline form. Although production of transparent Al_2O_3 is available by powder methods, it is rather challenging because of extremely high temperatures (up to 1900˚C), long soaking intervals (several hours) and high vacuum or pure hydrogen atmosphere required. Usage of microwaves gave rise to production of transparent Al_2O_3 with rapid and uniform heating at lower sintering temperatures (1750˚C) in shorter soaking times (15 min) providing finer microstructures [25].

In conclusion, microwave sintering method is advantageous for the production of fully densified monolithic Al_2O_3 ceramics. While it provides advantages on structural properties such as strength and abrasion resistance, other physical properties such as some optical transparency can be achieved via microwave processing. However, a well accepted explanation on the effective sintering mechanisms during microwave sinteringis still not available. Lowered activation energy, and hence increased diffisuvity of O^{2-} seems to be the most important factor in achieving enhanced densification at relatively milder sintering conditions.

2.4 Ceramic Nanocomposites

Despite their advantageous properties, brittleness of ceramic materials is the main drawback of the ceramic materials. To toughen the structural monolithic ceramics, composites have being used for many years. Especially for over a few decades incorporating particulates, fibers or whiskers to ceramic bodies have been studied by many researchers.

Nanocomposites are a newly developed concept to promote the mechanical properties of ceramics by dispersing second phase nano-particles into the matrix grains and on the grain boundaries [26]. Addition of second phase particles improves the fracture toughness, flexural strength [27], creep resistance [28], the wear resistance [29, 30] and hardness [31].

2.4.1 Alumina-SiC Nanocomposites

Silicon carbide (SiC) is an important second phase candidate to improve the mechanical properties of Al_2O_3 ceramics [2, 26, 27]. Dispersion of submicron-sized SiC particles into Al_2O_3 matrices, and hence forming nanocomposites is a developing concept which results in improved mechanical properties such as fracture toughness [32], creep resistance [33], hardness [34] and wear resistance [31]. Addition of second phase submicron sized SiC particles to ceramic materials have been first investigated by Niihara and co-workers in the 1991 which involve Si_3N_4/SiC and Al_2O_3/SiC composite systems. Niihara's study showed that even 5 vol% SiC addition to monolithic alumina (Al_2O_3) increases the strength from 380 MPa to 1 GPa and fracture toughness from 3.25 to 4.70 MPa·m$^{1/2}$ [35]. Following this initial work, various studies have been done to understand the effects of the SiC content (1, 2, 5, 10, 15, 20 wt% SiC), the particle size changes of SiC and/or Al_2O_3 from sub-micron to nanoscale to understand the toughening of monolithic Al_2O_3. The main mechanisms effective on the achieved fracture toughness enhancement, are: (1) fracture mode change from intergranular for monolithic Al_2O_3 to transgranular type for Al_2O_3/SiC nanocomposites, which increases with

SiC content [29-31, 36-39], (2) Zener pinning effect which reduces grain growth [40, 41], (3) crack impediment by intragranular particles [29], (4) weakening of the matrix with decreasing SiC grain size promoting transgranular type fracures [36]. In addition to these, thermal expansion mismatch between Al_2O_3 and SiC increases fracture toughness, hardness and flexural strength as a consequence of residual compressive stresses in the matrix [27].

Grain size of the dispersed SiC particles could be an important factor which affects mechanical properties significantly. Many studies have shown that smaller SiC particles located within the grains and larger particles dispersed on the grain boundaries lead to the reduction in the grain size of the matrix. However, there is a conflict between the results achieved by different groups. There are contradictory results about particle size of SiC. Some researches suggest that it should be in the sub-micron range to lower both grain size and the critical flaw size of the matrix to obtain toughness increment [38]. However, some researches show that decreasing SiC particle size optimizes the weakening effect on the matrix, and hence increases fracture toughness [36]. On the other hand, some of the studies did not reveal any dramatic effect of grain size reduction or SiC amount on the mechanical properties of Al_2O_3 [37].

Some of the studies on the mechanical properties showed that rather than SiC addition machining (grinding) induced surface residual stress and strength recovery behaviors in nanocomposites generate the enhancement of fracture toughness. According to these results, surface grinding increases the strength of Al_2O_3/SiC nanocomposites and after annealing, strength of Al_2O_3 decreases slightly, while strength of the Al_2O_3/SiC nanocomposites shows an enormous improvement as a consequence of residual compressive surface stresses introduced by machining, which can not be completely removed by annealing, and also healing of surface flaws after annealing process [42, 43]. However, full surface recovery of nanocomposites is not possible because of chips which are formed by machining. which did not heal with annealing as a consequence of the reduction in the local fracture stress [44].

Besides their toughening effect, sub-micron sized second phase particle additions have been shown to improve the creep resistance of Al_2O_3 as well [28, 30, 31, 33, 45, 46]. Creep behaviors of Al_2O_3 and nanocomposites are different from each other in the sense that Al_2O_3 reveal accelerated and steady state creep while transient creep prevails in the nanocomposites caused by the rotation and plunging of nanoparticles in the Al_2O_3 matrix during grain boundary sliding. As a result, creep rate of the monolith is higher and creep life is lower than the Al_2O_3/SiC nanocomposites. Also, the pinning of SiC particles on grain boundaries which limits grain boundary sliding increases creep resistance of nanocomposites. Furthermore, the interface of Al_2O_3/Al_2O_3 is weaker than the interface of Al_2O_3/SiC particles. Because, many TEM observations shows that at the Al_2O_3/Al_2O_3 interfaces there is glassy phase and wide atomic disorder in contrast to Al_2O_3/SiC interfaces. And that lowers the creep resistance of monolithic Al_2O_3 [33].

In addition, Al_2O_3 is a good alternative for abrading materials because it is a low cost mass production material compared with the other expensive abrasive materials such as diamond and boron nitride. Wear resistance of monolithic alumina increases with the decreasing grain size of the material. As addition of SiC particles hinder the grain growth and change the fracture mode, resulting substantial reduction in the wear rate of Al_2O_3/SiC nanocomposites compared to the monolithic Al_2O_3 with same grain. Changing the particle size of SiC does not reveal significant advantage on wear. Even though this is the case, use of moderate particle size and high proportion of intergranular SiC particles shows some beneficial effects. Such adjustments provide decrease in wear as well as area fraction of pullouts are resulted from the variations in the dimensions of the individual pullouts, which lead to the change of the fracture mode change from intergranular to transgranular [29, 30]. Wear behavior of monolithic Al_2O_3 depends on grain boundary sliding distance which rises with distance catastrophically. On the contrary, Al_2O_3/SiC nanocomposites show stable wear behavior most probably because of the improved grain boundary strength. With increase in the amount of SiC pitting increases which is the consequence of local

tensile stresses in the matrix resulting from thermal expansion mismatch between Al_2O_3 and SiC [31].

In addition to the mechanical property investigations, many researches have focused on different processing techniques of Al_2O_3/SiC nanocomposites with various motivations such as overcoming the high temperature and high pressure processing requirement [47] and suppressing glassy phase formation or reducing the particle sizes to nanoscale and providing a homogeneous second phase distribution [48, 49], or decreasing the shrinkage rate [50].

Up to date many of the studies mainly pointed out fracture mode change in the nanocomposites where most of the results are conflicting. Recently, there are some studies have focused on converting this fracture mode change to provide superior increase in the fracture toughness. Doping rare earth elements like Nd^{3+}, La^{3+}, Y^{3+} to Al_2O_3/SiC nanocomposites convertes fracture mode from transgranular for undoped composites to intergranular which increases crack deflection and hence results in fracture toughness improvement. The factor that causes fracture mode change is the segregation of rare earth dopants to the grain boundaries leading to weakening of the grain boundaries [39, 51]. To overcome the densification problem of Al_2O_3/SiC nanocomposites addition of Y_2O_3 and/or SiO_2 which form glassy phase on the grain boundaries, have been applied. Addition of Y_2O_3 to monolithic Al_2O_3 which had a positive influence on densification especially at 1550°C; however increasing the temperature to 1650°C causes increase in intragranular porosity resulting in of abnormal grain growth. Contrary to Y_2O_3, SiO_2 addition alone decreases densification because it causes excessive grain growth leading to isolated porosity within the grains of Al_2O_3. In case of Al_2O_3/SiC nanocomposite production, Si segregates on the grain boundaries of Al_2O_3 and thus hindering densification. Contrarily, although Y_2O_3 addition delay onset of the sintering, final densification enhanced despite of inhibition of sintering by SiC particles. Due to glassy phase formation between SiO_2, Al_2O_3 and Y_2O_3 final density of the added nanocomposites containing both Y_2O_3 and SiO_2 increased resulting in fracture toughness enhancement [52].

As a conclusion, SiC addition to Al_2O_3 ceramics provides some advantages on strength, fracture toughness, wear resistance and creep resistance when compared with monolithic Al_2O_3 of the equivalent grain size. So far there is no clear explanation available on strengthening mechanisms. However, fracture mode transition from intergranular to transgranular, crack tip bridging by the dispersed particles, healing of the cracks after machining and annealing as well as Zener pinning effect seem to be the main factors in the improvement of fracture toughness along with wear and creep resistances.

2.4.2 Alumina-Yttria Stabilized Zirconia Nanocomposites

Addition of second phase particles to oxide ceramics such as Y_2O_3 doped zirconia improves their fracture toughness [53, 54]. Zirconia has three crystallographic forms, from high to low temperatures: monoclinic, tetragonal and cubic phases. Transformation of tetragonal to monoclinic phase is at 1170°C, however, doping of CaO, MgO or Y_2O_3 suppresses this transformation temperature, thus at room temperature, stabilized zirconia with cubic and tetragonal structure could be obtained. Additionally, partially stabilized tetragonal zirconia could transform into monoclinic structure under stress which is accompanied by a volume expansion of 4 % [2, 55].

Partially stabilized zirconia doped alumina have higher fracture toughness and required stress to induce crack propagation compared to monolithic alumina utilizing this volume expansion of partially stabilized zirconia [55]. So, there is a trend to develop mechanically reliable ceramics for biomedical applications in addition to the high temperature applications [56, 57]. In recent years, there is a considerable increase in interest over alumina/zirconia nanocomposite materials with their improved mechanical properties [1]. Tuan W. H. et al. also showed that the addition of a small amount of ZrO_2 nanoparticles to Al_2O_3 reduced the grain size of Al_2O_3 matrix grains and this enhanced the strength of Al_2O_3 [58].

2.5 Aim of the Study

To investigate the efficiency of microwave sintering of ceramic materials in comparison to conventional processing under identical conditions. Monolithic alumina with or without sintering additives such as MgO, CaO, Y_2O_3 as well as nanometer-sized SiC or stabilized ZrO_2 particle-dispersed alumina matrix ceramic nanocomposites will be fabricated by both conventional and microwave sintering. Sintered ceramic materials will be characterized in terms of their densification, phase content, microstructural evolution and mechanical properties such as hardness and indentation fracture toughness.

CHAPTER 3

EXPERIMENTAL PROCEDURE

In the following section, detailed information about used raw materials, applied processing methods and characterization of microstructural and mechanical properties are presented.

3.1 Sample Preparation

3.1.1 Sample Preparation for Monolithic Alumina Samples

3.1.1.1 Powder Preparation Stage

To understand the effect of microwave heating on the sintering of ceramics, preliminary studies were conducted on monolithic Al_2O_3. In all of the experiments only one type of Al_2O_3 powder [α-Al_2O_3 (99.95%, Alfa Aeser GmbH & Co KG, Karlsruhe, Germany) with a mean particle size of 0.4 μm was used.

A comparison was made between conventional sintering and microwave sintering at different sintering temperatures for constant duration. In addition to the production of plain Al_2O_3 different sintering aids were added (MgO, Y_2O_3, CaO) with the weight percentage of 0.1 to enhance densification of Al_2O_3.

To distribute sintering additives homogeneously and to achieve coverage on the alumina powders which will create a thin glassy phase between Al_2O_3 grains for enhanced sintering, additives were added to Al_2O_3 in the liquid form. Solid sintering additives (MgO, CaO) were converted to aqueous solutions in the nitrate

form. To make aqueous solutions, sufficient amount of nitric acid was added to the MgO and CaO powders until a clear liquid solution was obtained. 1 cm^3 of obtained solutions was containing 25 mg sintering additive. Following formulas show the formation of nitrates.

$$MgO + 2HNO_3 \Rightarrow Mg(NO_3)_2 + H_2O \qquad \text{Eq. 3.1}$$

$$CaO + 2HNO_3 \Rightarrow Ca(NO_3)_2 + H_2O \qquad \text{Eq. 3.2}$$
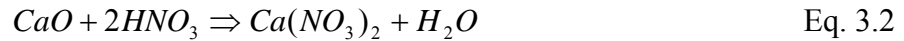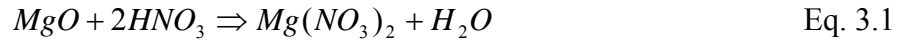
Another sintering additive was Y_2O_3 which was already in the crystal form of $Y(NO_3)_3.6H_2O$. To convert it to liquid form it was dissolved in the deionized water to obtain 25mg Y_2O_3/cm^3 of concentration.

Before the compaction stage, Al_2O_3 powder and aqueous solutions were mixed within a mortar in isopropyl alcohol medium. Following mixing, to remove NO_3 from the mixture, it was first heated to 100˚C to evaporate excess water and alcohol, then the temperature was raised to 600˚C with a heating rate of 4˚C /min and dwelled for 2 hours at that temperature. Obtained powders were then crushed in the mortar to eliminate agglomerates.

3.1.1.2 Powder Compaction Stage

To obtain disc-like compacts approximately 15 mm in diameter and 4 mm in thickness, uniaxial pressing method was applied using cold work tool steel dies with 15 mm inner diameter. Applied pressure was 60 MPa which is high enough to reach maximum achievable green density for the powder used and to produce pellets resistant to handling. Figure 3.1 shows the schematic of the steel die used for uniaxial compaction.
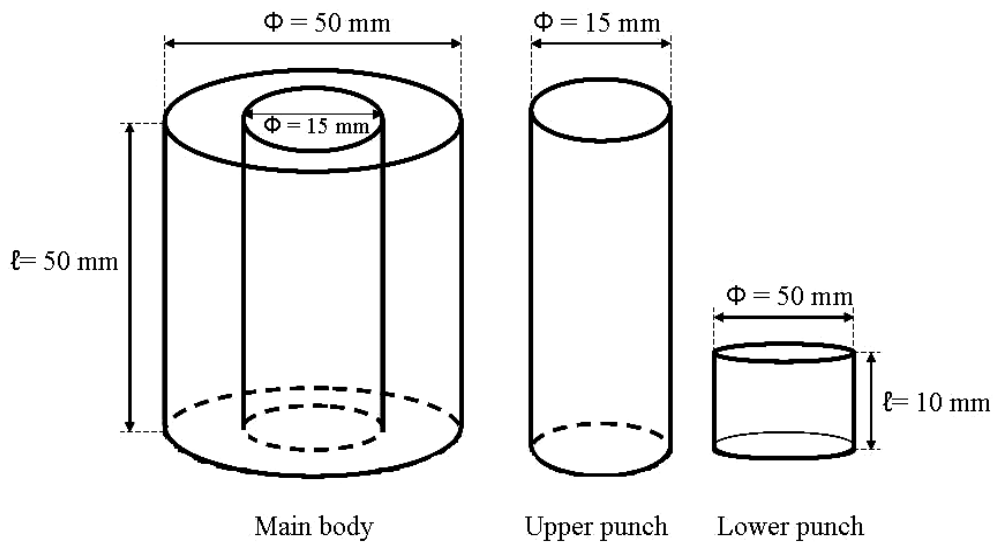
Figure 3.1 Schematic of the uniaxial compaction die made from cold work tool steel.

3.1.1.3 Sintering Stage

To compare the effectiveness of microwave and conventional sintering processes on the densification, monolithic Al_2O_3 samples were sintered at seven different temperatures of 1000, 1100, 1200, 1300, 1400, 1450, 1500, 1550 and 1600°C for 1 h using both methods. Conventional sintering experiments were conducted using a home-built muffle furnace capable of 1800°C of maximum operating temperature with its $MoSi_2$ heating elements.

Microwave sintering was conducted using a commercial 4.8 kW microwave sintering furnace (MKH-4.8, Linn High Therm GmbH, Eschenfelden, Germany) which has six magnetrons with 800 W maximum power each. Furthermore, output power of the magnetrons is adjustable from 15% to 100% of maximum level. Frequency of the electromagnetic waves produced by the magnetrons is 2.45 GHz +/- 0.05 GHz. Dimensions of the effective heating chamber are 135x135x135 mm. Temperature measurement was done from surfaces of the samples during sintering with an infrared pyrometer (Impac 140, LumaSense Technologies GmbH, Frankurt, Germany) which is located at the top of the furnace. In addition,

microwave furnace is capable of providing protective gas atmosphere (Argon, nitrogen or helium) as well as vacuum. Figure 3.2 shows the microwave furnace in this study which is located at the Electromagnetic Materials Laboratory of the Metallurgical and Materials Engineering Department of Middle East Technical University.
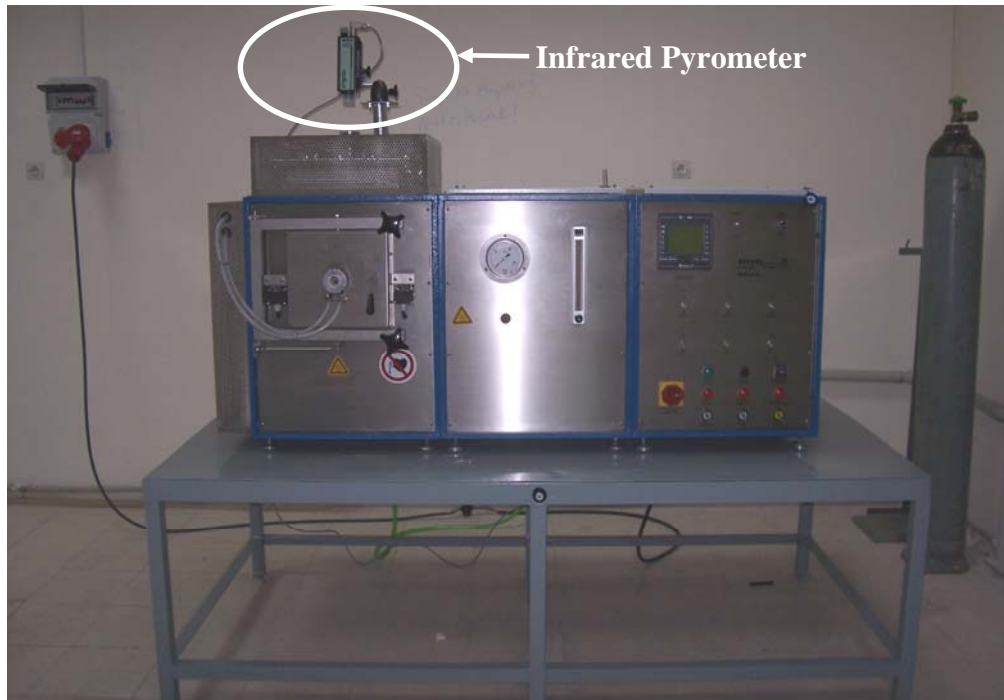
Figure 3.2 High temperature microwave sintering furnace.

An "insulation cage" (Fig. 3.3) built of high purity alumina insulation boards (Type: SALI-2, Zircar Ceramics, Inc., FL, USA) was designed and adapted to the heating chamber of the microwave sintering furnace (Fig. 3.4) in order to minimize heat losses from the specimen surface which has provided heating and soaking stability during sintering. SiC powder was used as the susceptor material which has provided initial heating until the alumina-based ceramics start to couple with the microwaves and generate heat by themselves. The samples were placed

in a high purity alumina crucible which was then placed to the center of a bigger high purity alumina crucible filled with the susceptor powder.
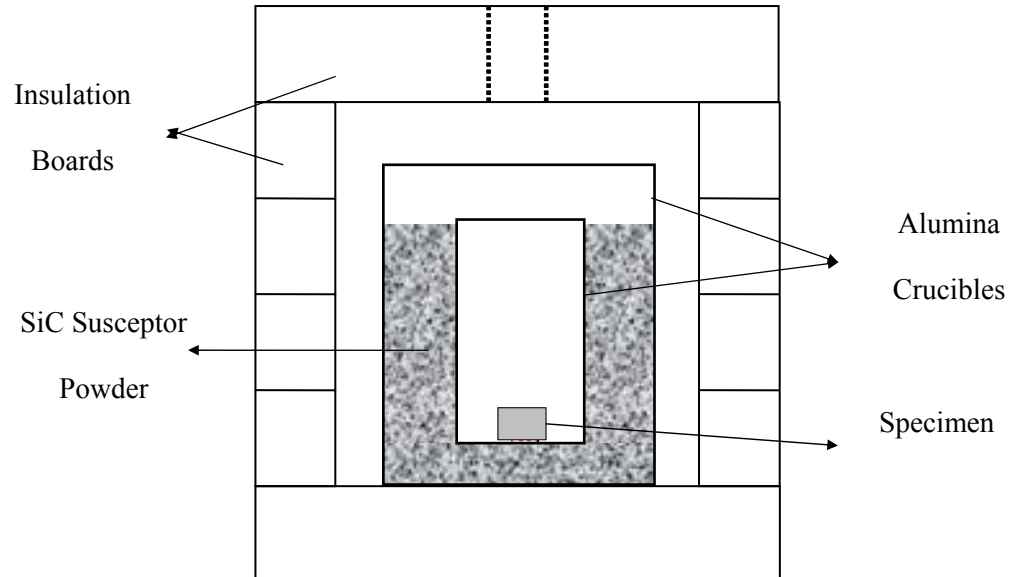
Figure 3.3 Home-built "insulation cage" composed of high purity alumina insulation boards and alumina crucibles providing holding cavity for the specimens and the SiC susceptor powder.

Figure 3.4 Picture of home-built "insulation cage" placed within the heating chamber of the microwave sintering furnace.

3.1.2 Production Al$_2$O$_3$/SiC and Al$_2$O$_3$/ZrO$_2$ Nanocomposites

3.1.2.1 Powder Preparation Stage

To compare densification and mechanical properties of the Al$_2$O$_3$-based nanocomposites formerly mentioned α-Al$_2$O$_3$ powder was used. As the second phase dispersion β-SiC powder (Alfa Aeser GmbH & Co KG) with an average particle size of 100 nm or yttria stabilized (3 and 8 mol% Y$_2$O$_3$) ZrO$_2$ powders (MSE Engineering, İstanbul, Turkey) with D$_{50}$ less than 0.5 μm were used as starting materials in this study.

Five different dispersant contents were selected to determine the optimum second phase content resulting in improvement in mechanical properties. 1, 5, 10, 15 and 20 wt% SiC or ZrO$_2$ particles were added to Al$_2$O$_3$ starting powder, and the mixtures were ball-milled for 16 hours in isopropyl alcohol using 10 and 1.5 mm

diameter yttria stabilized zirconia balls as the grinding medium. The mixture was then dried at 50°C in a drying oven for 4 hours. Dried lumps were crushed in the mortar and to inhibit agglomeration mixture was sieved using 140 mesh sieve.

3.1.2.2 Powder Compaction

For nanocomposites a different pressing method was applied compared to that used for monolithic Al_2O_3. Incorporation of the second phase particles decreased compaction efficiency, and hence achieved green and final densities. To overcome this problem compaction pressure had to be increased. However, during uniaxial compaction friction occurring between the walls of the die and the powders leads to stress formation and thus less uniform compaction and reduced green density. For this reason, increasing uniaxial compaction pressure is not a good solution to enhance compaction efficiency of nanocomposites [47]. To overcome this problem and obtain better compaction cold isostatic pressing has additionally been applied to uniaxially pressed green compacts.

In this set of materials, initially samples were uniaxially pressed at 30 MPa to obtain disk-shaped pellets approximately 15 mm in diameter and 4 mm in thickness following this green compacts were cold isostatically pressed (CIPed) at 150 MPa pressure to enhance densification and to provide homogeneous packing of the powders. Figure 3.5 shows the picture of home-built and custom-designed cold isostatic press in Electromagnetic Materials Laboratory of the Metallurgical and Materials Engineering Department of Middle East Technical University.

Figure 3.5 The pictures of home-designed and custom-built Cold Isostatic Press

3.1.2.3 Sintering Stage

Nanocomposites were sintered at 1300˚C and 1500˚C for 1 h under argon atmosphere, which were chosen as the most suitable conditions for the comparison of the efficiencies of microwave and conventional sintering methods. Schematic of heating and cooling cycles for conventional and microwave sintering is provided in Fig. 3.6 and Fig. 3.7, respectively.
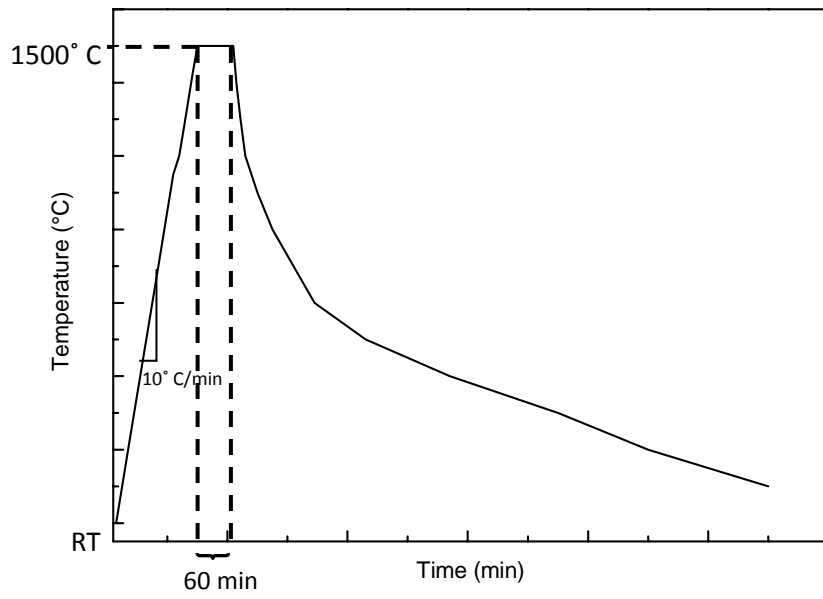
Figure 3.6 Heating and cooling cycle of conventional sintering process.
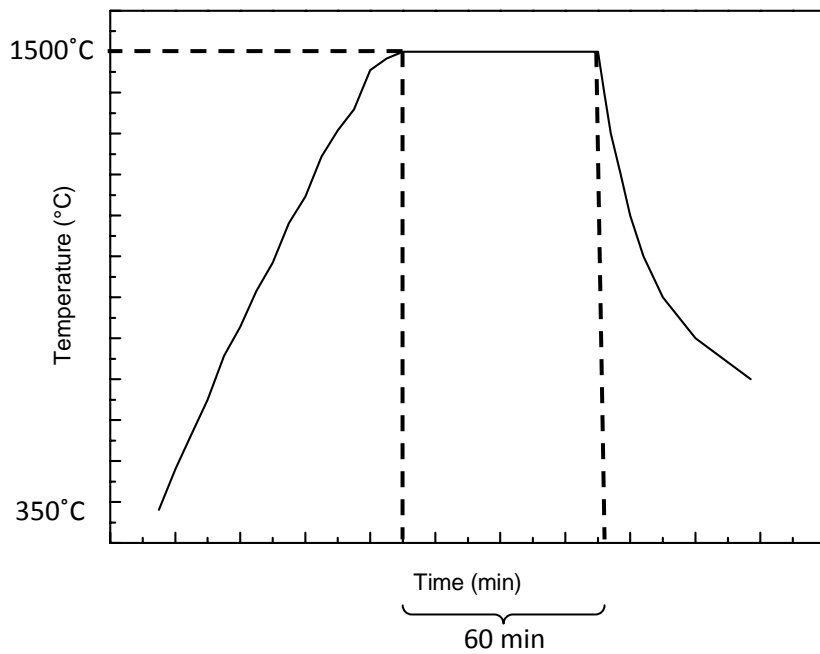
Figure 3.7 Heating and cooling cycle of microwave sintering process.

3.2 Materials Characterization

3.2.1 Density Measurements

Following the production stages, densities of all samples were measured using Archimedes' method in xylene as immersion medium to determine the densification of the samples with respect to their theoretical densities.

Theoretical density calculations were done according to rule of mixtures using the equation;

$$\rho_{theoretical} = \sum \omega_i \cdot \rho_i \qquad \text{Eq. 3.3}$$

where ω_i is the weight percent of the constituent and ρ_i is the theoretical density of the constituent in the mixture .

To calculate the densities of the samples after sintering Archimedes' method were used which has a formula of

$$\rho = \frac{\rho_{xylene} * W_{dry}}{W_{sat.} - W_{susp.}} \qquad \text{Eq.3.4}$$

where W_{dry} is the dry weight, W_{sat} is the saturated weight after keep the samples at 24 h in xylene and W_{susp} is the suspended weight of the sample. Density of the xylene is 0.86 g/cm^3. The inaccuracy during the density measurements was ca. 1% due to equipmental limitation.

3.2.2 Phase Analysis

Phase analysis was conducted by X-Ray Diffraction (XRD) method using a standart X-ray diffractometer (RINT 2200, Rigaku Co., Tokyo, Japan) using Cu_K$_\alpha$ radiation between 10 – 90° of 2θ values with 2°/min scan rate.

3.2.3 Surface Preparation

Following density measurement, surface preparation was performed on the sintered ceramics by using standard metallographic methods. The samples were ground in order to remove the surface roughness. After grinding, the surfaces of the samples were polished up to 0.25 µm surface finish by diamond slurry. Table gives brief information about the sample preparation steps.

Table 3. 1 Details of the grinding and polishing operations

	Grinding Operations		Polishing Operations			
	15 µm	9 µm	6 µm	3 µm	1 µm	0.25 µm
Wheel speed (rpm)	~300	~300	~150	~150	~150	~150
Duration (min)	120	300	300	360	360	360

3.2.4 Microstructural Characterization

Changes in the physical and chemical characteristics of the samples with the applied processing parameters may result in alterations in the densities, microstructures and mechanical characteristics of the components. To determine these alterations, microstructural observations were conducted on selected samples by scanning electron microscopy.

For the microstructural characterization sintered ceramics and nanocomposites were thermally etched for 15 min in air at a temperature 100˚C lower than the applied sintering temperature to reveal the grain boundaries. Thermally etched surfaces as well as fracture surfaces of the sintered ceramic and nanocomposite materials were observed using a field emission type scanning electron microscope (FE-SEM, Nova NanoSEM 430, FEI, Eindhoven, Netherlands). Fractured surfaces of nanocomposites and monolithic Al_2O_3 were studied observing fracture modes of the samples.

3.2.5 Mechanical Characterization

3.2.5.1 Hardness Measurement

Effect of ceramic particle (SiC and ZrO_2) addition on the mechanical characteristics of Al_2O_3 was studied applying hardness and indentation fracture toughness measurements. For both of the measurements Vickers indenter was employed. Hardness measurements were conducted using a microhardness tester (Shimadzu HMV 2 E, Shimadzu, Kyoto, Japan) with 1 N of maximum applied load and 10 s dwelling time. Hardness values, H_v, were calculated from the mean of the two diagonal lengths, a, of the residual impressions on the specimen surface using;

$$H_v = \frac{1.854\,P}{a^2}$$ Eq. 3.5

according to ASTM 1327-08 where P is the applied load.

3.2.5.2 Fracture Toughness Measurement

To determine the fracture toughness values of manufactured ceramics indentation fracture toughness, K_c, method was used. Vickers indentation was applied onto polished surfaces of the ceramics which created radial cracks emanating from the corners of the residual impressions. Observed crack lenghts are inversely proportional to the toughness of the material, and by measuring these crack lengths, fracture toughness can be estimated. Under small indentation loads small Palmqvist cracks (a<c) form which create residual tensile stress areas only around of the cracks (Fig. 3.9.a). If the c/a ratio is less than 3.5, Palmqvist crack model can be used to calculate K_c according to [59]

$$K_c = 0.018 \cdot H \cdot a^{1/2} \cdot \left(\frac{E}{H}\right)^{0.4} \left(\frac{a}{c}-1\right)^{-1/2}$$ Eq. 3.6

38

where c is the half length of the radial cracks, E is the Young's modulus of the specimen. E values of the specimens were calculated considering the remnant residual porosity inside the materials (closed pores) using

$$E = E_o(1 - 1.9p + 0.9p^2)$$ Eq. 3.6

where E_o is the modulus of elasticity of the nonporous material, and p is the porosity volume fraction in the sintered body [60].

However, Palmqvist crack method is not an effective method to calculate K_c for indentation cracks with c/a>3.5 (median cracks), which create residual tensile stress areas around both residual impression and emanating radial cracks as illustrated in Fig. 3.9.b [59]. Considering these limitations, Anstis et al. developed a simplified model for all types of cracks in order to calculate K_c [61];

$$K_C = \alpha \left(\frac{E}{H_V} \right)^{1/2} \left(\frac{P}{c^{3/2}} \right)$$ Eq. 3.8

where α is an indenter geometry dependent empirical constant which is 0.016 for the Vickers indenter. 200 N of indentation load, P, was applied using a standard hardness testing equipment to measure indentation fracture toughness, which has resulted in the best radial crack morphology at the corners of the residual impressions. In addition to this, in the majority of the studies reporting on the mechanical properties of bulk ceramics the model of Anstis is frequently preferred, which renders the results of the current study conveniently comparable with the literature data.
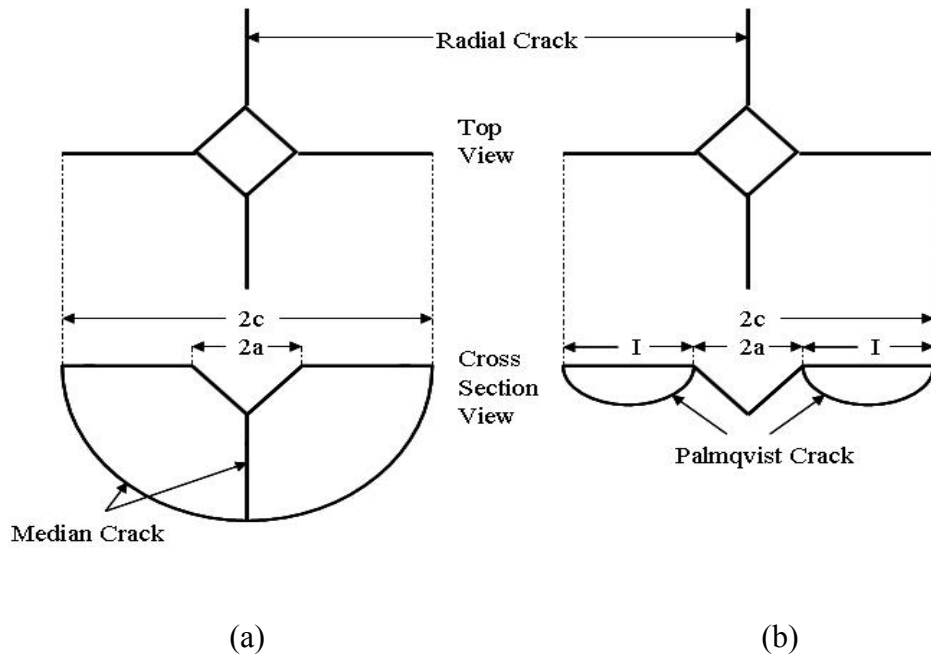
Figure 3.8 Crack formation and crack types by Vickers indentation [59].
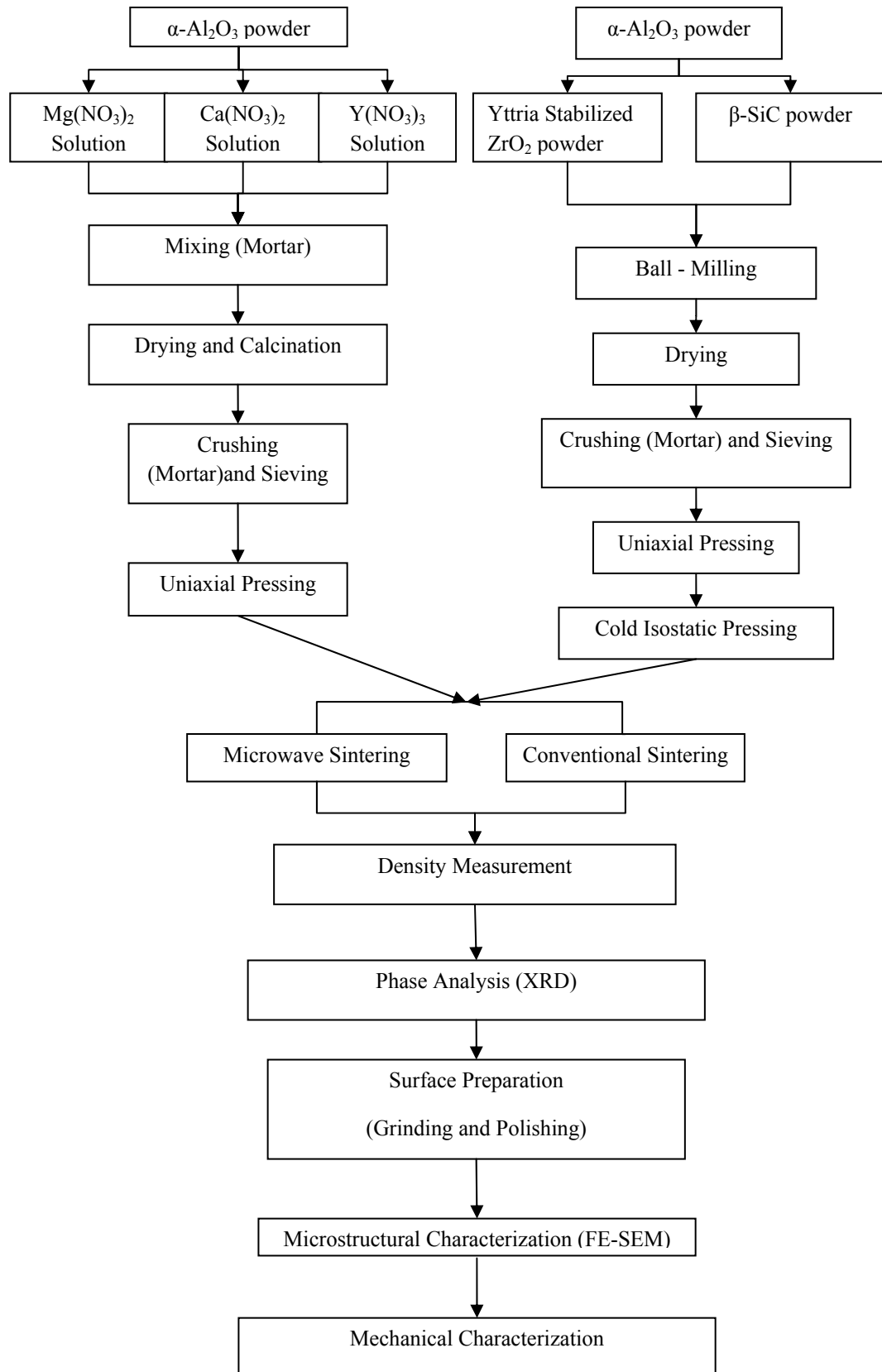
Figure 3.9 Flow chart summarizing the processing and characterization steps followed throughout this study.

41

CHAPTER 4

RESULTS AND DISCUSSION

Following sections include the results of densification, hardness, and indentation toughness measurements along with microstructural characterization of conventional and microwave sintered;

- Monolithic Al_2O_3 with three different kinds of sintering additives,
- Al_2O_3/SiC_p nanocomposites,
- Al_2O_3/YSZ_p nanocomposites.

4.1 Characterization of Monolithic Alumina

At the initial stage, the study has focused on the comparison of the sintering characteristics of monolithic Al_2O_3 fabricated using conventional and microwave sintering techniques. Average green densities of the samples following compaction were approximately 57±1%. Various combinations of sintering temperatures were applied to compare the effectiveness of conventional and microwave sintering on densification, microstructural evolution and mechanical properties of monolithic Al_2O_3. Figure 4.1 shows densification values of sintered monolithic Al_2O_3 relative to its theoretical density as a function of temperature achieved after 1 h of sintering in air by both methods. Theoretical density of α-Al_2O_3 was taken to be 3.98 g/cm^3 [7] throughout this study.
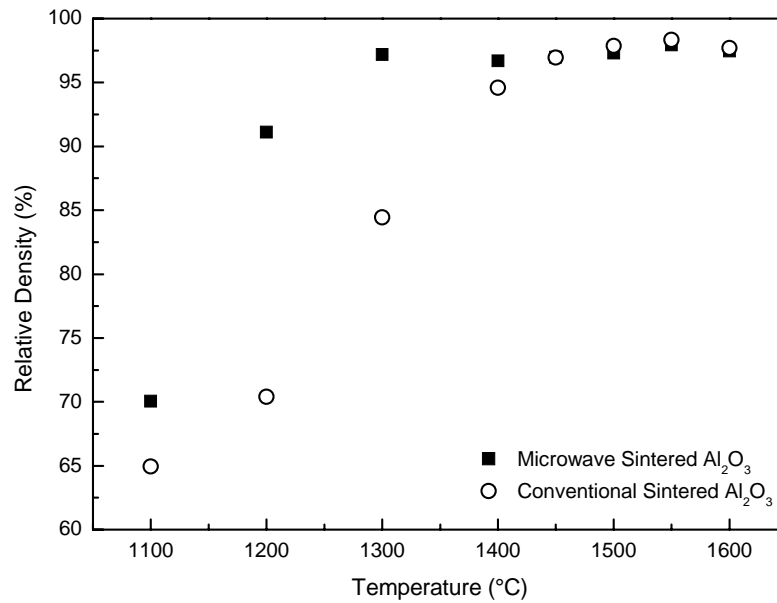
Figure 4.1 Comparison of densification efficiency achieved by microwave and conventional sintering on monolithic Al_2O_3.

It is clear that usage of microwave energy in sintering of Al_2O_3 is more effective on densification than conventional pressureless sintering especially at lower temperatures (<1400°C). Microwave sintering results in more than ~90% and 96% densification at temperatures as low as 1200°C and 1300°C, respectively, where conventionally sintered densities at these temperatures are ~15-20% lower. Slight deviations from the increasing trend line of densification achieved by microwave sintering results from the fluctuation of soaking temperature at values ≥1400°C. This effect is mainly caused by the difficulty in stabilizing temperature at elevated levels due to the higher temperature gradient from the hot specimen to the essentially colder furnace chamber. Despite this inaccuracy, which is in the uncertainity margin of the applied density measurements, obtained densification results seem to be consistent with the ones reported in the literature where almost full densification has been achieved at 1400°C for soaking periods ranging from zero and 30 min [18, 23].

As a baseline for comparison, SEM images of conventionally sintered and microwave sintered monolithic Al_2O_3 were taken. Thermally etched surfaces of the samples sintered at 1200, 1300, 1400, 1500 and 1600˚C are shown in Figure 4.2 (a)-(j). Microwave sintered ceramics seem to have a higher average grain size, compared to their counterparts conventionally sintered at identical temperatures, which is consistent with their higher densities. The reason may be attributed to the fact that microwave processing lowers the activation energy, and hence increases the diffusion coefficients, especially that of O^{2-}, which causes grain growth acceleration [17, 18]. This activation energy difference provides advantages predominantly for temperatures lower than 1400˚C where the microwave sintered ceramics reach to almost full densification. However, at elevated temperatures, 1500˚C≤, abnormal grain growth occurred during microwave sintering as a result of which closed pores started to remain within the grains which renders full densification almost impossible (Figure 4.2.j).
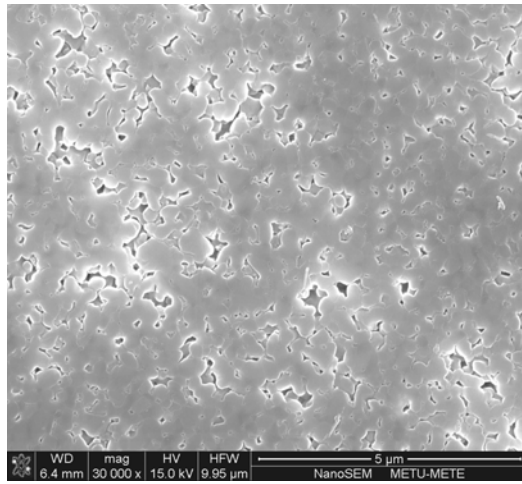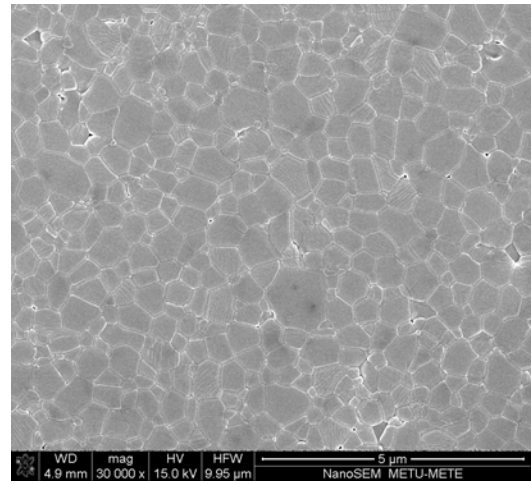
(a)   (b)
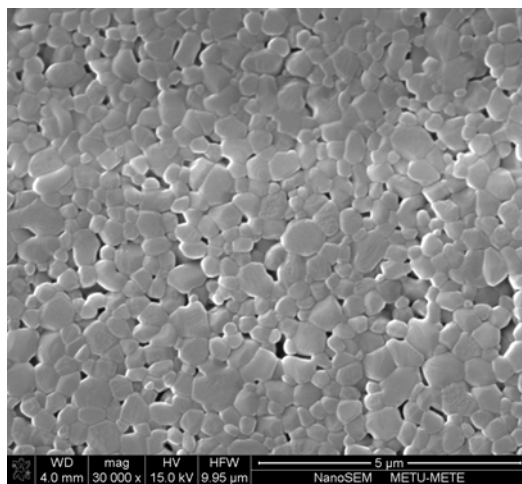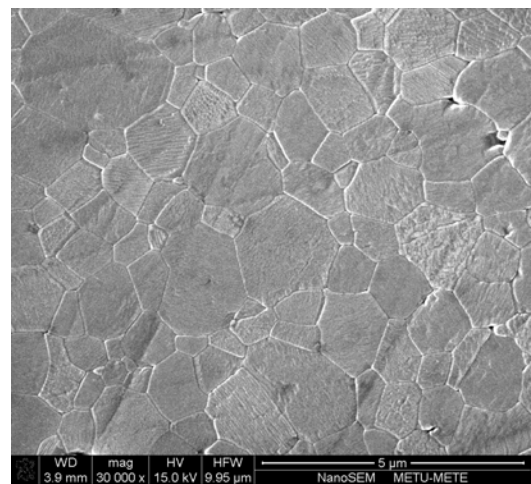
(c)   (d)

Figure 4.2 Microstructural changes of microwave and conventional sintered monolithic Al_2O_3 (a) conventional sintered at 1200˚C, (b) microwave sintered at 1200˚C, (c) conventional sintered at 1300˚C, (d) microwave sintered at 1300˚C, (e) conventional sintered at 1400˚C, (f) microwave sintered at 1400˚C, (g) conventional sintered at 1500˚C, (h) microwave sintered at 1500˚C, (i) conventional sintered at 1600˚C, (j) microwave sintered at 1600˚C.
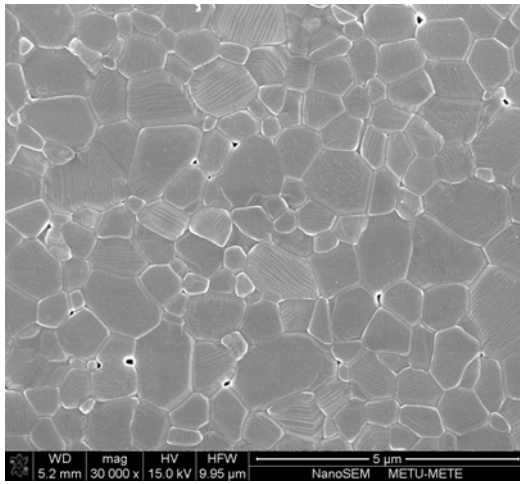
(e)
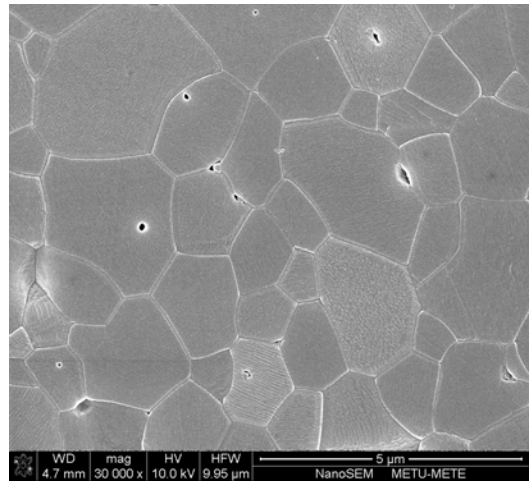
(f)
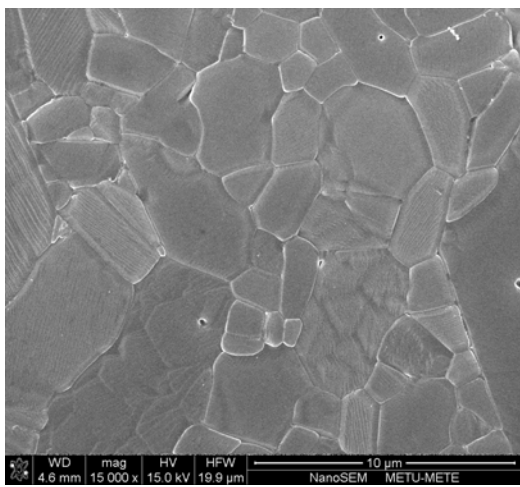
(g)
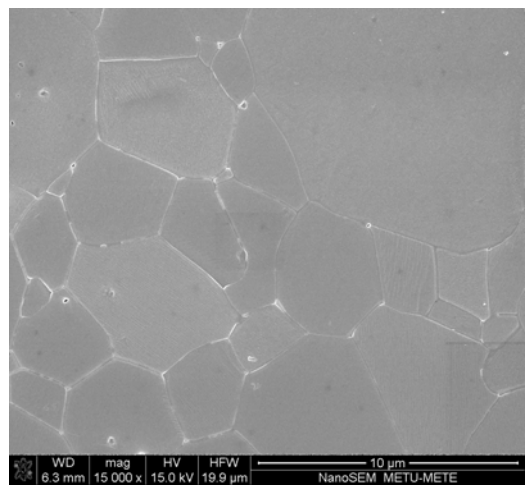
(h)
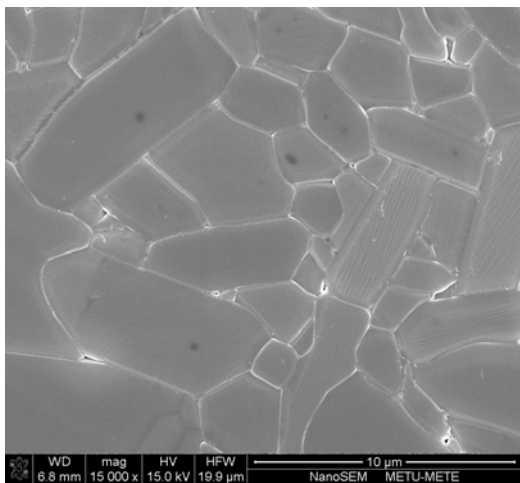
(i)
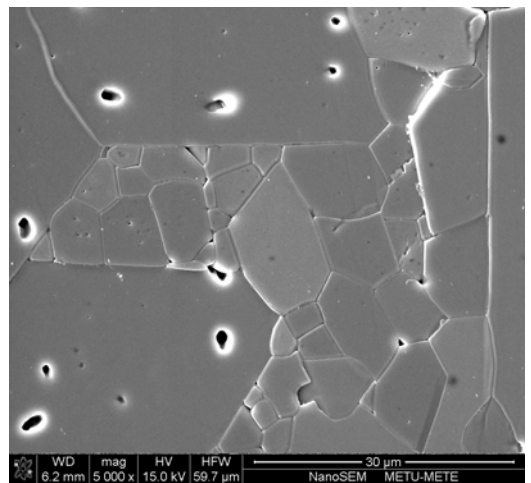
(j)

Figure 4.2 (Continued)

To compare the effect of conventional and microwave sintering on the mechanical properties of monolithic Al_2O_3, hardness and indentation toughness values of materials sintered by both of the methods were measured. Figure 4.3 shows the change of hardness with sintering temperature.
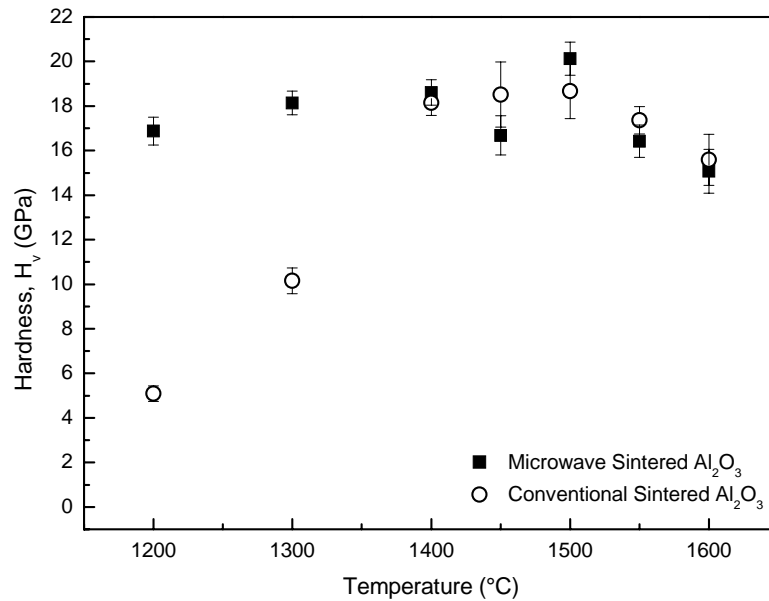
Figure 4.3 Hardness change of monolithic Al_2O_3 as function of temperature sintered by both microwave and conventional method.

Hardness of monolithic Al_2O_3 increases with sintering temperature up to 1500°C for both methods consistent with increasing densification rates. As expected from densification results and microstructural investigations, microwave sintered products reveal higher hardness values at sintering temperatures lower than 1500°C. However, after that point hardness starts to drop as a consequence of abnormal grain growth. Hardness values initially increase with increasing densification (lower pore content) where the grain structure was homogeneously forming with a uniform grain size distribution. When the microstructural evolution revealing an increase in grain size (Fig. 4.2 a-h) is analyzed together with the hardness data provided in Figure 4.3, the tendency seem to be

contradicting with the Hall-Petch relationship. Here, it should be noted that as sintering temperature increases, the ceramic body becomes densified with the coarsening of the grains. As a result, hardness, which is adversely affected by the porosity, shows an increasing trend at higher sintering temperatures with decreasing pore content although the average grain size rises. Nevertheless, at sintering temperatures higher than 1500°C, where almost full densification has been achieved, abnormal grain growth leads to a reduction in hardness values.

Figure 4.4 shows the change of indentation toughness of monolithic Al_2O_3 as a function of sintering temperature. Fracture toughness values showed a similar tendency with hardness values. Indentation fracture toughness increased with densification at higher temperatures. However, as a result of abnormal grain growth, fracture toughness started to decrease.
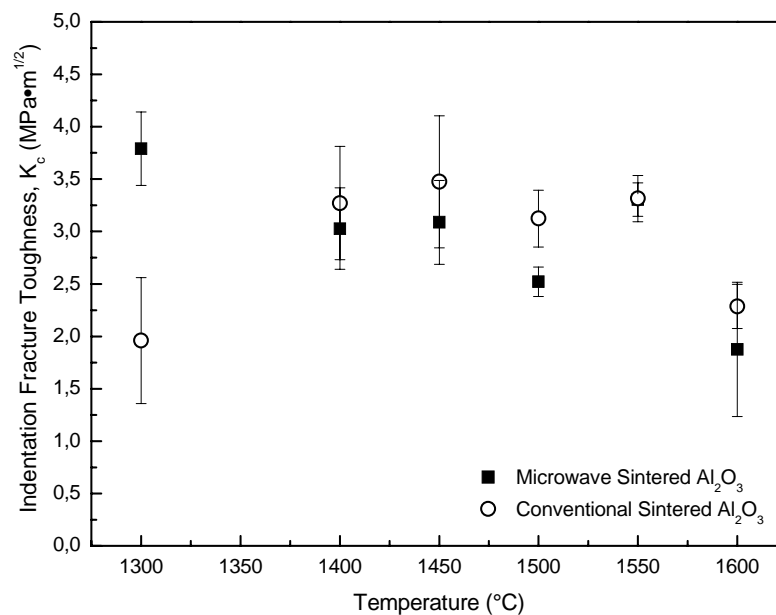
Figure 4.4 Indentation toughness of monolithic Al_2O_3 processed by microwave and conventional sintering as function of temperature.

Furthermore, indentation fracture toughness of almost fully densified conventionally sintered monolithic Al_2O_3 ceramics was higher than microwave sintered Al_2O_3 processed at temperatures above 1400°C, which can be attributed to finer average grain size achieved by conventional sintering especially at higher temperatures. Fracture mode of monolithic Al_2O_3 sintered by both methods is intergranular in which cracks propagate along the grain boundaries (Fig. 4.5 (a) and (b)). This can clearly be seen through the growth paths of the indentation cracks generated on the polished surfaces of the Al_2O_3 ceramics by Vickers indentations (Fig. 4.5 (c) and (d)). During propagation, cracks deflect at the junction points of the grains which cause loss of some portion of the crack energy resulting in the impediment of the cracks. From this point of view smaller grain size seems to be advantageous to inhibit crack propagation. However, in the case of large average grain size, as in Fig. 4.5 (d), cracks can move along the grain boundaries readily as an easy growth path without changing much in their direction (inefficient crack deflection), and thus fracture toughness decreases.
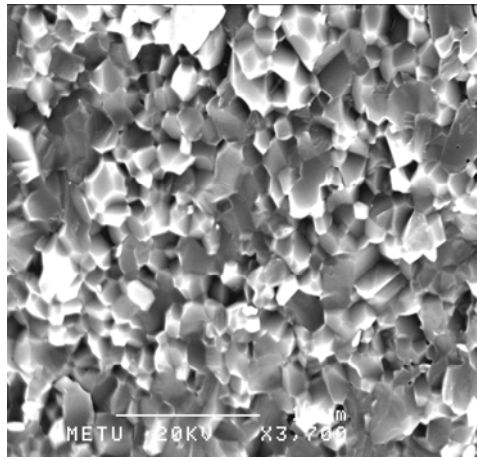
(a)
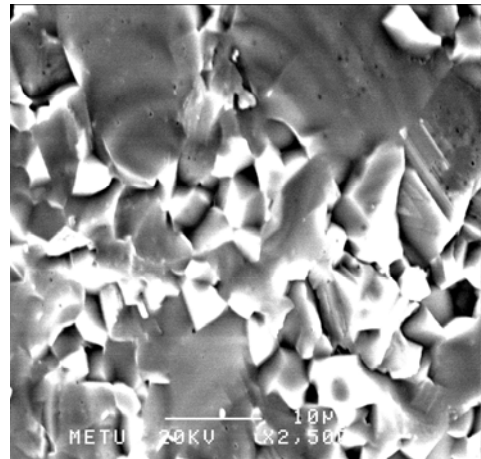
(b)
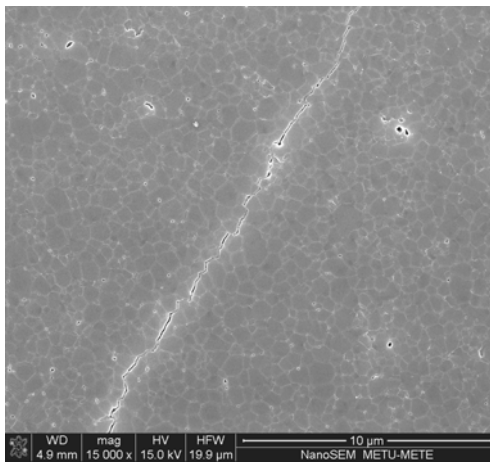
(c)
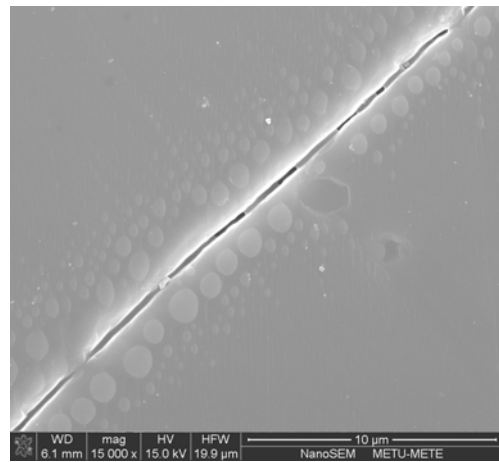
(d)

Figure 4. 5 Fracture surfaces and indentation crack growth paths of monolithic Al2O3 (a) fracture surface of conventional sintered Al_2O_3 at 1500˚C, (b) fracture surface of microwave sintered Al_2O_3 at 1500˚C, (c) indentation crack path of microwave sintered Al_2O_3 at 1200˚C (15000x) and (d) indentation crack path of microwave sintered Al_2O_3 at 1600˚C which propagates along the grain boundary between two large grains (15000x).

As it was already mentioned, comparison of microwave sintering to conventional sintering showed that usage of microwave heating is a very effective method especially for low temperatures (≤1400˚C) where densification of conventional sintered Al_2O_3 is at the intermediate stage level of sintering process, while that of microwave sintered one is at the final stage level. Conventional sintering requires temperatures higher than 1400˚C to reach densification values higher than 95% of the theoretical density. Figure 4.6 shows that to achieve comparable microstructures and mechanical properties, conventional sintering has to be conducted at temperatures 200˚C higher than microwave sintering. Owing to this difference in effective sintering temperatures between microwave and conventional processing, it can be said that microwave sintering provides energy and time saving.

(a)   (b)
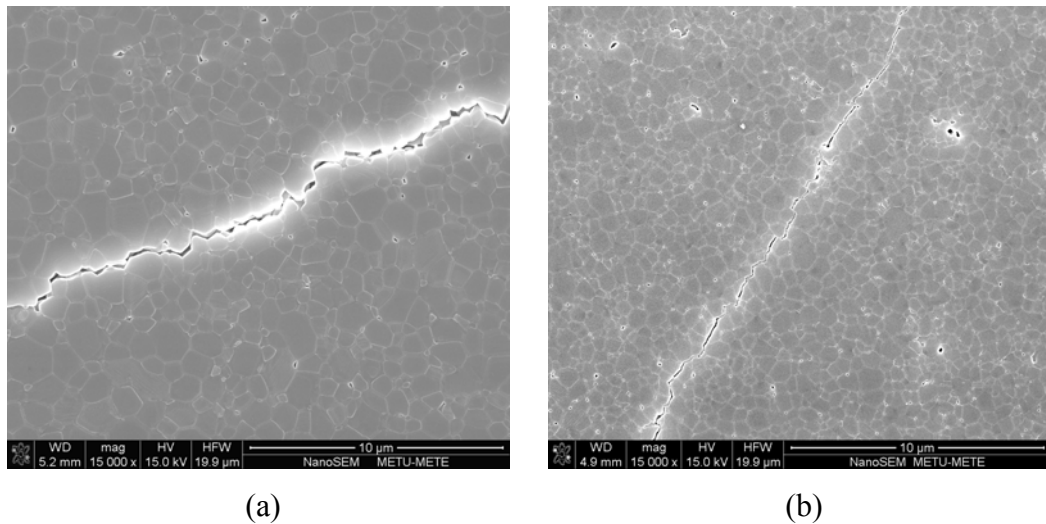
Figure 4.6 Indentation crack paths and microstructures of (a) conventional sintered Al_2O_3 at 1400˚C for 1 h, (b) microwave sintered Al_2O_3 at 1200˚C for 1 h.

4.2 Characterization of Monolithic Alumina Containing Sintering Additives

As mentioned before, abnormal grain growth is the most important obstacle standing in front of fully densified monolithic alumina production via solid state sintering. During densification and grain growth intergranular pores are removed from the grain boundaries with grain boundary diffusion; however, if some of the grains start to grow excessively; these pores are trapped within the grain interiors and cannot be removed easily. Abnormal grain growth can be the consequence of many different parameters such as; consolidation techniques, heating rates, purity and particle size of the starting powders, furnace environment, etc [62]. Usage of small amounts of sintering additives such as MgO, CaO, Y_2O_3 or SiO_2 could be beneficial to suppress abnormal grain growth and enhance densification.

In this section, effect of three different sintering additives on the densification of monolithic Al_2O_3 was investigated for both microwave and conventional sintering processes. To understand the effects of sintering additives on the sintering and abnormal grain growth behavior, sintering temperature interval of 1400-1600˚C was chosen. Figure 4.7 shows the densification change of conventional sintered monolithic Al_2O_3 and Al_2O_3 containing 0.1 wt% sintering additives (MgO, CaO or Y_2O_3). During conventional sintering, sintering additives generally showed similar effects on densification after 1450˚C, and eventually relative density reached to 98% of the theoretical value at 1550˚C. However, until 1400˚C densification trends were different, where alumina with MgO additive has the highest and alumina with Y_2O_3 additive has the lowest relative density values.
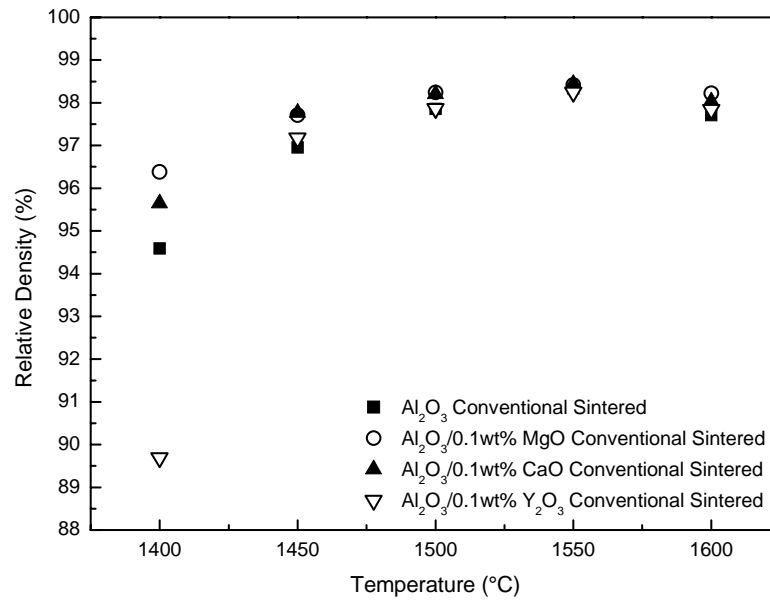
Figure 4.7 Comparison of densification efficiency achieved by conventional sintering on monolithic alumina with three different sintering additives.

Figure 4.8 shows the densification of microwave sintered alumina with the same amount of sintering additives as above. Unlike the conventional sintered Al_2O_3 ceramics with different additives, densification of the microwave sintered ceramics is different from each other. Up to 1600°C MgO additive seems to be the best one to enhance densification, and Y_2O_3 is the least efficient additive. The reason of this densification change with microwave sintering might be varying diffusion activation energies of different additive material ions in correlation with the ones of the O^{2-} and Al^{3+} ions of the parent material.
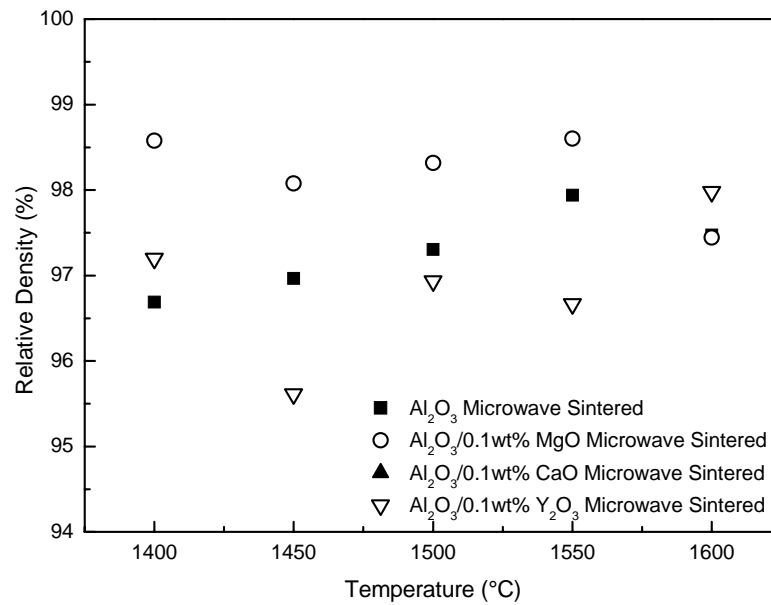
Figure 4.8 Comparison of densification efficiency achieved by microwave sintering on monolithic alumina with three different sintering additives.

To provide a comprehensive discussion on the effect of sintering additives on the densification of Al_2O_3 ceramics, microstructural investigation was done on the conventional and microwave sintered ceramics processed at 1500°C for 1 hour. It is evident from Fig. 4.9 that average grain size of the conventional sintered Al_2O_3 is smaller than that of the microwave sintered Al_2O_3 processed under identical condition.

(a)

(b)

(c)

(d)
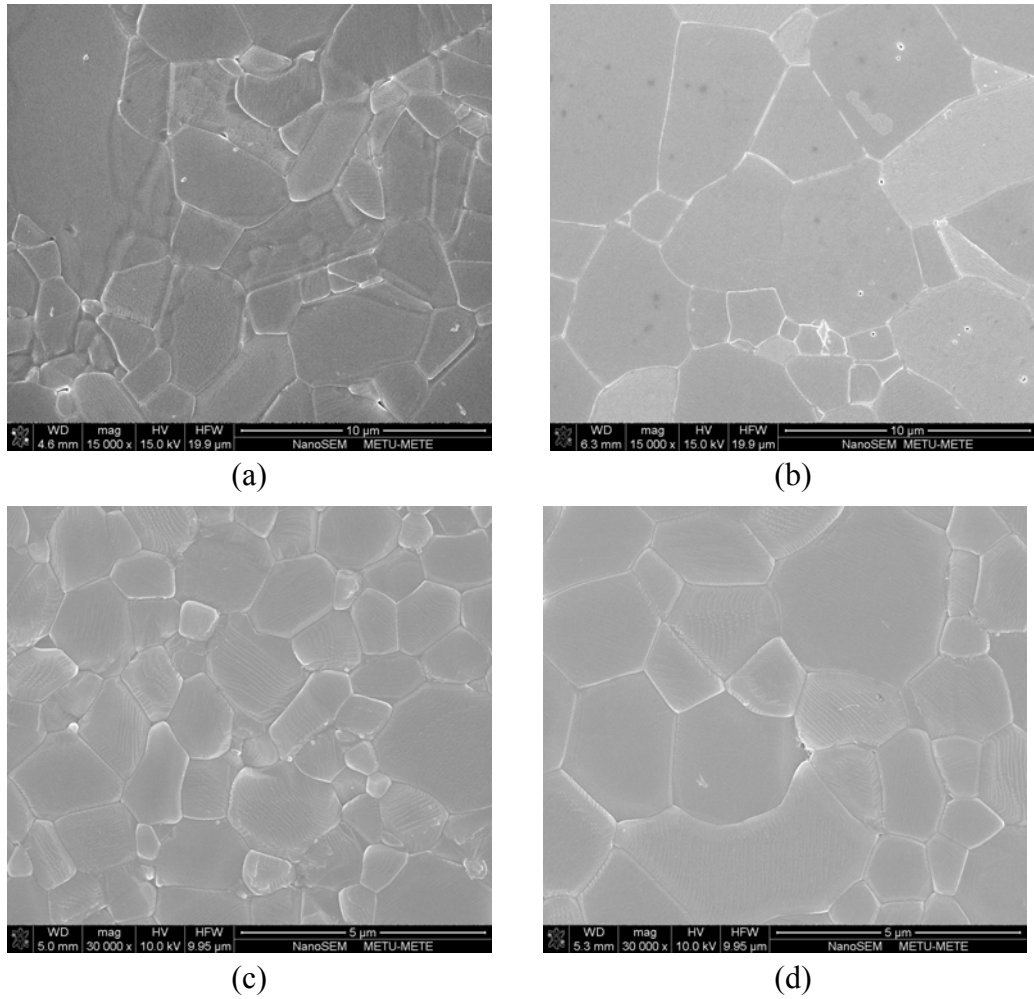
Figure 4.9 Microstructures of conventional and microwave sintered monolithic Al_2O_3 and Al_2O_3 containing sintering additives processed at 1500°C for 1 hour (a) conventional sintered plain Al_2O_3, (b) microwave sintered plain Al_2O_3, (c) conventional sintered $Al_2O_3/0.1$ wt% MgO, (d) microwave sintered $Al_2O_3/0.1$ wt% MgO, (e) conventional sintered $Al_2O_3/0.1$ wt% CaO, (f) microwave sintered $Al_2O_3/0.1$ wt% CaO, (g) conventional sintered $Al_2O_3/0.1$ wt% Y_2O_3, (h) microwave sintered $Al_2O_3/0.1$ wt% Y_2O_3.
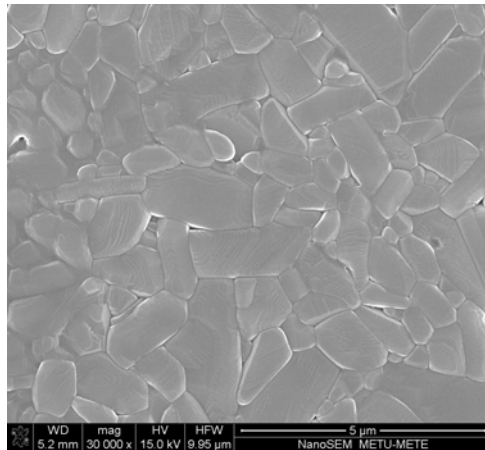
(e)
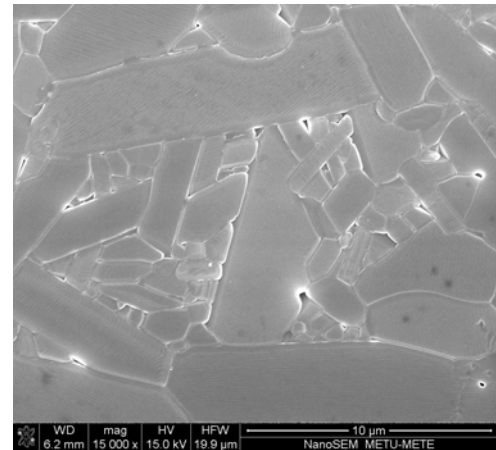
(f)
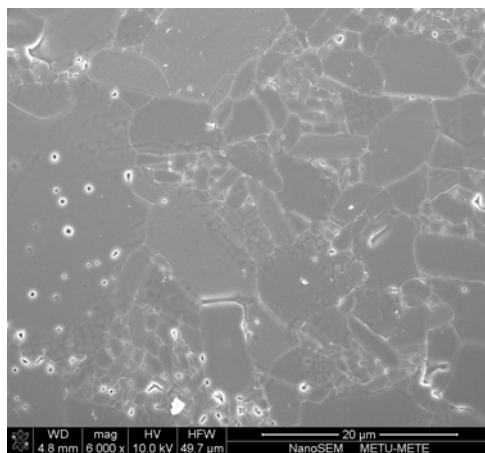
(g)
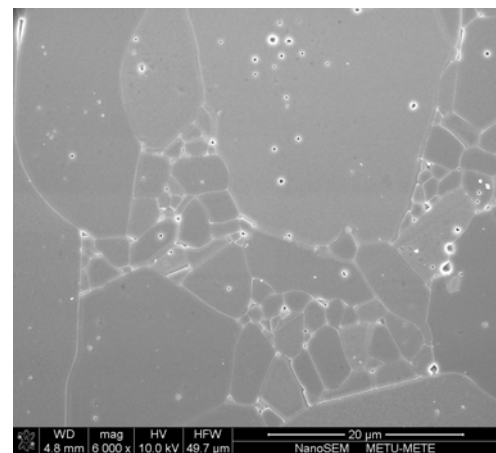
(h)

Figure 4.9 (Continued)

Figures 4.10 and 4.11 show the hardness change of conventional and microwave sintered Al_2O_3 ceramics as function of sintering temperature, respectively. The change of hardness with sintering temperature for conventional and microwave sintered Al_2O_3 is consistent with the densification data provided (Fig. 4.1).
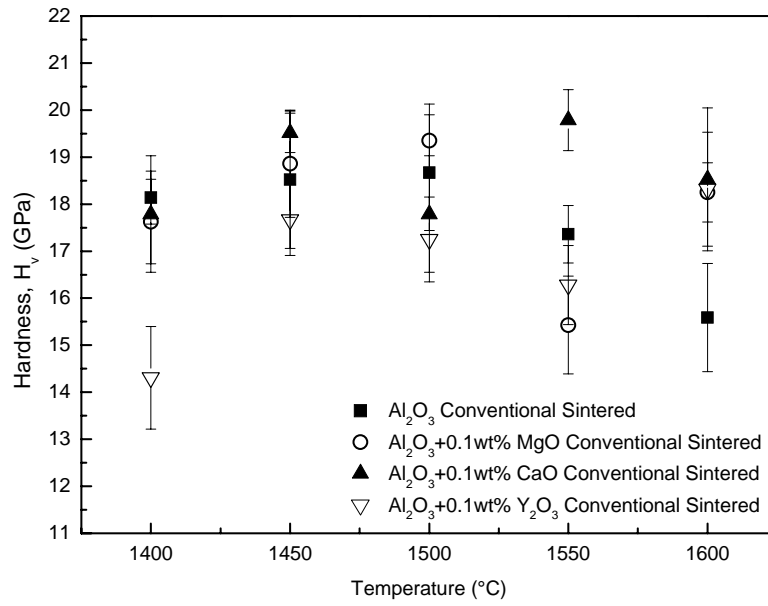
Figure 4.10 Hardness change of monolithic Al_2O_3 in the plain form and with sintering additives as function of sintering temperature processed by conventional method.
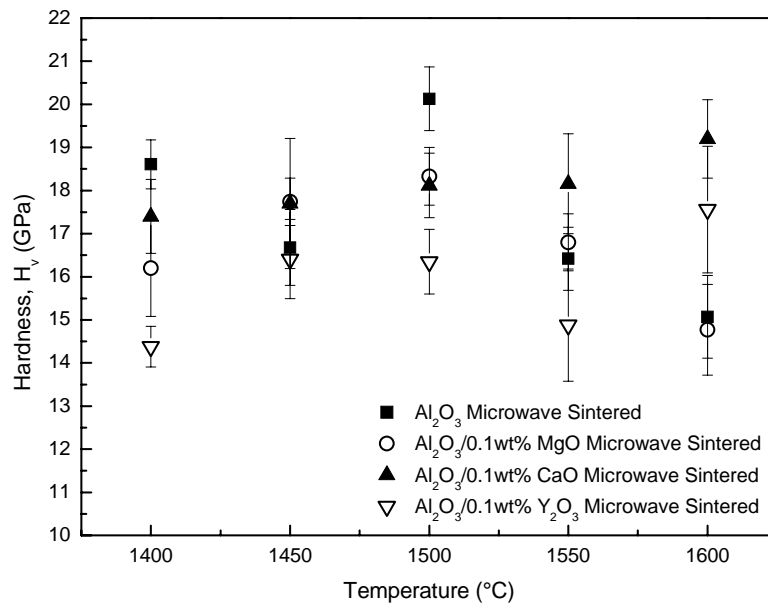
Figure 4.11 Hardness change of monolithic Al_2O_3 in the plain form and with sintering additives as function of sintering temperature processed by microwave heating.

57

Figures 4.12 and 4.13 present indentation fracture toughness values of monolithic Al_2O_3 in the plain form and with sintering additives processed by both conventional and microwave sintering as function of temperature. Indentation fracture toughness of conventional sintered ceramics decreases with temperature due to probably abnormal grain growth. At 1400˚C Al_2O_3 with 0.1 wt% Y_2O_3 additive has the highest fracture toughness because of smaller grain size along with microcracking present in the microstructure. At this temperature Y_2O_3 is still in solid form not in interaction with Al_2O_3 matrix inhibiting grain growth. However, after 1550˚C Y_2O_3 starts to interact with Al_2O_3, and hence results in pronounced grain growth rate leading to a reduction in indentation fracture toughness.

On the other hand, indentation fracture toughness values of microwave sintered Al_2O_3 ceramics did not show remarkable change with temperature and sintering additive type. This is a consequence of the comparable sintered characteristics of microwave processed Al_2O_3 ceramics including achieved densifications and resulting microstructures such as average grain sizes along with pore amounts and distributions.
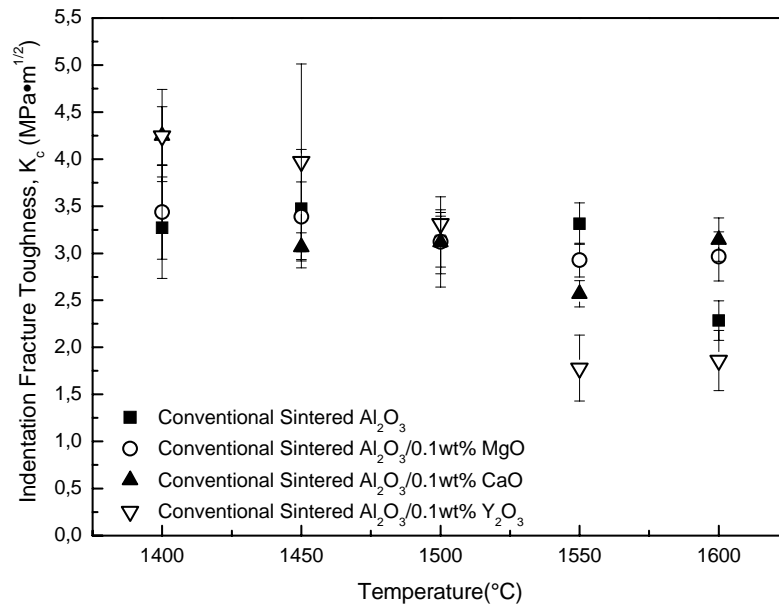
Figure 4.12 Indentation fracture toughness of monolithic Al_2O_3 in the plain form and with various sintering additives processed by conventional sintering as function of temperature.
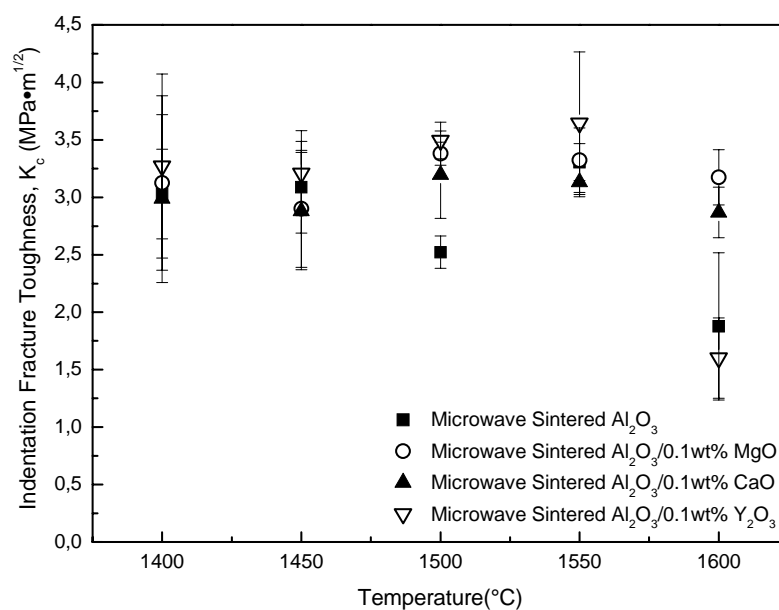
Figure 4.13 Indentation fracture toughness of monolithic Al_2O_3 in the plain form and with sintering additives processed by microwave sintering as function of temperature.

Densification studies on Al_2O_3 containing sintering additives showed that MgO is the most effective sintering aid with respect to others for microwave sintering. In order to understand the efficiency of MgO as a sintering aid at temperatures lower than 1400°C, plain Al_2O_3 and Al_2O_3/0.1 wt% MgO ceramics were sintered by microwave heating between 1000°C and 1600°C. Figure 4.14 shows the densification change of microwave sintered ceramics as a function of sintering temperature applied. Nevertheless, usage of MgO as a sintering aid did not provide a remarkable advantage at lower temperatures contrary to the anticipations. Densification behavior of microwave sintered plain Al_2O_3 and Al_2O_3 containing 0.1 wt% MgO is similar during microwave sintering. However, at 1100°C and 1200°C plain Al_2O_3 ceramics revealed slightly better relative densities being ~3% higher than those achieved in MgO containing Al_2O_3.
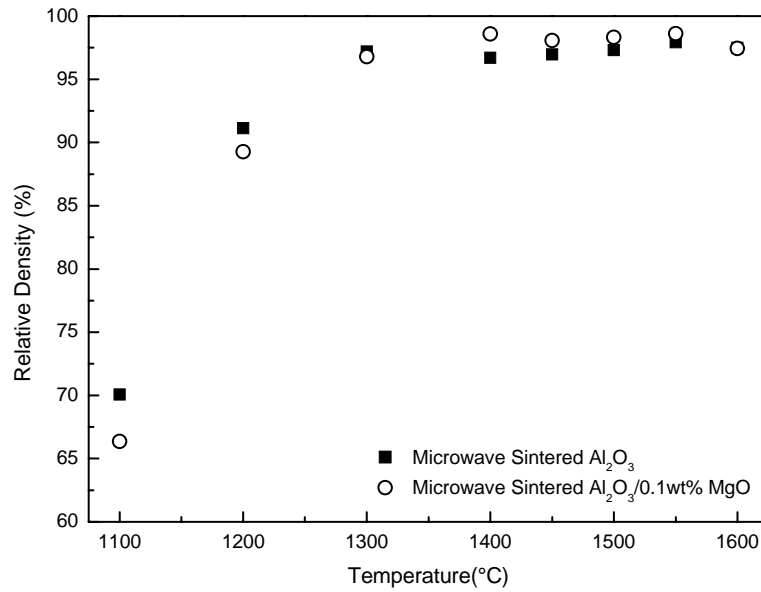
Figure 4.14 Comparison of densification efficiency of monolithic plain Al_2O_3 and Al_2O_3 containing 0.1 wt% MgO achieved by microwave sintering at different temperatures for 1 h.

Microstructures of plain Al_2O_3 and Al_2O_3 containing 0.1 wt% MgO ceramics sintered by microwave heating at 1100˚C and 1200˚C for 1h revealed that MgO addition increases porosity and inhibits grain growth suppressing sintering at low sintering temperatures. MgO starts to show its aid as an efficient sintering additive at temperatures higher than 1300˚C (Fig. 4.15).

(a)

(b)

(c)

(d)
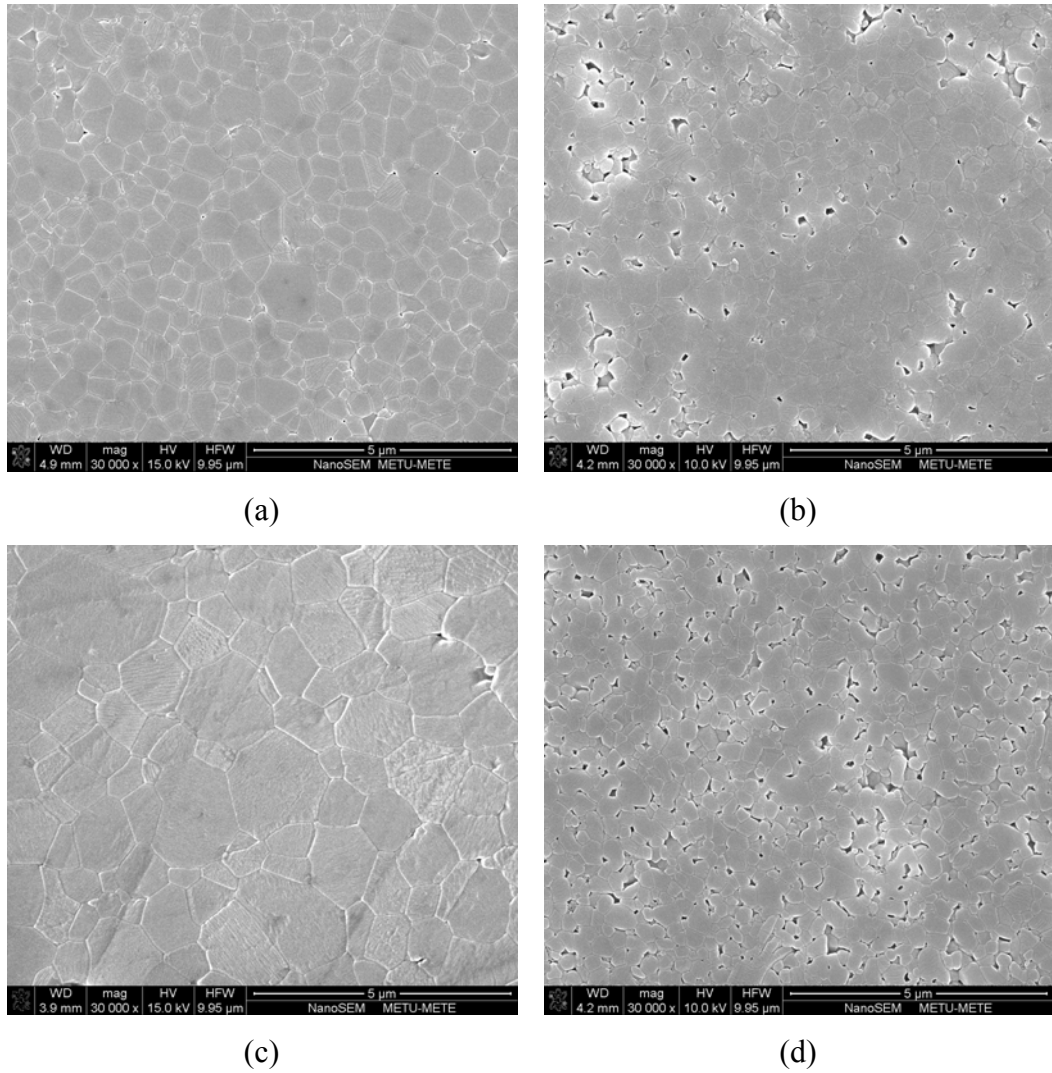
Figure 4.15 Microstructural changes of microwave sintered (a) monolithic Al_2O_3 sintered at 1100°C for 1 h, (b) Al_2O_3/0.1 wt% MgO sintered at 1100°C for 1 h, (c) monolithic plain Al_2O_3 sintered at 1200°C for 1 h, (d) Al_2O_3/0.1 wt% MgO sintered at 1200°C for 1 h.

In the light of the information given in Sections 4.1 and 4.2, for the sintering of monolithic Al_2O_3 use of microwave heating is more effective than conventional method. Plain monolithic Al_2O_3 can be sintered to remarkably high relative densities (~97%) at only 1300°C by microwave processing that is a considerably low temperature for ceramic processing at which such high densification values are quite hard to achieve by conventional sintering.

4.3 Characterization of Al_2O_3/SiC_p Nanocomposites

Following the initial part of this study where the effect of microwave heating on the densification of monolithic Al_2O_3 ceramics has been investigated, the study has focused on the SiC nanoparticle dispersion in Al_2O_3 and microwave sintering of the resulting Al_2O_3-based nanocomposites to achieve enhanced mechanical properties.

By using the information obtained from the microwave sintering studies on monolithic Al_2O_3 two optimum temperatures were chosen for the sintering of the ceramic nanocomposites. Firstly, 1300˚C was applied, since it appears to be the lowest temperature to achieve acceptable densification especially by microwave sintering. When compared with the data available in literature on this particular material, this temperature turns out to be considerably low for the fabrication of Al_2O_3 /SiC_p nanocomposites. Generally in the literature, studies on the processing of Al_2O_3 /SiC_p nanocomposites have been conducted at sintering temperatures above 1650˚C, where mostly pressure was applied simultaneously in the form of hot-pressing or hot isostatic pressing to approach the theoretical density as much as possible [29, 42, 63].

Varying amounts of SiC particles were added into Al_2O_3 by mechanical mixing to investigate the effect of second phase incorporation on the sinterability and mechanical properties of Al_2O_3 matrix nanocomposites. Figure 4.16 shows the change in densification with the increasing content of dispersed material after 1 h sintering at 1300˚C. It is obvious that increasing SiC content has a negative effect on the densification rate of Al_2O_3/SiC_p nanocomposites for both methods. This can be attributed to the decreasing grain boundary mobility due to the pinning effect of the well-dispersed nanometer-sized SiC particles in the alumina matrix, which suppresses grain growth, and hence densification.
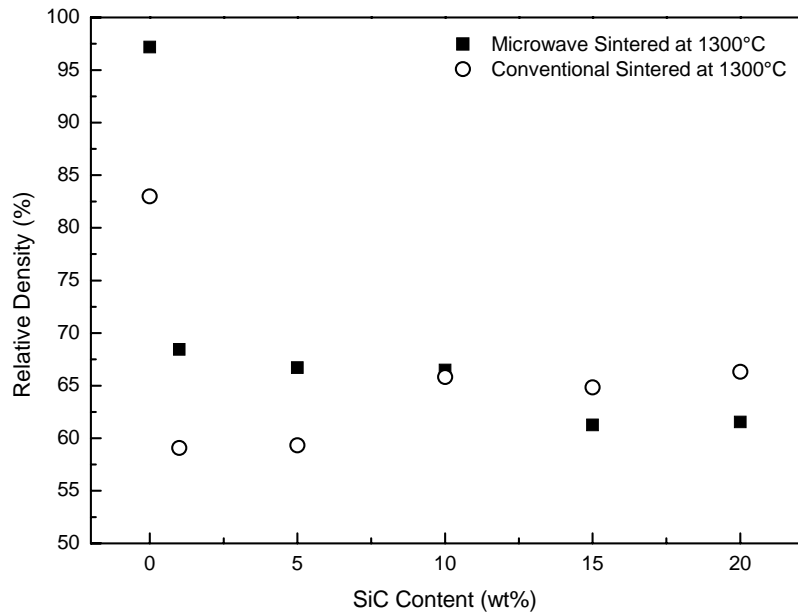
Figure 4.16 Change of densification with SiC content for the nanocomposites sintered by both microwave and conventional method at 1300°C for 1 h.

However, for SiC additions higher than 10 wt%, microwave sintered nanocomposites reveal lower densification rates. This is mainly the consequence of thermal expansion mismatch between Al_2O_3 ($\alpha=8.8 \times 10^{-6°}C^{-1}$) and SiC ($\alpha=4.7 \times 10^{-6°}C^{-1}$) which becomes more dominant at higher additive contents. During microwave sintering heating rates are considerably high (above 30°C/min) which results in the formation of residual stress fields in the matrix around the intragranular particles leading to cracking during sintering. As the dispersant content increases, the densification of microwave sintered nanocomposites decreases as a result of pronounced microcracking caused by the thermal expansion coefficient mismatch [36, 40]. Figure 4.17 shows the SEM pictures of the thermally etched surfaces of Al_2O_3 /SiC_p nanocomposites with 5, 10 and 20 wt% SiC all sintered at 1300°C for 1 h by both methods. Poor densification characteristic of the nanocomposites with increasing SiC content is evident from Fig. 4.17.

This is especially true for the material with 20 wt% SiC addition (Fig. 4.17 e and f), where no grain formation can be observed with a high amount of residual porosity.

(a)

(b)

(c)

(d)
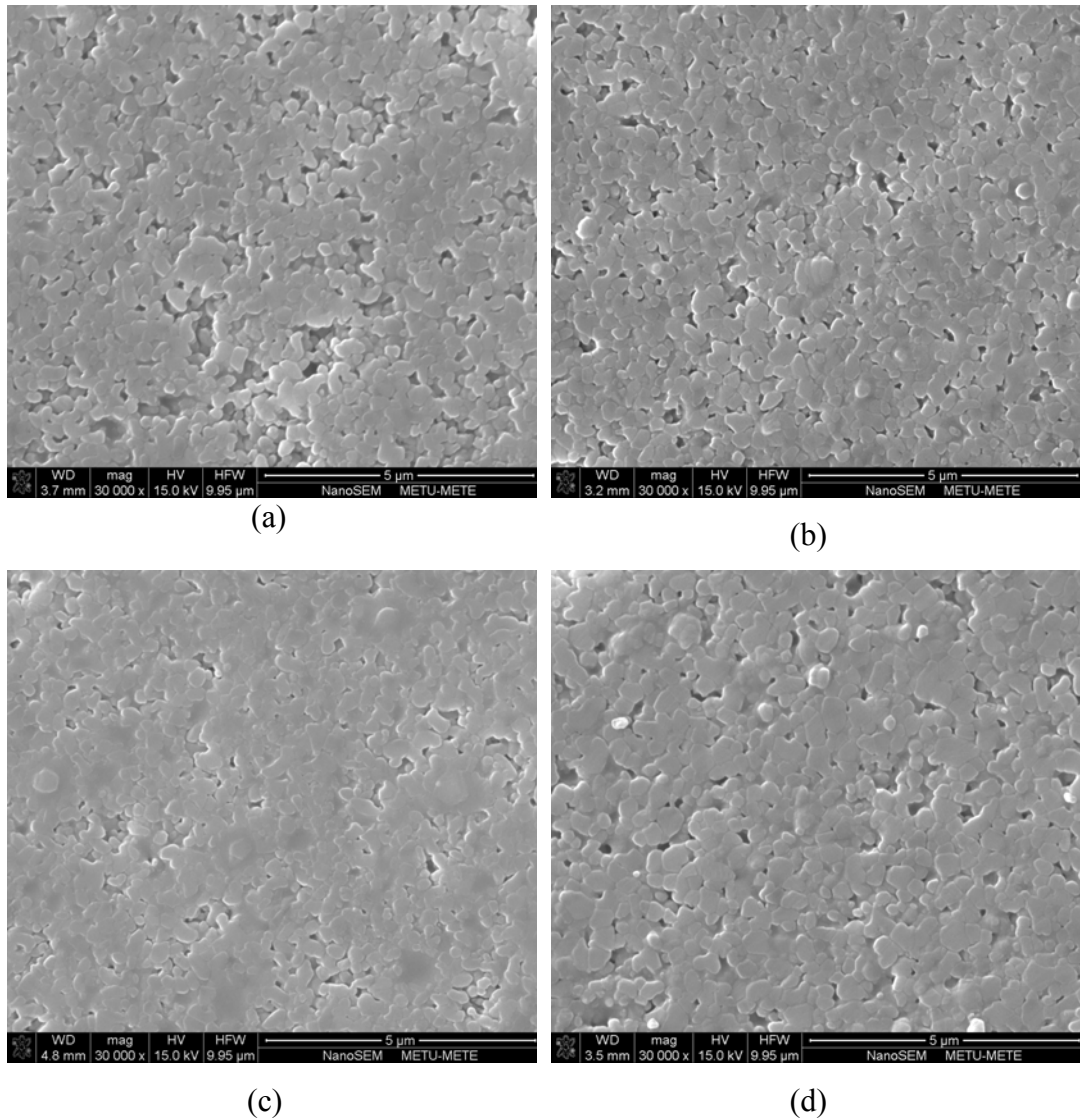
Figure 4.17 SEM micrographs of Al_2O_3/SiC_p nanocomposites with varying SiC content sintered at 1300°C for 1 h by both methods; (a), (b) 5 wt% SiC conventional and microwave sintered, (c), (d) 10 wt% SiC conventional and microwave sintered, (e), (f) 20 wt% SiC conventional and microwave sintered.

(e)   (f)
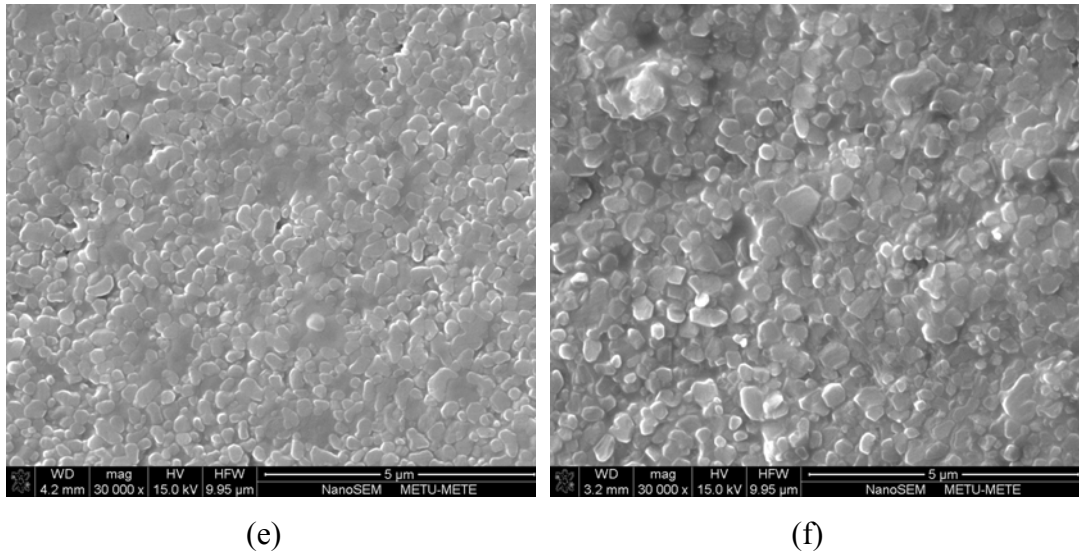
Figure 4.17 (Continued)

To reveal the mechanical properties of Al_2O_3 /SiC_p nanocomposites with varying SiC content sintered at 1300˚C for 1 hour microhardness measurements were conducted. As anticipated from the densification data presented in Fig. 4.16 along with the achieved microstructures shown in Fig. 4.17, measured hardness values of the Al_2O_3 matrix nanocomposites are considerably lower than that of the monolithic Al_2O_3 (Fig. 4.18).
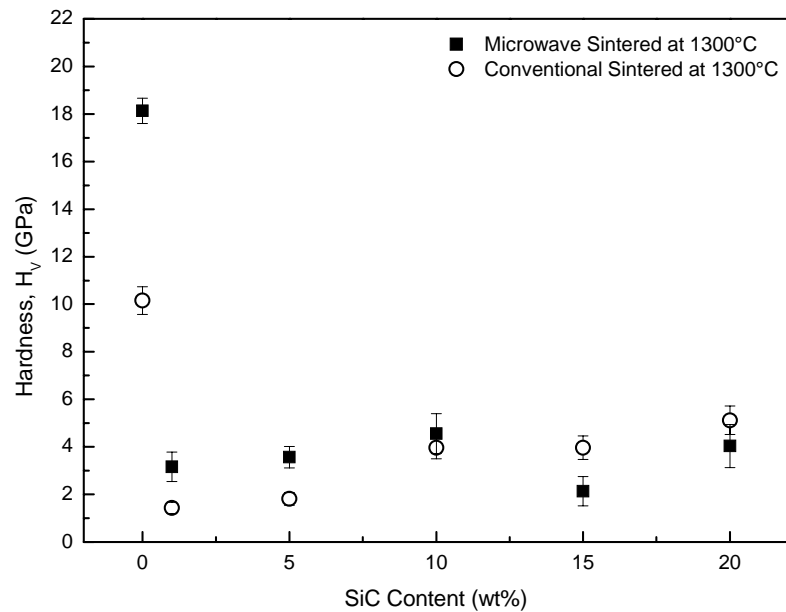
Figure 4.18 Hardness of Al_2O_3 nanocomposites as function of SiC content sintered by both microwave and conventional method at 1300°C for 1 h.

As mentioned above, sintering of Al_2O_3 /SiC_p nanocomposites at 1300°C was not sufficient to achieve densified ceramic nanocomposites with improved properties compared to those of monolithic Al_2O_3. To overcome this problem 1500°C was applied as the second sintering temperature, since it seems to be the lowest temperature to achieve the highest possible and comparable densification levels by both microwave and conventional processing. Although 1500°C is a moderately high temperature for the pressureless sintering of most common engineering ceramic materials, it is still considerably low for the fabrication of Al_2O_3 /SiC_p nanocomposites [49, 64].

For comparison same amounts of SiC particles were added into Al_2O_3 which were sintered at 1500°C for 1 hour applying either heating method. Figure 4.19 shows the change in densification with the increasing content of dispersed second phase. It is obvious that increasing SiC content still has a negative effect on the densification rate of Al_2O_3/SiC_p nanocomposites for both methods mainly because

of the reasons explained previously. However, relative densities achieved at 1500˚C range from ~73 to 93% of the theoretical densities for varying SiC contents, which were changing between ~60 and 70% for all SiC amounts after sintering at 1300˚C.
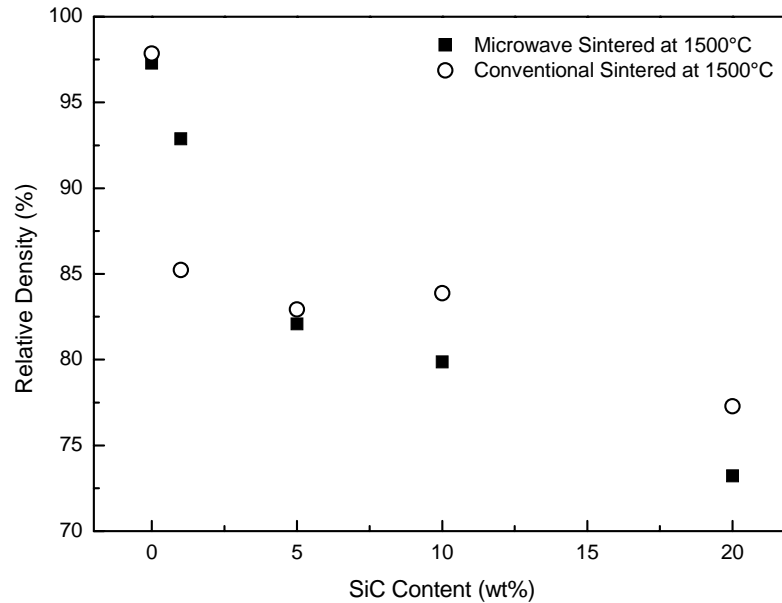
Figure 4.19 Change of densification with SiC content for the nanocomposites sintered by both microwave and conventional method at 1500˚C for 1 h.

XRD of the monolithic Al_2O_3 and Al_2O_3/SiC_p nanocomposites after the sintering process at 1500˚C were investigated to determine the phases present. Obtained XRD patterns of conventional sintered monolithic Al_2O_3 and 1 and 5 wt% SiC containing Al_2O_3 matrix nanocomposites are given in Fig. 4.20. Increasing SiC content causes some mullite $(3Al_2O_3 \cdot 2SiO_2)$ formation because of the decomposition of SiC which was not observed in the obtained spectra.
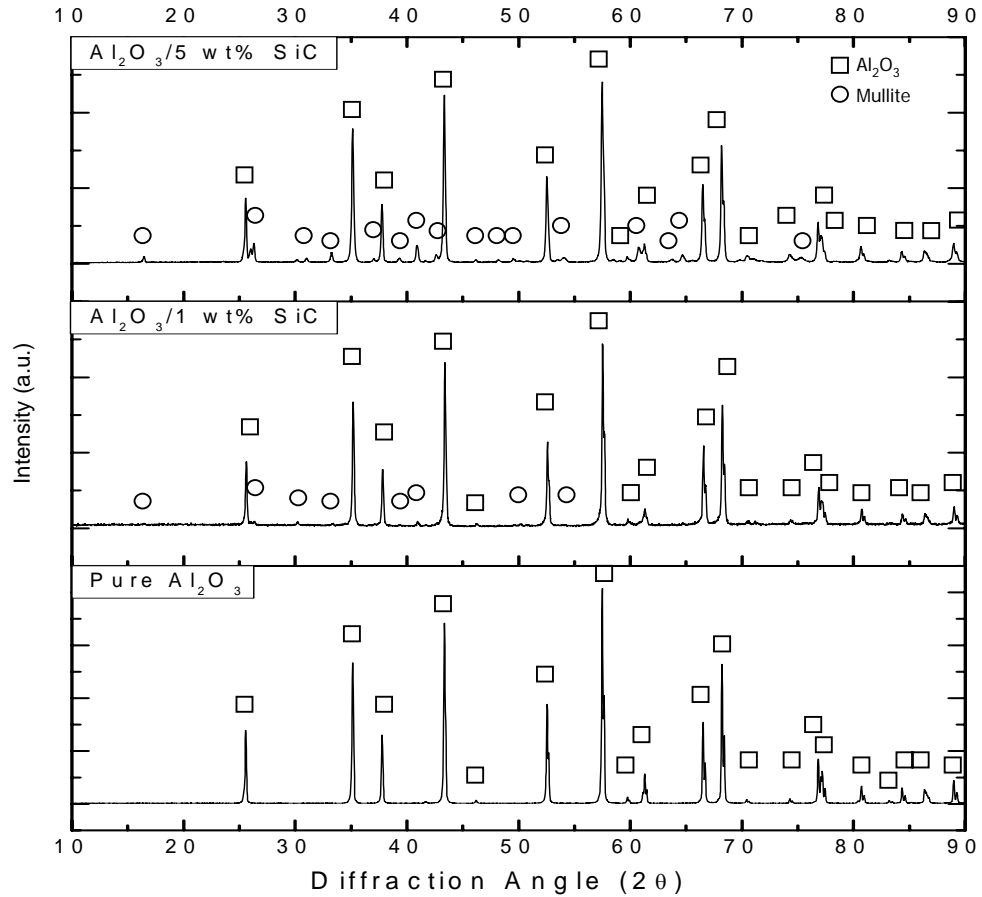
Figure 4.20 XRD spectra of conventional sintered monolithic alumina and Al_2O_3 /SiC_p nanocomposites after sintering at 1500°C for 1 h.

Figure 4.21 shows the XRD spectra of microwave sintered monolithic Al_2O_3 and 1 and 5 wt% SiC containing Al_2O_3 matrix nanocomposites. Compared to the results of conventional sintering, mullite formation is more pronounced during conventional sintering caused by differing sintering atmospheres. Microwave sintering experiments were conducted under Ar atmosphere, while conventional sintering experiments were carried out in air resulting in higher decomposition rate of SiC leading to increased amount of mullite formation following the interaction of the decomposition products with the Al_2O_3 matrix.
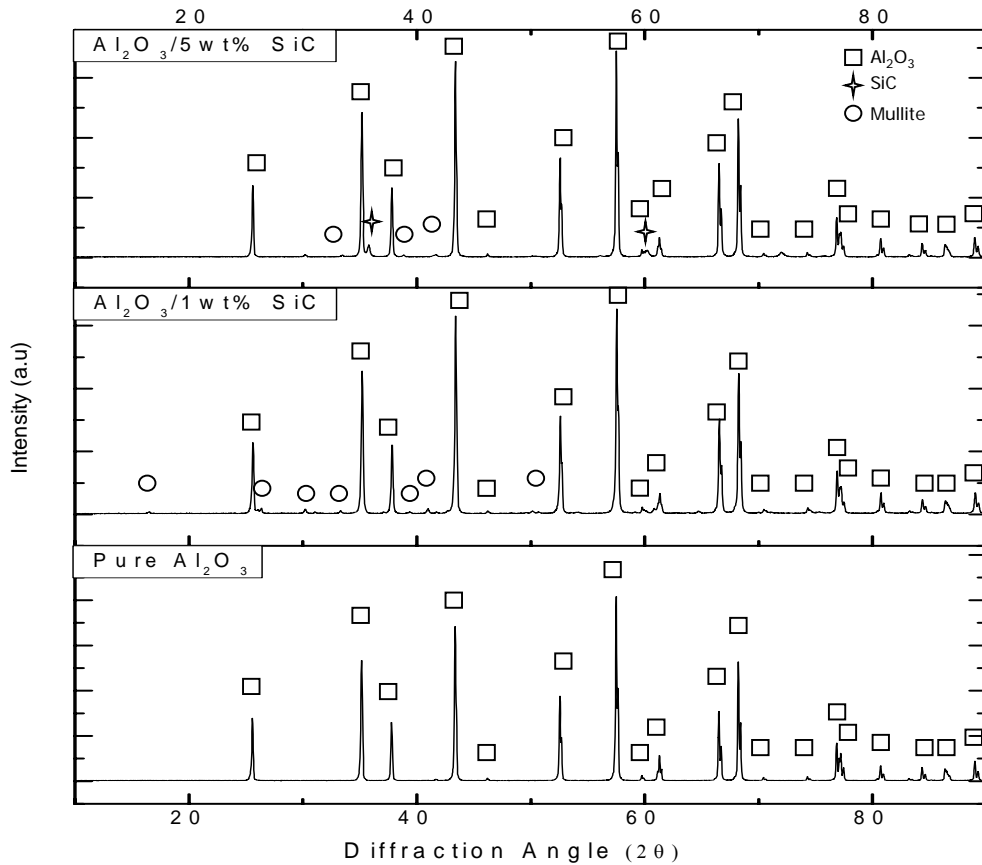
Figure 4.21 XRD spectra of microwave sintered alumina and Al_2O_3 /SiC_p nanocomposites after sintering at 1500°C for 1 h.

To understand the effect of temperature increase on the sintering of Al_2O_3 /SiC_p nanocomposites, their microstructures were examined on their thermally etched surfaces. From Fig. 4.22 it is evident that increasing sintering temperature gave rise to grain growth and elimination of the pores at lower SiC contents (<5 wt%) especially for microwave sintered samples. However, 1500°C was still not sufficient even for microwave sintering to provide full densification in the case of ceramic nanocomposites. For both methods increment in SiC content resulted in the increase of the pore amount and pore size, and thus decreasing densification because of the thermal expansion mismatch between the matrix and the particles which becomes more dominant at higher additive contents.

70

(a)

(b)

(c)

(d)
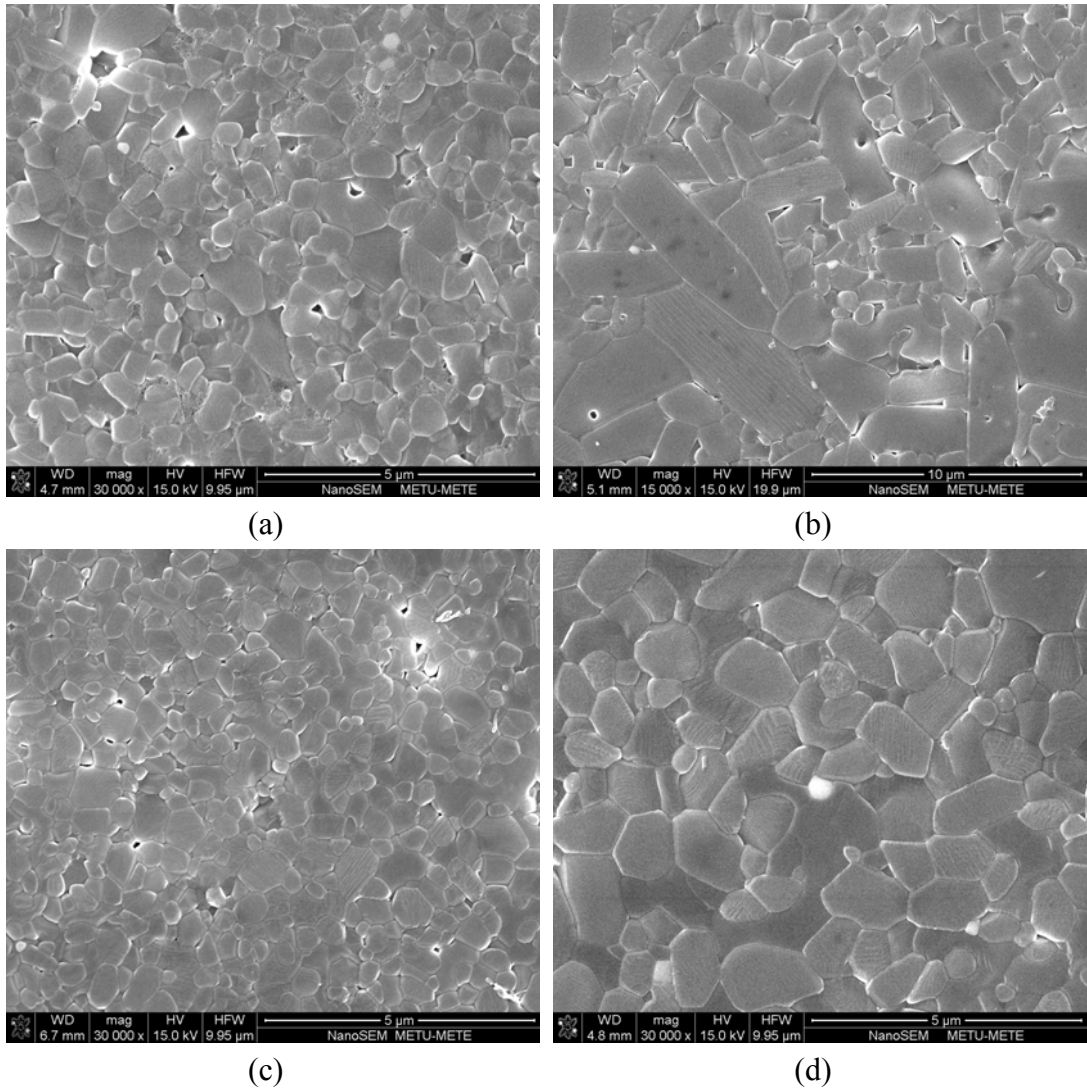
Figure 4.22 Microstructural changes of $Al_2O_3/SiCp$ nanocomposites sintered by both conventional and microwave heating at 1500°C for 1 h; (a), (b) 1 wt% SiC conventional and microwave sintered, (c), (d) 5 wt% SiC conventional and microwave sintered, (e), (f) 10 wt% SiC conventional and microwave sintered, (g), (h) 15 wt% SiC conventional and microwave sintered, (i), (j) 20 wt% SiC conventional and microwave sintered.
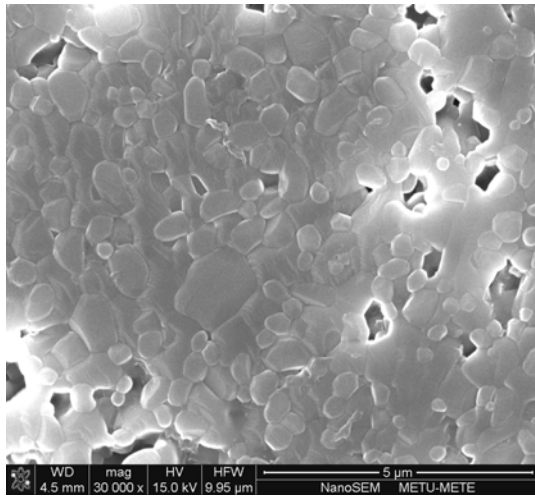
(e)
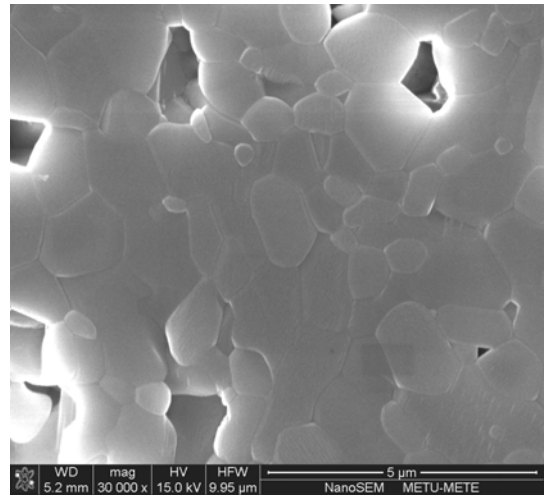
(f)
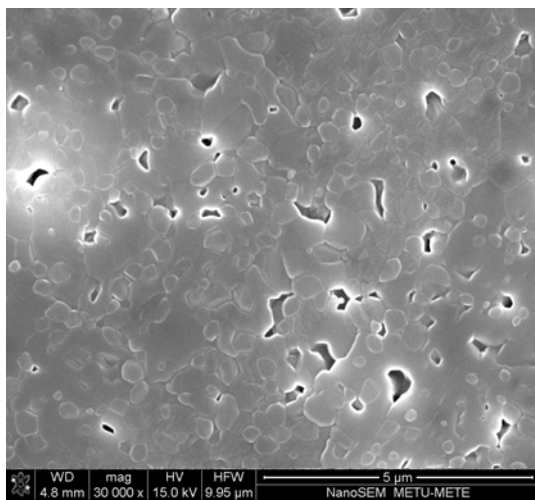
(g)
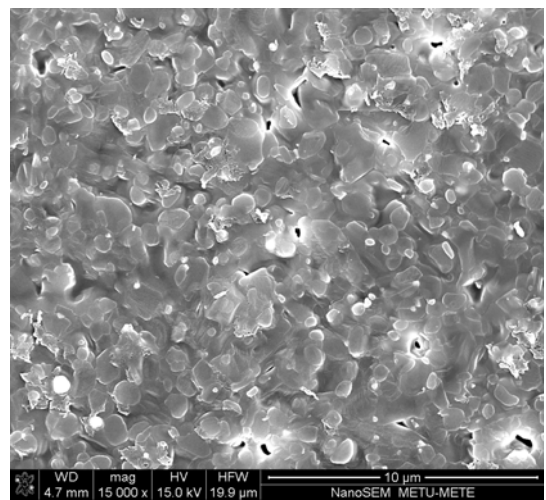
(h)
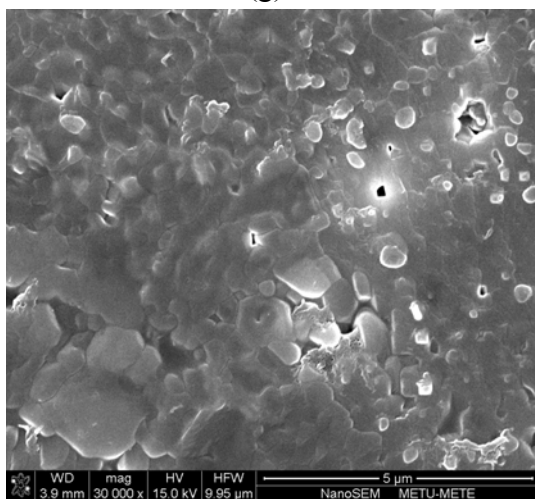
(i)
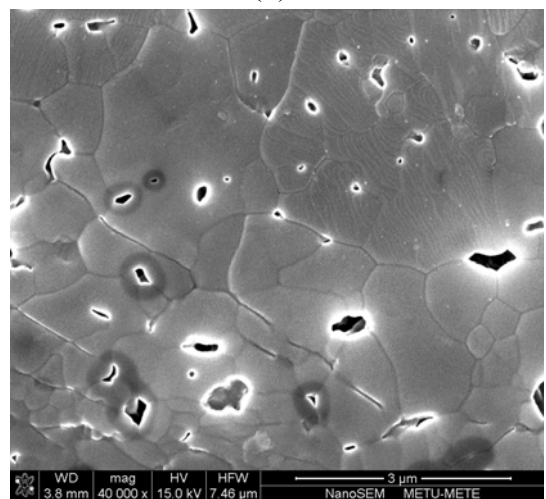
(j)

Figure 4.22 (Continued)

Following the densification and microstructural evolution investigations, mechanical properties of Al_2O_3 /SiC_p nanocomposites were examined by hardness and indentation toughness measurements. Figure 4.23 shows the change of hardness with SiC content for the nanocomposites sintered at 1500°C for 1 h. It is clear that although increasing temperature enhanced the hardness values of Al_2O_3/SiC_p nanocomposites when compared to those sintered at a lower temperature (Fig. 4.23), hardness of monolithic Al_2O_3 decreases with increasing SiC content for both of the sintering methods. This result is consistent with the densification data presented in Fig. 4.19 which shows the decreasing sintering efficiency with increasing second phase content.
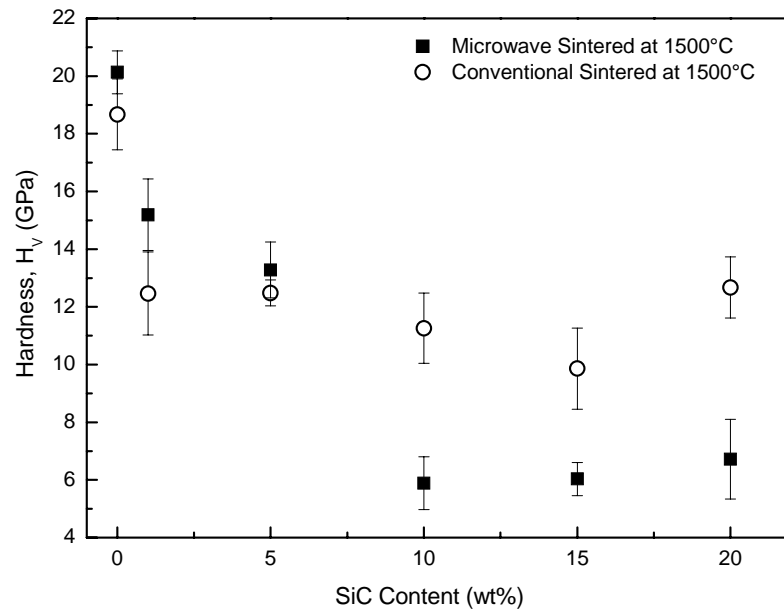
Figure 4.23 Hardness of Al_2O_3 /SiC_p nanocomposites with varying SiC content sintered by both microwave and conventional method at 1500°C for 1 h.

For the conventionally sintered nanocomposites, there is a slight decrease in hardness with increasing SiC content up to 15 wt%, which is followed by a little rise for 20 wt% SiC. This is thought to be a combined consequence of the applied

microhardness measurement technique and the relatively smaller grain and pore sizes observed for this nanocomposite (Fig. 4.22 (i)). Hardness values measured for the 20 wt% SiC containing conventionally sintered nanocomposite seem to have been taken from regions free from pores and microcracks, which are microstructural features with a negative effect on the hardness of ceramic materials. Therefore, this value does not seem to reflect the average mechanical property of this material, and thus should not be considered as deteriorating the observed decreasing trend in hardness with increasing SiC content. In the case of the microwave sintered nanocomposites the decrease in hardness is more dramatic which can be attributed to increasing amount of microcracking with SiC content due to the aforementioned thermal expansion mismatch in the structure caused by the residual stress due to considerably higher heating rates typical to microwave heating. Nevertheless, compared to the hardness value of 19.2 GPa reported for 5 wt% SiC containing Al_2O_3 matrix nanocomposite processed by hot-pressing at 1775°C for 4 h [42], 14 GPa of hardness achieved in the current study for the same SiC content by microwave sintering at relatively milder processing conditions is notable.

Figure 4.24 presents the change of indentation fracture toughness of the Al_2O_3/SiC_p nanocomposites as a function of SiC content. For both of the sintering methods SiC addition seems to increase the indentation toughness of the monolithic Al_2O_3. This is consistent with the results of the previous studies reporting on the toughening effect of SiC addition due to the strength of the Al_2O_3/SiC interfaces which were the consequence of residual compressive stresses forming in the matrix upon cooling because of the thermal expansion mismatch [27]. Even though the error margin of the measurements is considerable, from Fig. 4.24 it is evident that indentation toughness shows an increasing trend with SiC content in the case of microwave sintering. The highest indentation toughness value of ~4 $MPa.m^{1/2}$ achieved by microwave sintering for 15 and 20 wt% SiC containing nanocomposites was ca. 50% higher than that of monolithic Al_2O_3 processed under identical conditions. This result is consistent with the data of the previous studies on the fracture toughness improvement by

SiC particle addition [35, 36, 42], where indentation toughness values such as 3.25 to 4.70 MPa·m$^{1/2}$ were reported [35, 36, 42]. In addition to the previously mentioned mechanisms, increasing amount of microcracking might have a positive contribution on this value, which is consistent with the low densification (Fig. 4.19) and hardness (Fig. 4.23) values of microwave sintered nanocomposites containing 15 and 20 wt% SiC. In the case of conventionally sintered nanocomposites there is a similar increasing trend on indentation toughness with SiC content most probably due to the similar effects discussed previously.
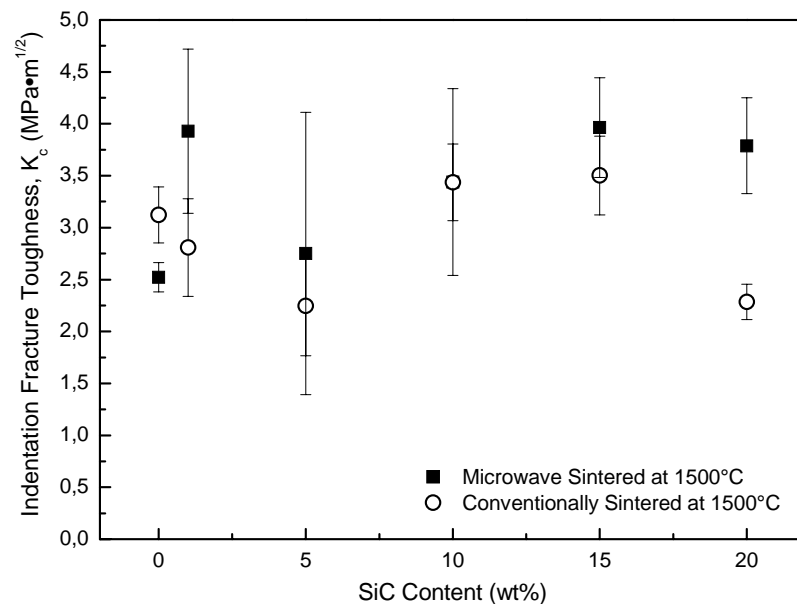
Figure 4.24 Indentation toughness of the Al$_2$O$_3$ /SiCp nanocomposites processed by microwave and conventional sintering at 1500˚C for 1 h with varying SiC content.

Many previous studies which reported toughness improvement have attributed related the results to the change of fracture mode from inter to transgranular type along with crack impediment by intragranular particles [29]. Fracture surfaces of the nanocomposites containing 20 wt% SiC sintered at 1500˚C for 1 h by

conventional and microwave processing are shown in Fig. 4.25 a and b, respectively. Fracture mode for both of the materials seems to be a mixture of intergranular and transgranular type. Nevertheless, microwave sintered nanocomposites reveal a higher fraction of transgranular type of fracture. The expected change in the fracture mode from inter to transgranular by the addition of SiC particles into Al_2O_3 has been achieved dominantly by microwave sintering in the present case.

(a)   (b)
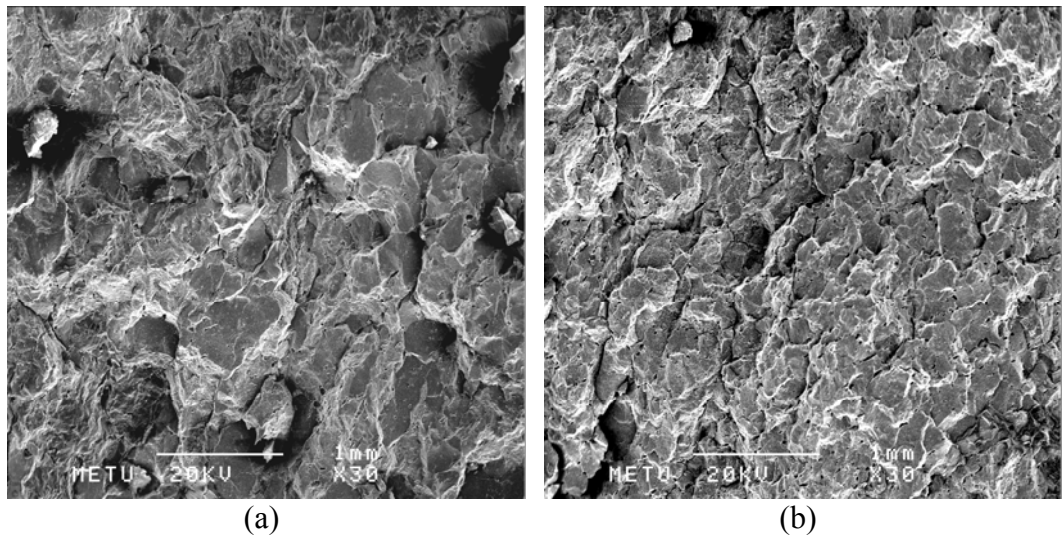
Figure 4.25 Fracture surfaces of Al_2O_3 /SiC_p nanocomposites (a) conventional and (b) microwave sintered at 1500˚C for 1 hour.

4.4 Characterization of Al_2O_3/Yttria Stabilized ZrO_2 Particle (YSZ$_p$) Nanocomposites

Stabilized zirconia particles are frequently being added to alumina matrix in order to achieve ceramic composites with improved mechanical properties. In the scope of the present study, in addition to the efforts on Al_2O_3/SiC$_p$ nanocomposites, investigations were also conducted on yttria stabilized ZrO_2 particle (YSZ$_p$) dispersed Al_2O_3 matrix nanocomposites. Two different sized stabilized zirconia powders were used and both of the resulting nanocomposites were sintered at 1300˚C and 1500˚C. However, different than the studies on SiC particle dispersed nanocomposites, low temperature sintering behavior of Al_2O_3/YSZ$_p$ nanocomposites was studied at 1300˚C only for a single second phase content of 5 wt% YSZ.. This part of the investigation was mainly concentrated on the sintering studies at 1500˚C to make a better comparison between SiC and yttria stabilized ZrO_2 dispersed nanocomposites.

5 wt% partially stabilized ZrO_2 (3 mol% Y_2O_3) and stabilized ZrO_2 (8 mol% Y_2O_3) powders were added to alumina by mechanical mixing method and sintered at 1300˚C for 1 h by both conventional and microwave sintering techniques. Similar to Al_2O_3/SiC$_p$ nanocomposites, this temperature was insufficient to achieve full densification in Al_2O_3/YSZ$_p$ by conventional sintering.

Table 4.1 shows the densification, hardness and indentation toughness values of Al_2O_3/5 wt% ZrO_2 (3 mol%Y_2O_3) and Al_2O_3/5 wt% ZrO_2 (8 mol%Y_2O_3) nanocomposites, respectively. Prior to sintering green densities of all compacts were around 55±1% of the theoretical density. After sintering, although conventional sintered samples did not show any noticeable densification, microwave sintered nanocomposites revealed remarkable densifications values reaching to ~89% of their theoretical densities.

Table 4.1 Comparison of Al_2O_3/5 wt% ZrO_2 (3 mol%Y_2O_3) and Al_2O_3/5 wt% ZrO_2 (8 mol%Y_2O_3) nanocomposites sintered by conventional and microwave methods at 1300˚C for 1 h.

	Al_2O_3/5 wt% ZrO_2 (3 mol%Y_2O_3)		Al_2O_3/5 wt% ZrO_2 (8 mol%Y_2O_3)	
	Conventional Sintered	Microwave Sintered	Conventional Sintered	Microwave Sintered
Relative Density (%)	58.8	89.1	57.9	88.7
Hardness (GPa)	2.02±0.44	17.27±1.72	1.69±0.65	17.46±1.35
Fracture Toughness, K_c (MPa·m$^{1/2}$)	2.02±0.44	3.02±0.45	1.16±0.58	2.61 ±0.75

Figure 4.26 (a)–(d) shows the SEM micrographs of conventional and microwave sintered nanocomposites sintered at 1300˚C for 1 h. The microstructure formation under the applied condition presented in this figure is compatible with the one observed in Al_2O_3/SiC_p nanocomposites (Fig. 4.17) under identical sintering conditions. From these microstructures it is evident that conventional sintered nanocomposites are at the beginning of the intermediate stage of the solid state sintering process identified by the presence of an open pore network; where microwave sintered nanocomposites seem to be close to the final stage of the sintering process with the closed and isolated pore sturucture. In the case of the microwave sintered nanocomposites, YSZ particles are located on the grain boundaries pinning them, and thus providing finer grain size formation.

(a)   (b)

(c)   (d)
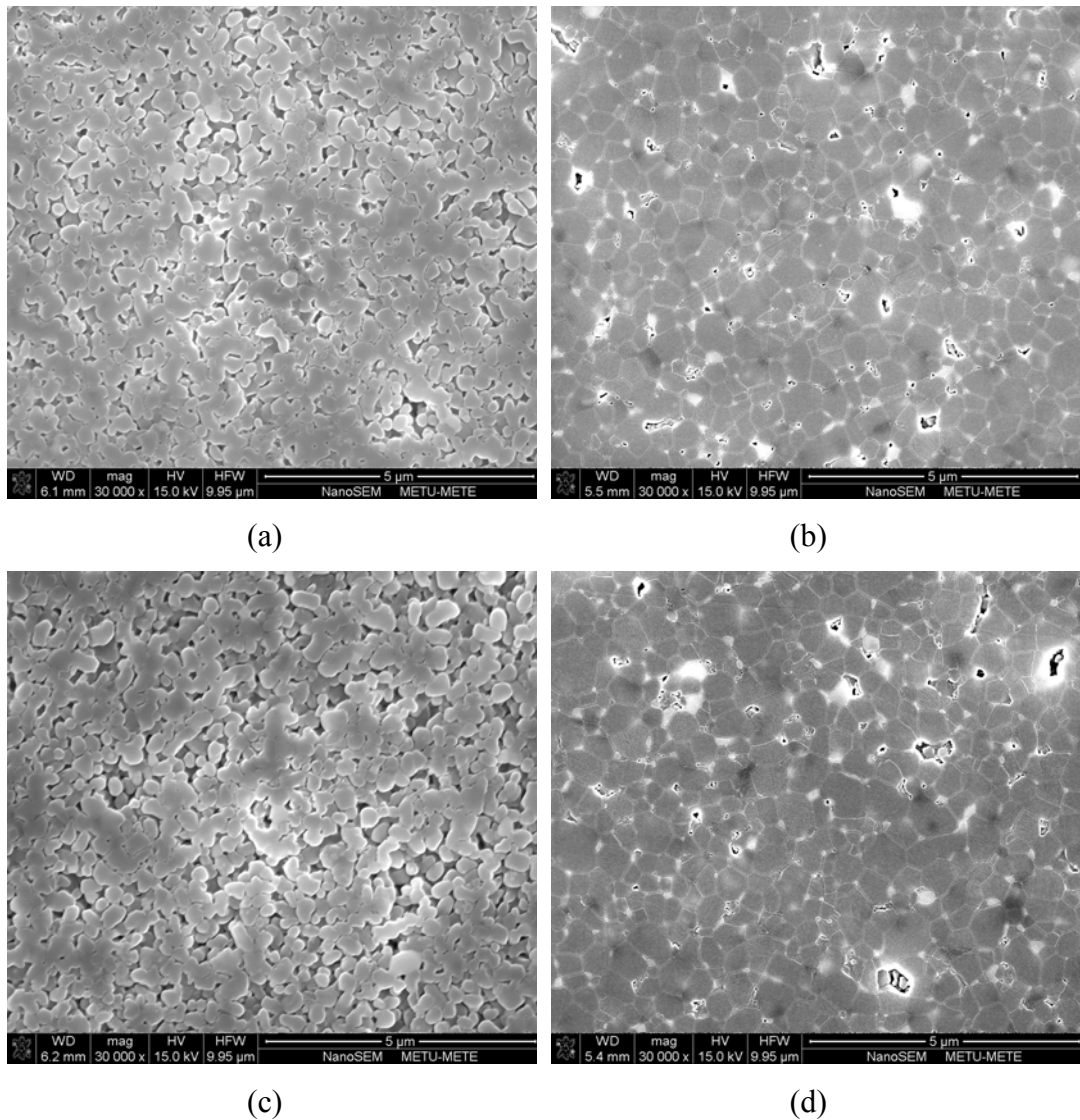
Figure 4.26 SEM micrographs of nanocomposites (a) Al_2O_3/5 wt% ZrO_2 (3 mol%Y_2O_3) conventionally sintered at 1300˚C, (b) Al_2O_3/5 wt% ZrO_2 (3 mol%Y_2O_3) microwave sintered at 1300˚C, (c) Al_2O_3/5 wt% ZrO_2 (8 mol%Y_2O_3) conventionally sintered at 1300˚C, (d) Al_2O_3/5 wt% ZrO_2 (8 mol%Y_2O_3) microwave sintered at 1300˚C.

Although densification, hardness and fracture toughness values and microstructure of microwave sintered nanocomposites are superior compared to those of the conventional sintered nanocomposites, sintering at 1300˚C was not sufficient to improve the mechanical properties of monolithic alumina by the second phase addition. As a result, to improve densification, hardness and fracture toughness and to make a clear comparison between the improvements achieved in

Al$_2$O$_3$/SiC$_p$ / and Al$_2$O$_3$/YSZ$_p$ nanocomposites, additional sintering experiments were conducted at 1500˚C for 1 h for stabilized zirconia dispersed nanocomposites. Furthermore, a brief comparison between the effect of identical particle sized partially stabilized and stabilized ZrO$_2$ powder addition on the properties of Al$_2$O$_3$ will be discussed.

Figure 4.27 shows the relative density change with the addition of partially stabilized zirconia (3 mol% Y$_2$O$_3$) for both conventional and microwave sintering. Increasing zirconia content decreased the densification as expected from the earlier studies due to similar reasons discussed above. However, the negative effect of zirconia addition on densification was less compared to that observed in SiC addition. This can be attributed to the thermal expansion coefficients of alumina and zirconia which are closer to each other than alumina and SiC. With 20 wt% ZrO$_2$ addition densification drops to ~88% of the theoretical density which has decreased to ~73% for the same amount of SiC addition.
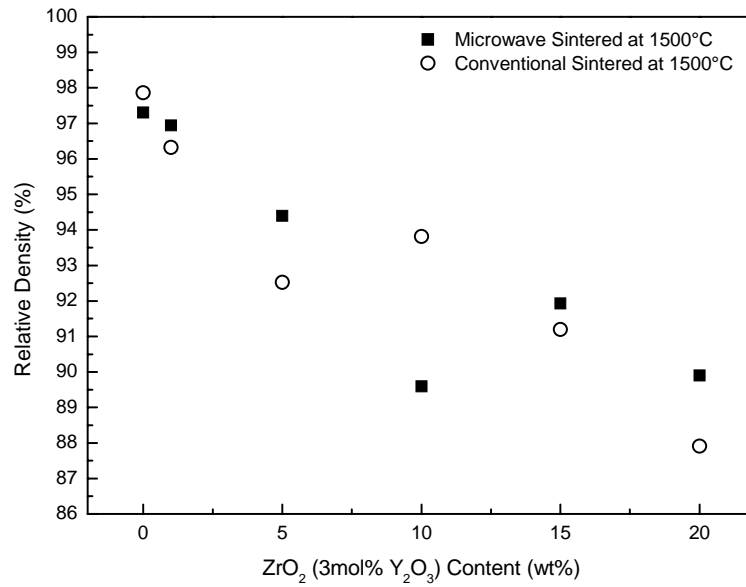
Figure 4.27 Change of densification with ZrO_2 (3mol% Y_2O_3) content for the nanocomposites sintered by both conventional and microwave method at 1500°C for 1 h.

Figure 4.28 shows the XRD spectra of 5 wt% partially stabilized ZrO_2 (3 mol% Y_2O_3) containing Al_2O_3 matrix nanocomposites both conventional and microwave sintered at 1500°C for 1 h. Obtained XRD patterns revealed that independent of the applied technique processed composites mainly contain Al_2O_3 and Yttrium Zirconium Oxide (ICDD 30-1468) phases as expected.
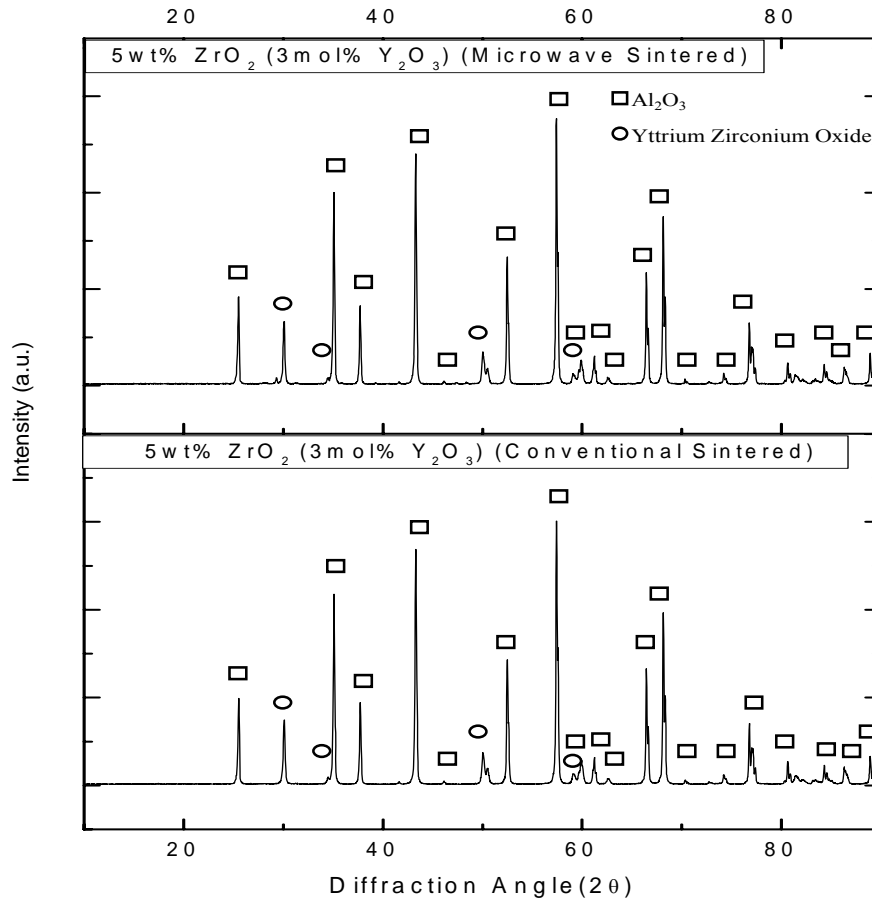
Figure 4.28 XRD spectra of 5 wt% partially stabilized ZrO_2/Al_2O_3 matrix nanocomposites after conventional and microwave sintering at 1500˚C for 1 h.

Figure 4.29 shows the microstructure of Al_2O_3/partially stabilized ZrO_2 (3 mol%Y_2O_3) particle nanocomposites. It is clear that addition of partially stabilized ZrO_2 particles as the second phase inhibits grain growth compared to monolithic Al_2O_3 as discussed in section 4.1. The nanocomposites which contains 1 wt% partially stabilized ZrO_2 (is the only exception of this observation where abnormal grain growth occured. Unlike the ZrO_2 particles (white particles in the micrographs) either located on the grain boundaries or on the tripol junctions for higher second phase contents, in the case of 1 wt% addition ZrO_2 particles seem to be trapped within the grains leading to observed abnormal grain growth due to inefficient particle-grain boundary interactions.

(a)

(b)

(c)

(d)
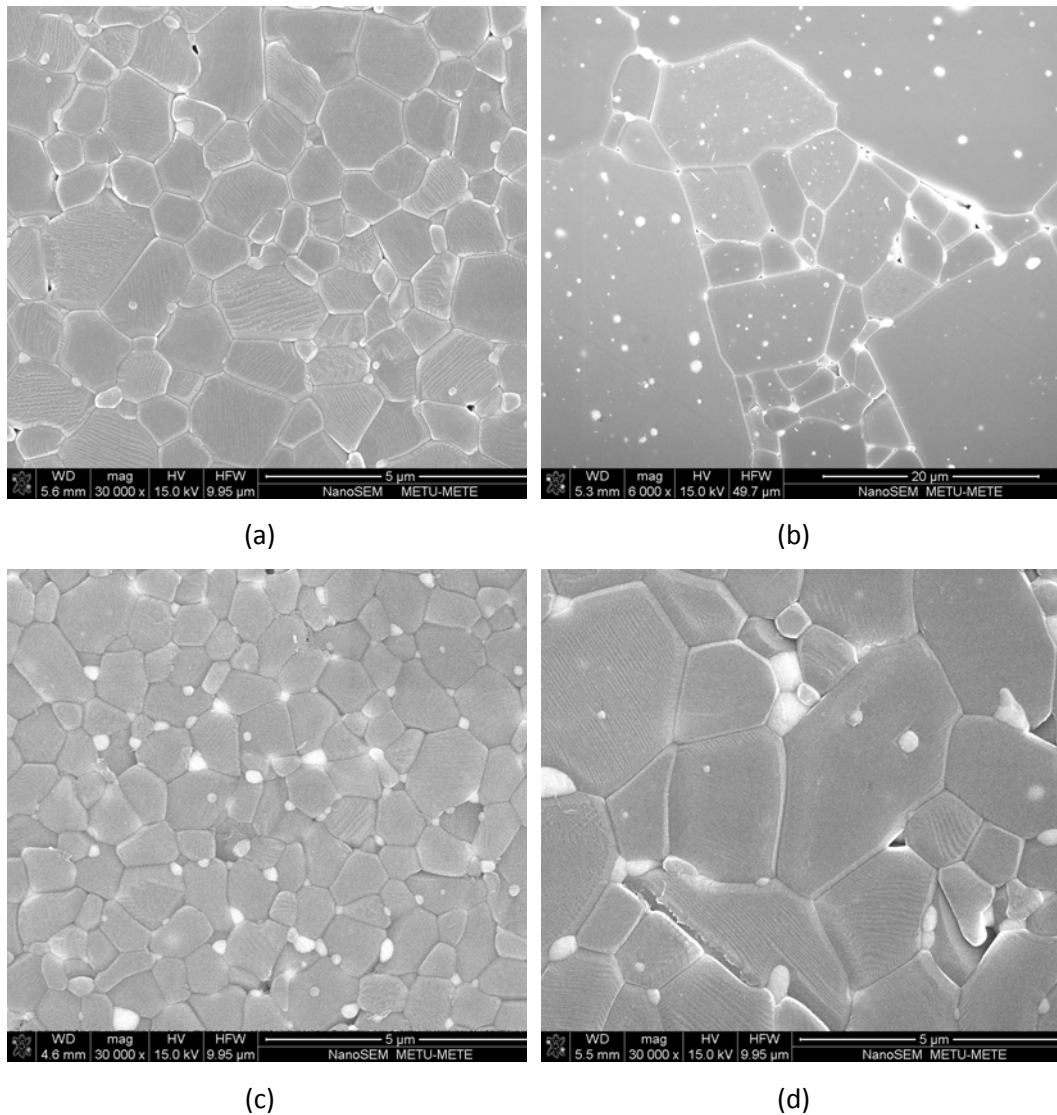
Figure 4.29 Microstructural changes of Al$_2$O$_3$/partially stabilized ZrO$_2$ (3mol% Y$_2$O$_3$) nanocomposites processed by conventional and microwave sintering at 1500˚C for 1 h (a) conventional sintered Al$_2$O$_3$/1 wt% ZrO$_2$, (b) microwave sintered Al$_2$O$_3$/1 wt% ZrO$_2$, (c) conventional sintered Al$_2$O$_3$/5 wt% ZrO$_2$, (d) microwave sintered Al$_2$O$_3$/5 wt% ZrO$_2$, (e) conventional sintered Al$_2$O$_3$/10 wt% ZrO$_2$, (f) microwave sintered Al$_2$O$_3$/10 wt% ZrO$_2$, (g) conventional sintered Al$_2$O$_3$/15 wt% ZrO$_2$, (h) microwave sintered Al$_2$O$_3$/15 wt% ZrO$_2$, (i) conventional sintered Al$_2$O$_3$/20 wt% ZrO$_2$, (j) microwave sintered Al$_2$O$_3$/20 wt% ZrO$_2$.
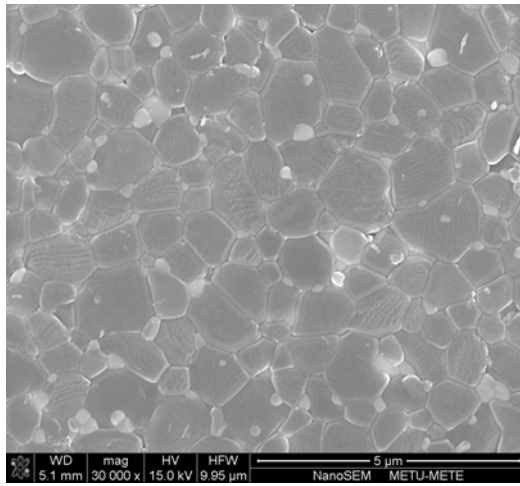
(e)
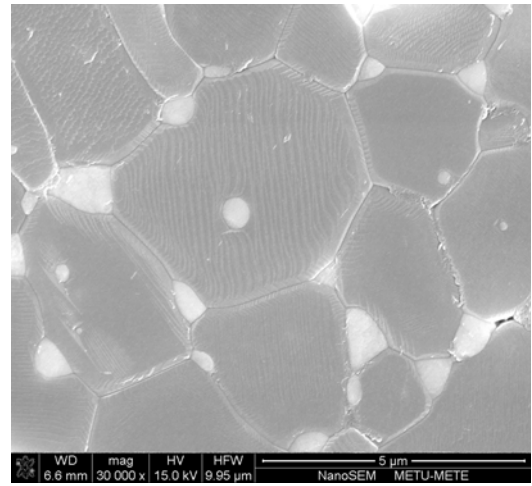
(f)
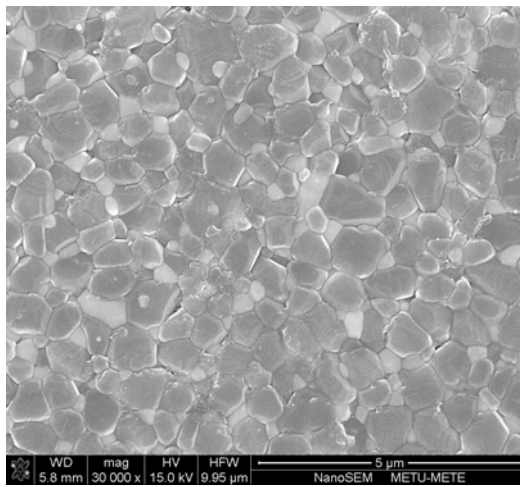
(g)
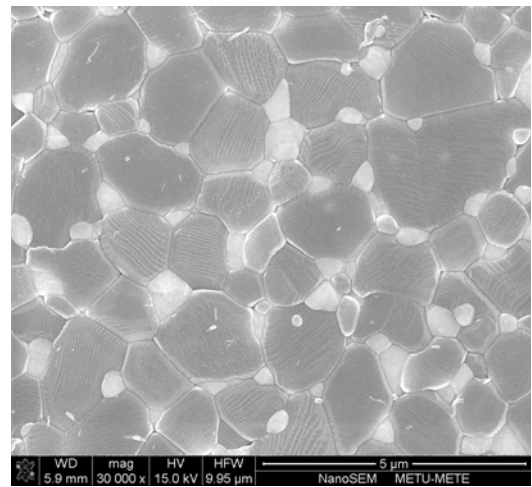
(h)
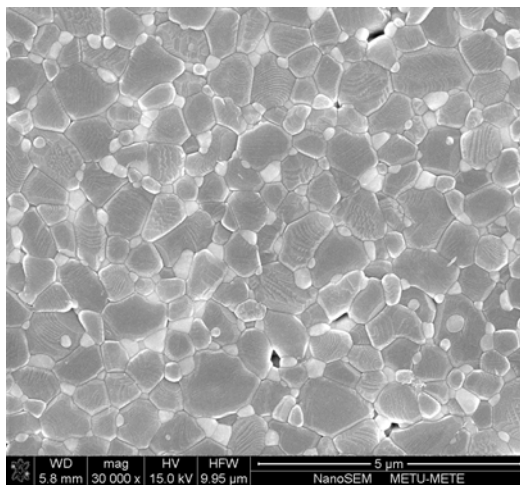
(i)
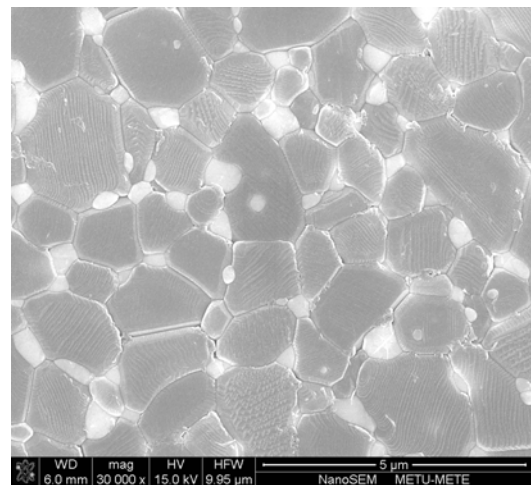
(j)

Figure 4.29 (Continued)

Figure 4.30 shows the change of hardness of the nanocomposites with increasing partially stabilized ZrO_2 (3 mol% Y_2O_3) content. Although densification decreased up to ~88% of the theoretical density, hardness remained at the same level with that of the monolithic Al_2O_3. Moreover, small addition of YSZ (1 wt%) increased the hardness value which is consistent with the previous studies in the literature which reported that the addition of a small amount of ZrO_2 nanoparticles to Al_2O_3 reduced the grain size of Al_2O_3 matrix grains enhancing its strength [58, 65]. Although there is not a reduction in the grain size in this study (Fig.4.29-b) in the case of 1wt% YSZ_p addition contrarily to the results of the previous study similar hardess increase obtained.
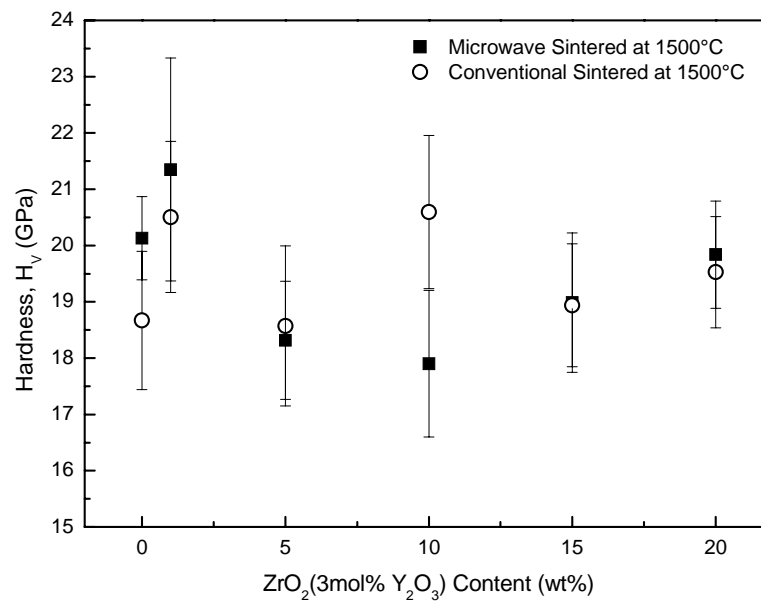
Figure 4.30 Hardness of nanocomposites as function of partially stabilized ZrO_2 (3 mol% Y_2O_3) content sintered by both conventional and microwave method at 1500˚C for 1 h.

Figure 4.31 shows the change of indentation fracture toughness of the nanocomposites as a function of partially stabilized ZrO_2 (3 mol% Y_2O_3) content. The highest fracture toughness was obtained for Al_2O_3/5 wt% ZrO_2 nanocomposite. This increase can be attributed to the formation of microcracking in the structure resulting from the thermal expansion mismatch between alumina and stabilized zirconia which are $8.8 \times 10^{-6 \circ}C^{-1}$ and $10.5 \times 10^{-6 \circ}C^{-1}$, respectively. At higher second phase additions, indentation fracture toughness starts to decrease with increasing ZrO_2 content mainly due to reduction in densification. Although indentation fracture toughness follows a decreasing trend at high additive contents because of the densification drop, measured values for the nanocomposites are still comparable to that of the monolithic Al_2O_3.
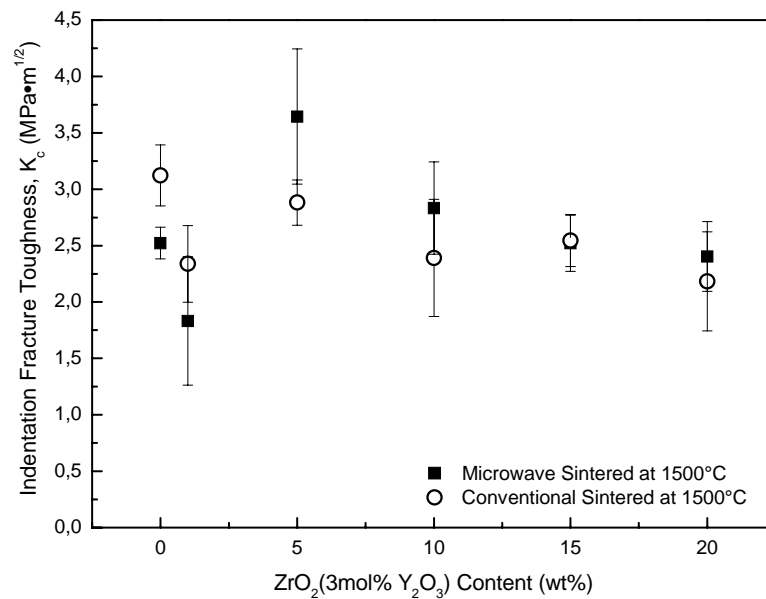
Figure 4.31 Indentation fracture toughness of the nanocomposites processed by microwave and conventional sintering at 1500°C for 1 h as function of partially stabilized ZrO_2 (3 mol% Y_2O_3) content.

8 to 15 mol% Y_2O_3 is added to ZrO_2 to inhibit polymorphic transformation from tetragonal or cubic phase to monoclinic phase. Such ceramics are called fully stabilized zirconia. In literature generally studies have focused on alumina/partially stabilized zirconia composites and their properties. However, usage of fully stabilized zirconia could be useful to improve mechanical properties of alumina as well.

For this reason, in the present study ZrO_2 fully stabilized with the addition of 8 mol% Y_2O_3 has also been used as a second phase dispersion in Al_2O_3 matrix nanocomposites. Figure 4.32 shows the change in densification of Al_2O_3/stabilized ZrO_2 (8 mol% Y_2O_3) nanocomposites for five different additive contents. The decrease in the densification with the addition of stabilized ZrO_2 is evident from this figure as in the case of SiC and partially stabilized zirconia additions. However, different than the other results following an initial drop densification did not show considerable ZrO_2 dependence. This can be attributed to the locating of second phase particles preferentially on the grain boundaries rather than being trapped within the grains. As a consequence, both pore elimination and suppression of excessive grain boundary mobility seem to be balanced leading to the uniform densification behavior.
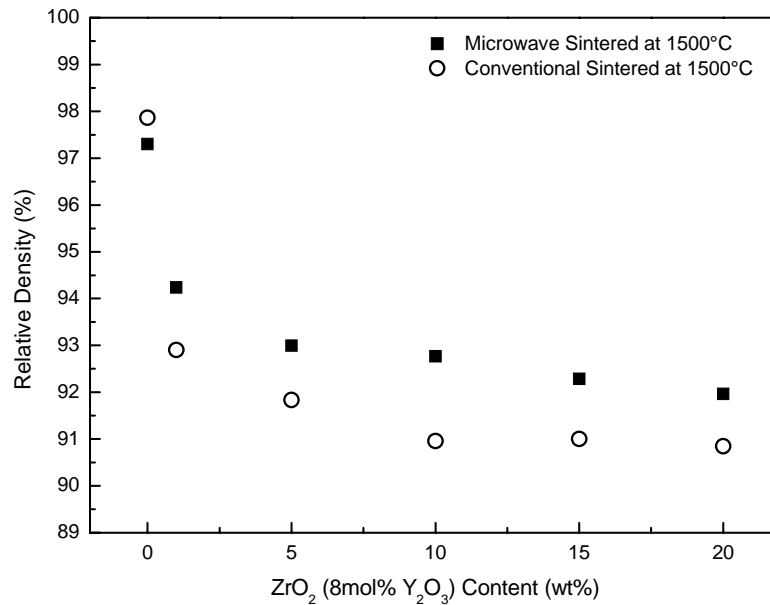
Figure 4.32 Change in densification with ZrO_2 (8 mol% Y_2O_3) content for the nanocomposites sintered by both conventional and microwave method at 1773 K for 1 h.

Figure 4.33 shows XRD spectra of 5 wt% stabilized ZrO_2 (8 mol% Y_2O_3) containing Al_2O_3 matrix nanocomposites sintered by either conventional or microwave methods at 1500°C for 1 h. Observed results are similar to those of Al_2O_3 /partially stabilized ZrO_2 (3 mol%Y_2O_3) nanocomposites. Detected peaks belong to Al_2O_3 and Yttrium Zirconium Oxide phases. However, in the case of microwave sintered Al_2O_3 /5wt% stabilized ZrO_2 nanocomposite, mullite peaks are present in the spectrum most probably caused by deposition of mullite on the surface of the sintered body due to decomposition of the susceptor material (SiC) interacting with the Al_2O_3 in the system under the sintering temperatures applied.
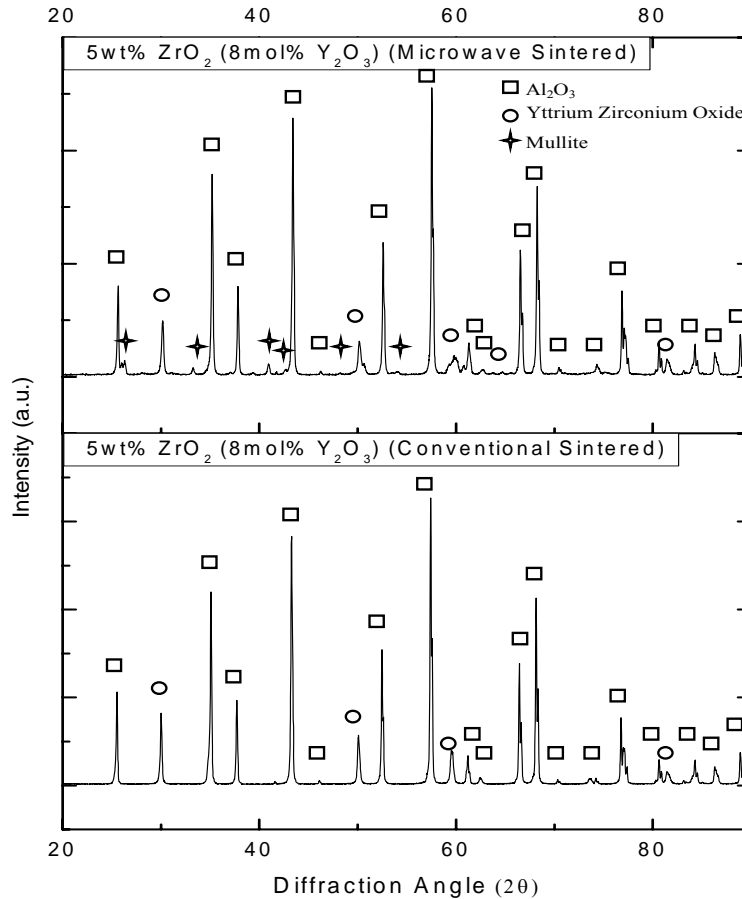
Figure 4.33 XRD spectra of 5 wt% stabilized ZrO_2 (8 mol% Y_2O_3) containing Al_2O_3 matrix nanocomposites sintered by either conventional or microwave methods at 1500°C for 1 h.

Comparison of the microstructures of Al_2O_3/stabilized ZrO_2 composites showed similar behavior with the one observed in partially stabilized zirconia added Al_2O_3 nanocomposites (Fig. 34.a - j). With increasing ZrO_2 content, grain size of the matrix decreased especially in the case of conventional sintered nanocomposites. Microwave sintered materials reveal higher average grain size than conventional sintered composites. Similar to Al_2O_3/partially stabilized zirconia nanocomposite, microwave sintered 1 wt% stabilized ZrO_2 containing Al_2O_3 also showed abnormal grain growth. However, this time structure appears to be more porous. The difference in grain size could be one of the reasons of enhanced densification

achieved by microwave sintering compared to that obtained by conventional sintering.

Furthermore, microstructural observations on all fabricated materials including SiC and ZrO_2 dispersed Al_2O_3 nanocomposites revealed that second phase particles generally pin the grain boundaries limiting their mobility, and thus leading to a decrease in the average grain size of the fabricated nanocomposites. Nevertheless, with the increasing grain growth rate, as in the case of the microwave sintering, grain boundaries rip off the second phase particles leaving them trapped within the grains. Such a high grain boundary mobility also sets a barrier against effective pore elimination leading to isolated intragranular porosity detrimental for full densification.

(a)

(b)

(c)

(d)
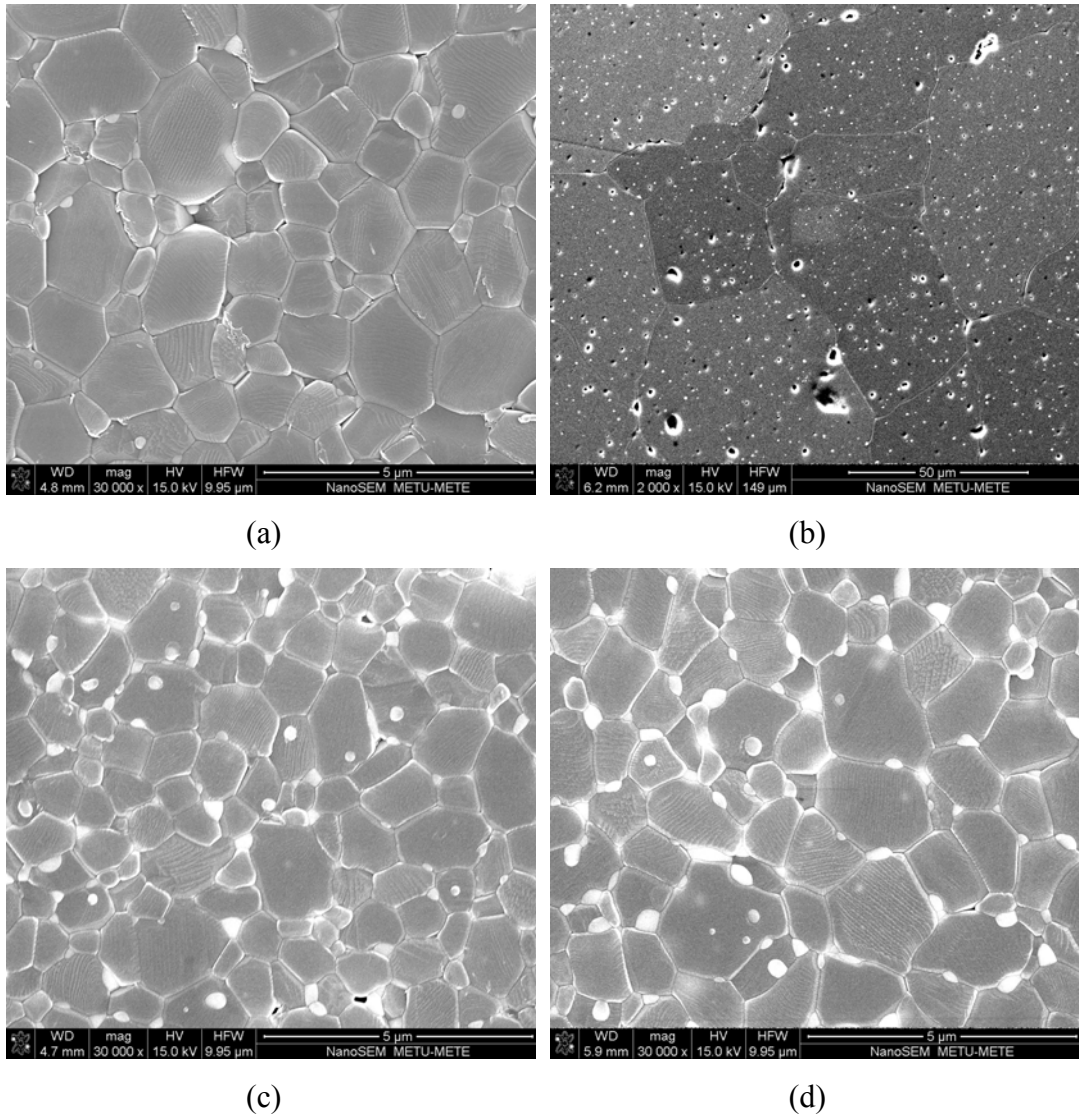
Figure 4.34 Microstructural comparison of Al_2O_3/stabilized ZrO_2 (8 mol% Y_2O_3) nanocomposites processed by conventional and microwave sintering at 1500°C for 1 h (a) conventional sintered Al_2O_3/1 wt% stabilized ZrO_2, (b) microwave sintered Al_2O_3/1 wt% stabilized ZrO_2, (c) conventional sintered Al_2O_3/5 wt% stabilized ZrO_2, (d) microwave sintered Al_2O_3/5 wt% stabilized ZrO_2, (e) conventional sintered Al_2O_3/10 wt% stabilized ZrO_2, (f) microwave sintered Al_2O_3/10 wt% stabilized ZrO_2, (g) conventional sintered Al_2O_3/15 wt% stabilized ZrO_2, (h) microwave sintered Al_2O_3/15 wt% stabilized ZrO_2, (i) conventional sintered Al_2O_3/20 wt% stabilized ZrO_2, (j) microwave sintered Al_2O_3/20 wt% stabilized ZrO_2.
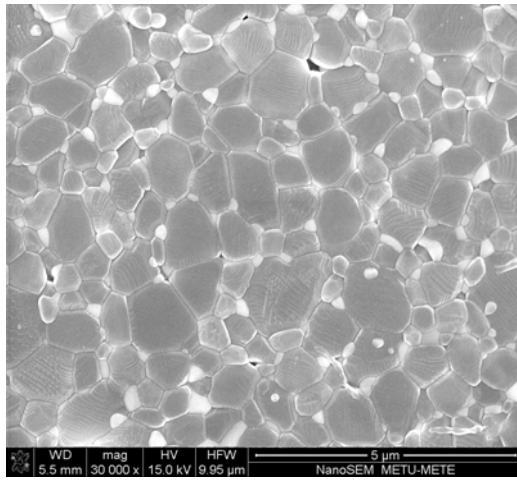
(e)
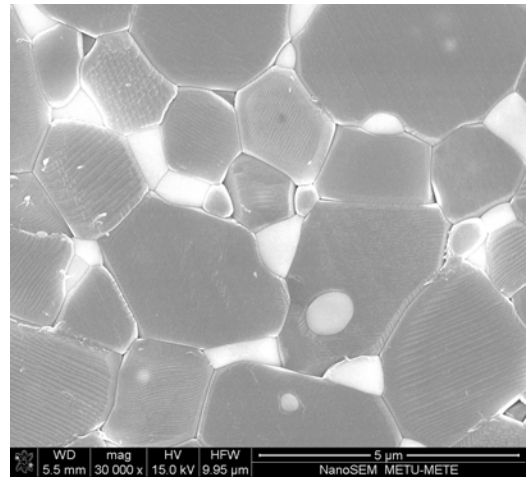
(f)
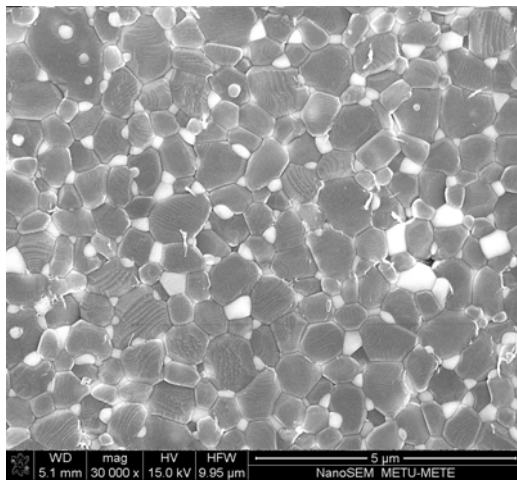
(g)
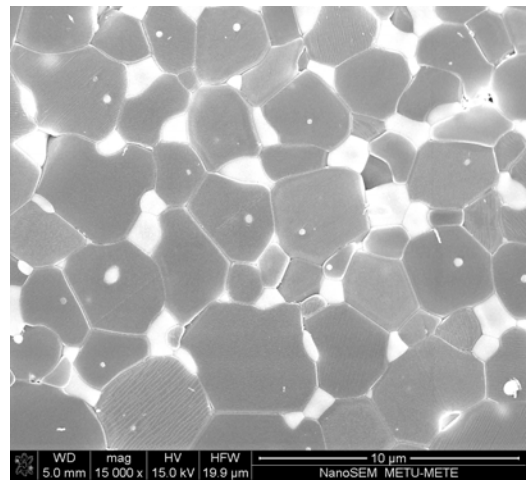
(h)
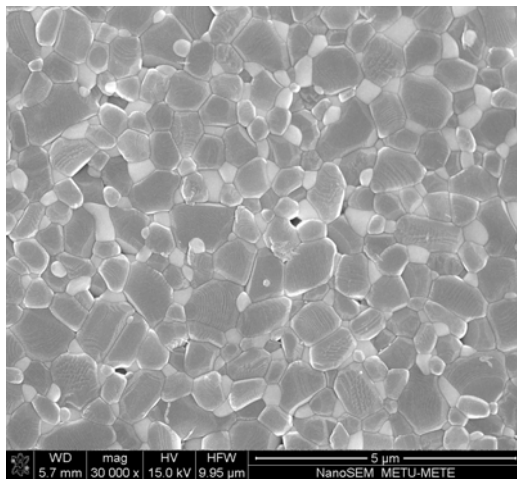
(i)
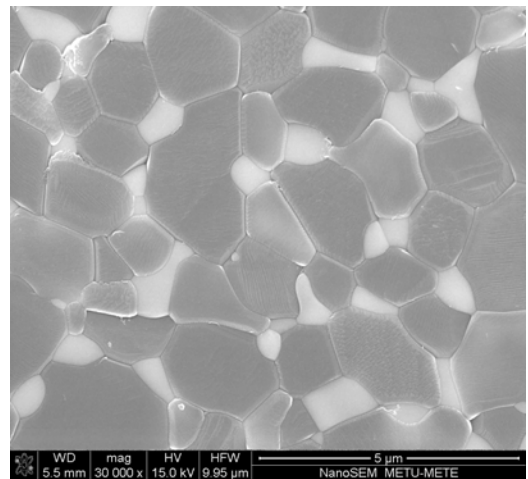
(j)

Figure 4.34(Continued)

In Fig. 4.35, hardness of Al_2O_3/stabilized ZrO_2 (8mol% Y_2O_3) nanocomposites is presented for varying second phase content. In the case of stabilized zirconia addition, hardness of the nanocomposites did not show a strong second phase content dependence. There is a slight fluctuation in the measured hardness values for all compositions which is almost within the error margin of the measurements. This observation can be attributed firstly to the lower densification of nanocomposites with respect to monolithic Al_2O_3, and secondly to the weak grain boundary structure because of thermal expansion mismatch between the matrix and the second phase particles. In order to make a more accurate comparison, investigations have to be done on fully densified nanocomposites and corresponding monolithic matrix.
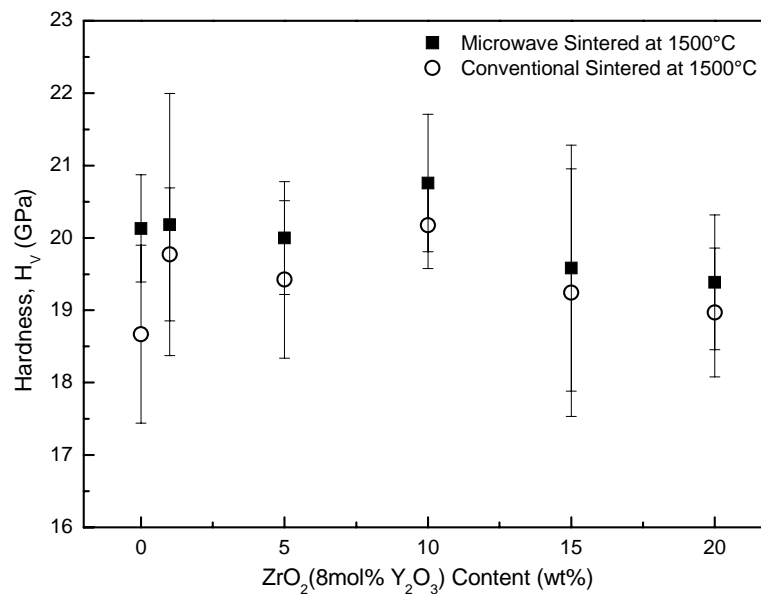
Figure 4.35 Hardness of nanocomposites as function of fully stabilized ZrO_2 (8 mol% Y_2O_3) content sintered by both conventional and microwave method at 1500°C for 1 h.

As can be seen in Fig. 4.36 indentation fracture toughness of the Al_2O_3/stabilized zirconia, nanocomposites showed very similar trend with Al_2O_3/partially stabilized zirconia materials. Both types of Al_2O_3/zirconia nanocomposites showed lower indentation fracture toughness values with respect to Al_2O_3/SiC_p nanocomposites, although they reveal higher densification and hardness which can be attributed to the considerably larger particle size of the zirconia compared to SiC along with the relative thermal expansion coefficient differences between Al_2O_3, SiC and ZrO_2. Zirconia has the highest thermal coefficient among these ceramics causing it to shrink more during cooling stage than Al_2O_3 which creates residual compressive stresses at the particle/matrix interface. As a result of this, the efficiency of crack impediment by the relatively large zirconia particles surrounded by a compressive stress field decreases. For the effective crack impediment, particle/matrix interface should reveal a controlled "weakness" mostly by the presence of limited residual tensile stresses so that crack deflection can operate leading to a net increase in the total path of the advancing crack. Despite this fact indentation fracture toughness values of Al_2O_3/zirconia nanocomposites are still between 2.0 to 3.5 $MPa.m^{1/2}$ range which is due to the fine average grain size and crack impediment by the second phase particles.

On the other hand, Al_2O_3/SiC_p nanocomposites revealed indentation fracture toughness improvement with increasing SiC particle content. Lower thermal expansion coefficient of SiC compared to Al_2O_3 matrix results in the formation of residual tensile stresses at the particle/matrix interface upon cooling from the process temperature. Consequently, nanometer sized SiC particles homogeneously distributed within the Al_2O_3 matrix, which posses a residual tensile stress field around them, are extremely effective in deflecting an advancing crack, and hence dissipating its energy leading to an enhancement in fracture toughness.
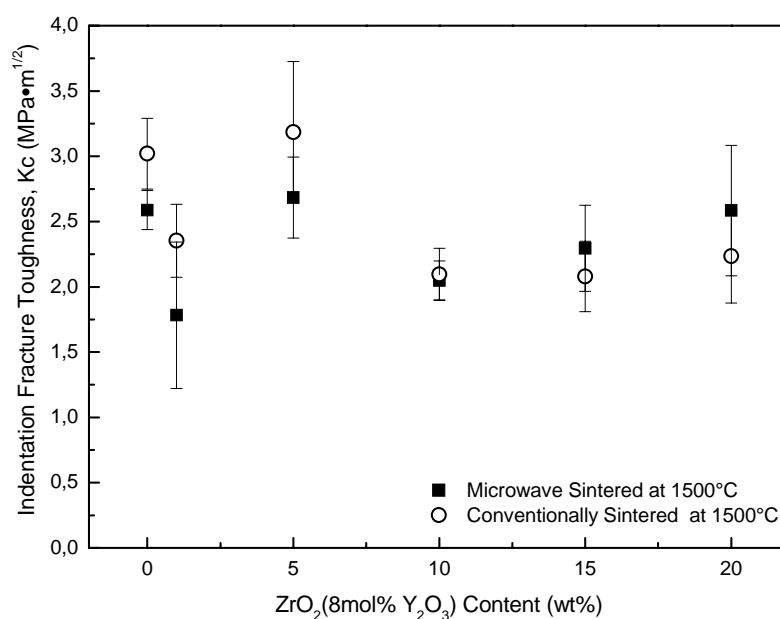
Figure 4.36 Indentation toughness of the nanocomposites processed by microwave and conventional sintering at 1500°C for 1 h as function of ZrO_2 (8mol% Y_2O_3) content.

Figure 4.37 shows fracture surfaces of Al_2O_3/5 wt% ZrO_2 (3 mol% Y_2O_3) and Al_2O_3/5 wt% ZrO_2 (8 mol% Y_2O_3) nanocomposites as representative for all Al_2O_3/YSZ_p nanocomposites. All of the Al_2O_3 matrix nanocomposites independent of the type or amount of the ZrO_2 addition revealed intergranular fracture as evident from the fractographs provided in Fig. 4.34.

<div align="center">(a)   (b)</div>
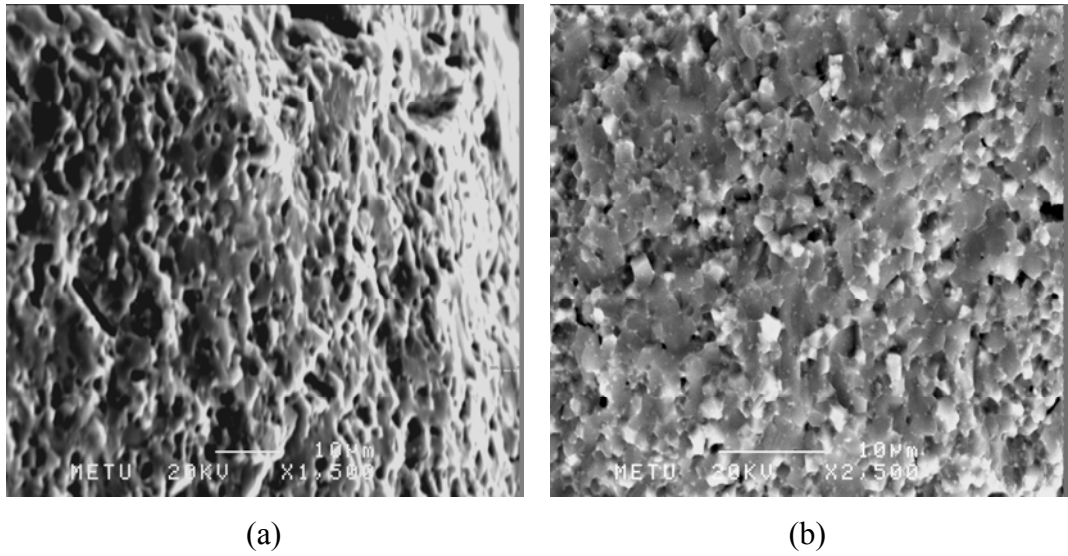
Figure 4.37 Fracture surfaces of Al_2O_3/ZrO_2 nanocomposites microwave sintered at 1500˚C for 1 hour (a) Al_2O_3/5 wt% ZrO_2 (3 mol% Y_2O_3), (b) Al_2O_3/5 wt% ZrO_2 (8 mol% Y_2O_3).

CHAPTER 5

CONCLUSIONS

In the present study, effect of microwave sintering on the densification, microstructural evolution and mechanical properties of monolithic Al_2O_3 with or without sintering additives as well as of nanometer-sized SiC or YSZ particle-dispersed Al_2O_3 matrix nanocomposites containing varying amounts of second phase particles has been studied in comparison to conventional sintering. To understand the effect of microwave sintering on the resulting properties of the matrix material used in this study, preliminary experiments were conducted on monolithic plain Al_2O_3 at temperatures between 1000˚C and 1600˚C. In addition to this, three different types of sintering aids (MgO, CaO, Y_2O_3) were added to Al_2O_3 to enhance its densification by eliminating abnormal grain growth. According to the results achieved from the experiments on monolithic Al_2O_3, microwave and conventional sintering studies on Al_2O_3 matrix nanocomposites were conducted at two different selected temperatures, which were 1300˚C and 1500˚C. These were the lowest applied temperatures revealing a reasonably high densification level in monolithic Al_2O_3 by microwave sintering. As a result of this study, the following conclusions can be drawn:

1. Microwave heating is more effective in sintering Al_2O_3 compared to conventional pressureless sintering especially at lower temperatures (<1400˚C). To achieve comparable microstructures and mechanical properties, conventional sintering has to be conducted at temperatures ~200˚C higher than those used for microwave sintering. Consequently, microwave sintering provides energy and time saving owing to its higher efficiency.

2. Hardness and indentation fracture toughness values of monolithic Al_2O_3 increased with densification achieved at higher sintering temperatures. Especially elimination of residual pores with increased temperature had a positive effect on hardness of monolithic Al_2O_3 resulting in a tendency which is in accordance with the Hall-Petch relationship. However, as a result of abnormal grain growth hardness and fracture toughness values started to decrease for both conventional and microwave sintering after 1500˚C.

3. Incorporation of SiC and YSZ particles to form Al_2O_3/SiC_p and Al_2O_3/YSZ_p nanocomposites caus es reduction in densification rate compared to monolithic Al_2O_3 for both conventional and microwave sintering methods. However, the negative effect of zirconia addition on densification was less pronounced compared to that observed in SiC addition.

4. Hardness values of the Al_2O_3/SiC_p nanocomposites are considerably lower than that of the monolithic Al_2O_3 due to the inefficient densification at the selected sintering temperatures of 1300˚C and 1500˚C. Hardness of the nanocomposites did not show a strong second phase content dependence.

5. For both of the sintering methods SiC addition improved indentation toughness of monolithic Al_2O_3. Especially in microwave sintering, fracture mode of Al_2O_3 changed from inter to transgranular by the addition of SiC particles.

6. At higher second phase contents, indentation fracture toughness of Al_2O_3/YSZ_p nanocomposites starts to decrease mainly due to reduction in densification.

7. Resulting nanocomposites revealed poorer densification, and hence hardness compared to monolithic Al_2O_3; however, they showed remarkable improvement in fracture toughness corresponding to crack growth impediment caused by the crack deflection at the dispersed particles as well as at the grain boundaries.

Following remarks could be stated for possible future studies in the field of microwave sintering of alumina-based ceramics to complete and improve the results achieved in this study. Firstly, higher sintering temperatures could be applied for the processing of alumina matrix nanocomposites to obtain higher densification levels. Shorter sintering periods at higher temperatures could be applied in order to demonstrate the pronounced efficiency of microwave sintering compared to its conventional counterpart. These studies could be supported by complementary XRD analyses to provide insights on the effects of the resulting phase content on the mechanical properties of the fabricated alumina matrix nanocomposites. Furthermore, microwave sintering behavior of the polymorphs of Al_2O_3 could be studied in comparison to conventional sintering.

REFERENCES

1. Wang, F., K. Zhang, and G. Wang, *Texture in superplastically deformed alumina-zirconia composites.* Materials Science and Engineering A, 2008. **491**(1-2): p. 476-482.

2. Barsoum, M.W., *Fundamentals of Ceramics.* Materials Science and Engineering, ed. B.C.a.M.J. Goringe. 2003, UK: IOP Publishing Ltd.

3. Rahaman, M.N., *Sintering of Ceramics.* 2008, USA: CRC Press.

4. A. M. Guzmán, P.Rodriguez and.E.Sereno, *Development of AZS Refractories for the Glass Industry.* Advances in Technology of Materials and Materials Processing 2004. **6**: p. 69-76

5. De Jonghe, L.C. and M.N. Rahaman, *4.1 Sintering of Ceramics*, in *Handbook of Advanced Ceramics.* 2003, Academic Press: Oxford. p. 187-264.

6. Thümmler, F. and R. Oberacker, *An Introduction to Powder Metallurgy*, ed. I. Jenkins and J.V. Wood. 1993, London: The Institute of Materials.

7. German, R.M., *Sintering Theory and Practice.* 1996, New York, NY: A Wiley-Interscience Publication.

8. Lange, F.F., *Powder processing science and technology for increased reliability.* Journal of the American Ceramic Society, 1989. **72**(1): p. 3-15.

9. Reed, J.S., *Introduction to the principles of ceramic processing.* 1988, New York : Wiley: A Wiley-Interscience publication.

10. Gupta, M. and E. Wong Wai Leong, *Microwaves and Metals.* 2007, Singapore: John Wiley & Sons (Asia) Pte Ltd.

11. Serway, R.A., *Physics for Scientists and Engineers with Modern Physics.* Third ed. Saunders Golden Sunburst Series. 1992, Orlando, Florida: Saunders College Publishing.

12. Katz, J.D., *Microwave sintering of ceramics.* Annual Review of Materials Science, 1992. **22**(1): p. 153-170.

13. Janney, M.A., C.L. Calhoun, and H.D. Kimrey, *Microwave Sintering of Solid Oxide Fuel Cell Materials: I, Zirconia-8 mol% Yttria.* Journal of the American Ceramic Society, 1992. **75**(2): p. 341-346.

14. Freer, R. and F. Azough, *Microstructural engineering of microwave dielectric ceramics.* Journal of the European Ceramic Society, 2008. **28**(7): p. 1433-1441.

15. Viswanathan, V., T. Laha, K. Balani, A. Agarwal, and S. Seal, *Challenges and advances in nanocomposite processing techniques.* Materials Science and Engineering R: Reports, 2006. **54**(5-6): p. 121-285.

16. Thostenson, E.T. and T.W. Chou, *Microwave processing: fundamentals and applications.* Composites Part A: Applied Science and Manufacturing, 1999. **30**(9): p. 1055-1071.

17. Brosnan, K.H., G.L. Messing, and D.K. Agrawal, *Microwave sintering of alumina at 2.45 GHz.* Journal of the American Ceramic Society, 2003. **86**(8): p. 1307-1312.

18. Xie, Z., J. Yang, and Y. Huang, *Densification and grain growth of alumina by microwave processing.* Materials Letters, 1998. **37**(4-5): p. 215-220.

19. Wilson, J. and S.M. Kunz, *Microwave Sintering of Partially Stabilized Zirconia.* Journal of the American Ceramic Society, 1988. **71**(1): p. C-40-C-41.

20. Agrawal, D.K., *Microwave processing of ceramics.* Current Opinion in Solid State and Materials Science, 1998. **3**(5): p. 480-485.

21. Nath, S., B. Basu, and A. Sinha, *A comparative study of conventional sintering with microwave sintering of hydroxyapatite synthesized by chemical route.* Trends in Biomaterials and Artificial Organs, 2006. **19**(2): p. 93-98.

22. Lee, W.E. and W.M. Rainfoth, *Ceramic Microstructures, Property control by processing.* First ed. 1994, London: Chapman & Hall, 2-6 Boundary Row, London SE1 8HN, UK.

23. Xie, Z., J. Yang, X. Huang, and Y. Huang, *Microwave processing and properties of ceramics with different dielectric loss.* Journal of the European Ceramic Society, 1999. **19**(3): p. 381-387.

24. Tian, Y.L., D.L. Johnson, and M.E. Brodwin, *Ultrafine Microstructure of Al_2O_3 Produced by Microwave Sintering*, in *Ceramic Transactions, Vol. 1, Ceramic Powder Science IIB*, G.L. Messing, E.R. Fuller, and H. Hausner, Editors. 1988, American Ceramic Society: Westerville, OH. p. 925-32.

25. Cheng, J., D. Agrawal, Y. Zhang, and R. Roy, *Microwave sintering of transparent alumina.* Materials Letters, 2002. **56**(4): p. 587-592.

26. Choi, S.M. and H. Awaji, *Nanocomposites - A new material design concept.* Science and Technology of Advanced Materials, 2005. **6**(1): p. 2-10.

27. Dong, Y.L., F.M. Xu, X.L. Shi, C. Zhang, Z.J. Zhang, J.M. Yang, and Y. Tan, *Fabrication and mechanical properties of nano-/micro-sized Al_2O_3/SiC composites.* Materials Science and Engineering A, 2009. **504**(1-2): p. 49-54.

28. Ohji, T., A. Nakahira, T. Hirano, and K. Niihara, *Tensile creep behavior of alumina/silicon carbide nanocomposite.* Journal of the American Ceramic Society, 1994. **77**(12): p. 3259-3262.

29. Limpichaipanit, A. and R.I. Todd, *The relationship between microstructure, fracture and abrasive wear in Al_2O_3/SiC nanocomposites and microcomposites containing 5 and 10% SiC.* Journal of the European Ceramic Society, 2009. **29**(13): p. 2841-2848.

30. Ortiz-Merino, J.L. and R.I. Todd, *Relationship between wear rate, surface pullout and microstructure during abrasive wear of alumina and alumina/SiC nanocomposites.* Acta Materialia, 2005. **53**(12): p. 3345-3357.

31. Chen, H.J., W.M. Rainforth, and W.E. Lee, *Wear behavior of Al_2O_3-SiC ceramic nanocomposites.* Scripta Materialia, 2000. **42**(6): p. 555-560.

32.   Deng, Z.Y., J.L. Shi, Y.F. Zhang, D.Y. Jiang, and J.K. Guo, *Pinning Effect of SiC Particles on Mechanical Properties of Al$_2$O$_3$-SiC Ceramic Matrix Composites.* Journal of the European Ceramic Society, 1998. **18**(5): p. 501-508.

33.   Ohji, T., T. Hirano, A. Nakahira, and K. Niihara, *Particle/matrix interface and its role in creep inhibition in alumina/silicon carbide nanocomposites.* Journal of the American Ceramic Society, 1996. **79**(1): p. 33-45.

34.   Dong, Y.L., F.M. Xu, X.L. Shi, C. Zhang, Z.J. Zhang, J.M. Yang, and Y. Tan, *Fabrication and mechanical properties of nano-/micro-sized Al$_2$O$_3$/SiC composites.* Materials Science and Engineering A, 2009. **504**(1-2): p. 49-54.

35.   Niihara, K., *New design concept of structural ceramics. Ceramic nanocomposites.* Journal of the Ceramic Society of Japan. International ed., 99 (10), 1991: p. 945-952.

36.   Levin, I., W.D. Kaplan, D.G. Brandon, and A.A. Layyous, *Effect of SiC submicrometer particle size and content on fracture toughness of alumina-SiC 'nanocomposites'.* Journal of the American Ceramic Society, 1995. **78**(1): p. 254-256.

37.   Perez-Rigueiro, J., J.Y. Pastor, J. Llorca, M. Elices, P. Miranzo, and J.S. Moya, *Revisiting the mechanical behavior of alumina/silicon carbide nanocomposites.* Acta Materialia, 1998. **46**(15): p. 5399-5411.

38.   Sciti, D., J. Vicens, and A. Bellosi, *Microstructure and properties of alumina-SiC nanocomposites prepared from ultrafine powders.* Journal of Materials Science, 2002. **37**(17): p. 3747-3758.

39.   Deng, Z.Y., Y. Zhou, M.E. Brito, J.F. Yang, and T. Ohji, *Fracture-Mode Change in Alumina-Silicon Carbide Composites Doped with Rare-Earth Impurities.* Journal of the American Ceramic Society, 2003. **86**(10): p. 1789-1792.

40.   Perez-Rigueiro, J., J.Y. Pastor, J. Llorca, M. Elices, P. Miranzo, and J.S. Moya, *Revisiting the mechanical behavior of alumina/silicon carbide nanocomposites.* Acta Materialia, 1998. **46**(15): p. 5399-5411.

41.   Xu, Y., A. Zangvil, and A. Kerber, *SiC Nanoparticle-Reinforced Al$_2$O$_3$ Matrix Composites: Role of Intra- and Intergranular Particles.* Journal of the European Ceramic Society, 1997. **17**(7): p. 921-928.

42.   Zhao, J., L.C. Stearns, M.P. Harmer, H.M. Chan, and G.A. Miller, *Mechanical behavior of alumina-silicon carbide 'nanocomposites'.* Journal of the American Ceramic Society, 1993. **76**(2): p. 503-510.

43.   Wu, H.Z., C.W. Lawrence, S.G. Roberts, and B. Derby, *The strength of Al$_2$O$_3$/SiC nanocomposites after grinding and annealing.* Acta Materialia, 1998. **46**(11): p. 3839-3848.

44.   Osada, T., W. Nakao, K. Takahashi, K. Ando, and S. Saito, *Strength recovery behavior of machined Al$_2$O$_3$/SiC nano-composite ceramics by crack-healing.* Journal of the European Ceramic Society, 2007. **27**(10): p. 3261-3267.

45.   Ohji, T., *Creep inhibition of ceramic/ceramic nanocomposites.* Scripta Materialia, 2001. **44**(8-9): p. 2083-2086.

46.   Sedláček J., D. Galusek[b], P. Švančárek[b], R. Riedel[c], Alan Atkinson[d] and Xin Wang, *Abrasive wear of Al$_2$O$_3$-SiC and Al$_2$O$_3$-(SiC)-C composites with micrometer- and submicrometer-sized alumina matrix grains.* Journal of the European Ceramic Society, 2008. **28**(15): p. 2983-2993.

47.   Baron, B., C.S. Kumar, G. Le Gonidec, and S. Hampshire, *Comparison of different alumina powders for the aqueous processing and pressureless sintering of Al$_2$O$_3$-SiC nanocomposites.* Journal of the European Ceramic Society, 2002. **22**(9-10): p. 1543-1552.

48.   Ananthakumar, S., U.S. Hareesh, A.D. Damodaran, and K.G.K. Warrier, *Microwave processing of boehmite coated SiC composite precursors for alumina - Silicon carbide nanocomposites.* Journal of Materials Science Letters, 1997. **17**(2): p. 145-148.

49.   Gustafsson, S., L.K.L. Falk, E. Lidén, and E. Carlström, *Alumina/silicon carbide composites fabricated via in situ synthesis of nano-sized SiC particles.* Ceramics International, 2009. **35**(3): p. 1293-1296.

50. Sakka, Y., D.D. Bidinger, and I.A. Aksay, *Processing of silicon carbide-mullite-alumina nanocomposites.* Journal of the American Ceramic Society, 1995. **78**(2): p. 479-486.

51. Deng, Z.Y., Y. Zhou, M.E. Brito, Y. Tanaka, and T. Ohji, *Effects of rare earth dopants on grain boundary bonding in alumina-silicon carbide composites.* Journal of the European Ceramic Society, 2004. **24**(2): p. 511-516.

52. Shapiro, I.P., R.I. Todd, J.M. Titchmarsh, and S.G. Roberts, *Effects of Y$_2$O$_3$ additives and powder purity on the densification and grain boundary composition of Al$_2$O$_3$/SiC nanocomposites.* Journal of the European Ceramic Society, 2009. **29**(9): p. 1613-1624.

53. CLAUSSEN, N., *Fracture Toughness of Al$_2$O$_3$ with an Unstabilized ZrO$_2$ Dispersed Phase.* Journal of the American Ceramic Society, 1976. **59**(1-2): p. 49-51.

54. Heuer, A.H. and L.W. Hobbs, *Zirconia-an overview. In Science and Technology of Zirconia.* Vol. 3. 1981, Columbus, OH, USA: The American Ceramic Society

55. Aza, A.H., J. Chevalier, G. Fantozzi, M. Schehl, and R. Torrecillas, *Slow-Crack-Growth Behavior of Zirconia-Toughened Alumina Ceramics Processed by Different Methods.* Journal of the American Ceramic Society, 2003. **86**(1): p. 115-120.

56. Chevalier, J., A.H. De Aza, G. Fantozzi, M. Schehl, and R. Torrecillas, *Extending the lifetime of ceramic orthopaedic implants.* Advanced Materials, 2000. **12**(21): p. 1619-1621.

57. Piconi, C. and G. Maccauro, *Zirconia as a ceramic biomaterial.* Biomaterials, 1999. **20**(1): p. 1-25.

58. Tuan, W.-H., J.-R. Chen, and C.-J. Ho, *Critical zirconia amount to enhance the strength of alumina.* Ceramics International, 2008. **34**(8): p. 2129-2135.

59. Strecker, K., S. Ribeiro, and M.-J. Hoffmann, *Fracture toughness measurements of LPS-SiC: a comparison of the indentation technique and the SEVNB method.* 2005, scielo. p. 121-124.

60.   Kingery, W.D., H.K. Bowen, and D.R. Uhlmann, *Introduction to Ceramics*. 1976, New York: John Wiley & Sons, Inc.

61.   Anstis, G.R., B.R. Lawn, D.B. Marshall, *A Critical Evaluation of Indentation Techniques for Measuring Fracture Toughness: I, Direct Crack Measurements*. 1981. p. 533-538.

62.   So, I.B. and S. Baik, *Critical concentration of MgO for the prevention of abnormal grain growth in alumina*. Journal of the American Ceramic Society, 1994. **77**(10): p. 2499-2504.

63.   Schmid, H.K., M. Aslan, S. Assmann, R. Nass, and H. Schmidt, *Microstructural characterization of Al_2O_3-SiC nanocomposites*. Journal of the European Ceramic Society, 1998. **18**(1): p. 39-49.

64.   Sternitzke, M., *Review: Structural ceramic nanocomposites*. Journal of the European Ceramic Society, 1997. **17**(9): p. 1061-1082.

65.   Tekeli, S., *Fracture toughness (K_{IC}), hardness, sintering and grain growth behaviour of $8YSCZ/Al_2O_3$ composites produced by colloidal processing*. Journal of Alloys and Compounds, 2005. **391**(1-2): p. 217-224.